Optical and dc conductivity of the two-dimensional Hubbard model in the pseudogap regime and across the antiferromagnetic quantum critical point including vertex corrections

Dominic Bergeron,[*] Vasyl Hankevych, Bumsoo Kyung, and A.-M. S. Tremblay[†]

Département de physique, Regroupement Québécois sur les Matériaux de Pointe (RQMP) and Canadian Insitute for Advanced Research (CIFAR), Université de Sherbrooke, Québec, Canada

The conductivity of the two-dimensional Hubbard model is particularly relevant for high-temperature superconductors. Vertex corrections are expected to be important because of strongly momentum-dependent self-energies. To attack this problem, one must also take into account the Mermin–Wagner theorem, the Pauli principle, and crucial sum rules in order to reach nonperturbative regimes. Here, we use the two-particle self-consistent approach that satisfies these constraints. This approach is reliable from weak to intermediate coupling. A functional derivative approach ensures that vertex corrections are included in a way that satisfies the f-sum rule. The two types of vertex corrections that we find are the antiferromagnetic analogs of the Maki–Thompson and Aslamasov–Larkin contributions of superconducting fluctuations to the conductivity but, contrary to the latter, they include nonperturbative effects. The resulting analytical expressions must be evaluated numerically. The calculations are impossible unless a number of advanced numerical algorithms are used. These algorithms make extensive use of fast Fourier transforms, cubic splines, and asymptotic forms. A maximum entropy approach is specially developed for analytical continuation of our results. These algorithms are explained in detail in the appendices. The numerical results are for nearest-neighbor hoppings. In the pseudogap regime induced by two-dimensional antiferromagnetic fluctuations, the effect of vertex corrections is dramatic. Without vertex corrections the resistivity increases as we enter the pseudogap regime. Adding vertex corrections leads to a drop in resistivity, as observed in some high-temperature superconductors. At high temperatures, the resistivity saturates at the Ioffe–Regel limit. At the quantum critical point and beyond, the resistivity displays both linear and quadratic temperature dependence and there is a correlation between the linear term and the superconducting transition temperature. A hump is observed in the mid-infrared range of the optical conductivity in the presence of antiferromagnetic fluctuations.

I. INTRODUCTION

The calculation of transport quantities in strongly correlated electron systems is particularly challenging, but is a necessary step to make contact with a wide class of experiments. Even for the simplest model, namely the single-band Hubbard model, this is a formidable task. Taking up the challenge is all the more important for the two-dimensional case (2D) that acts as the minimal model for the high-temperature cuprate superconductors,[1] layered organic superconductors,[2] and a number of other materials.

Even in cases where one has a good handle on the single-particle Green's function, the difficulty of calculating transport in the 2D Hubbard model stems from the fact that one cannot neglect the effect of vertex corrections when strong momentum-dependent correlations are present. Those vertex corrections are the analog of the self-energy, but for the two-particle response functions. When vertex corrections are not included, conservation laws can be violated and results inaccurate. In the case of small finite systems tractable by exact diagonalization or quantum Monte Carlo (QMC) calculations, the correlation function is directly evaluated and vertex corrections are not an issue. However, those results are more relevant for finite frequency conductivity and strong coupling, where correlations are mainly local.[3–8]

Consider for example the electrical conductivity for the 2D Hubbard model. For the infinite system, optical and DC conductivity calculations have been performed without vertex corrections using dynamical mean-field theory (DMFT)[9] and cellular DMFT (CDMFT).[10] Those calculations have also been done with the composite operator method[11] but vertex corrections cannot all be taken into account. For the $t − J$ model, the strong coupling limit of the Hubbard model, a number of approaches have been used, in particular the extended dynamical cluster approximation (DCA),[12,13] but vertex corrections[14,15] have been neglected. However, recent optical conductivity calculations for the Hubbard model with the DCA took vertex corrections into account.[16,17] The effects were found to be important only at high frequencies. Despite this recent advance, the calculation of vertex corrections with DCA or CDMFT, considered the best available ones at strong coupling,[18–20] is still an open problem.

At weak coupling, the Boltzmann equation offers a tractable approach that satisfies conservation laws when one includes scattering-in terms. For linear response, its variational formulation has been used for example to compute the effect of spin fluctuations within the self-consistent renormalized approach[21] and also to investigate the resistivity near the quantum critical point (QCP) in the clean[22] and disordered cases.[23,24] The drawbacks of this approach are that it assumes the existence of quasiparticles and that this assumption is not valid in two dimensions, especially near the pseudogap regime and QCP. Green's function approaches that do not assume quasiparticles are preferable. Hence, some resistivity calculations without vertex corrections were done with the T-matrix approximation[25] and with the fluctuation-exchange (FLEX) approximation.[26] Other FLEX calculations take into

account some vertex corrections due to spin and charge fluctuations.[27,28] In these works, only the antiferromagnetic Maki–Thompson (MT) diagrams were included. The antiferromagnetic analogs of the Aslamasov–Larkin (AL) diagrams were neglected, claiming that the latter are negligible. We will see that in the DC case this is true only in the presence of particle-hole symmetry. A review on those calculations is given in Ref. 29. In Ref. 30, which takes into account superconducting fluctuations, AL diagrams are taken into account for superconducting fluctuations but they are neglected for the spin fluctuations. A recent calculation using field-theory methods of the conductivity at the QCP[31] includes all vertex corrections but only at $T = 0$. The renormalized classical regime where a pseudogap appears has also been considered, but focusing only on the hot spots[32] or neglecting the AL contribution.[33] There are also analytical results for the conductivity with vertex corrections using Fermi-liquid theory.[34,35]

Despite all these results, the electrical resistivity at weak to intermediate coupling has not been reliably computed for all dopings and temperatures because particle-hole symmetry, where the AL term vanishes, does not generally hold and because there are regimes where Fermi-liquid theory is no longer valid. Fermi-liquid theory breaks down in the pseudogap regime, near the antiferromagnetic QCP and in the Ioffe–Regel limit. Hence, in this paper, we extend the two-particle self-consistent (TPSC)[36–39] approach to include the effect of vertex corrections in the calculation of the resistivity and optical conductivity of the one-band, square-lattice, nearest-neighbor 2D Hubbard model for weak to intermediate coupling. This regime corresponds to values of the interaction strength U below the critical value for the Mott transition. We present numerical results as examples and discuss possible links with experiments on cuprates. In particular, we consider the origin of the mid-infrared hump in the electron-doped materials, the Ioffe–Regel limit, insulating behavior in the pseudogap regime, and the link between linear resistivity, quantum critical behavior, and superconductivity.

The TPSC approach has the following strengths that make it a good choice for the present purposes. In two dimensions, the Mermin–Wagner theorem[40,41] prevents the occurrence of antiferromagnetic long-range order at finite temperature. Not many theories can handle that constraint. Because long-range order is prohibited, there is a wide range of temperatures where there are huge antiferromagnetic [or spin-density wave (SDW)] fluctuations in the paramagnetic state. It is in this regime that a fluctuation-induced pseudogap can appear.[37,42–44] The standard way to treat fluctuations in many-body theory, the random-phase approximation (RPA), leads instead to long-range order and misses this effect. The RPA also violates the Pauli principle in an important way.[36] The FLEX[45,46] approximation and the self-consistent renormalized theory of Moriya–Lonzarich[47–49] satisfy the Mermin–Wagner theorem but they do not satisfy the Pauli principle and consistency between one- and two-particle quantities. Strengths and weaknesses of these approaches are discussed further in Refs. 37,38. Weak coupling renormalization group approaches become uncontrolled when the antiferromagnetic fluctuations begin to diverge.[50–53] Other approaches include the effective spin-Hamiltonian approach.[54] The TPSC approach does not assume a Migdal theorem for

spin fluctuations, and Kanamori–Brueckner renormalization of the bare interaction is included without adjustable parameters. The conditions for the appearance of a pseudogap induced by antiferromagnetic fluctuations have been verified experimentally in electron-doped cuprates.[55] In addition to the above theoretical considerations, the TPSC approach has been extensively benchmarked against QMC calculations in regimes where the latter is available.[36,37,39,43,56–58] The agreement between the one-particle spectral function of TPSC and QMC approaches in the pseudogap regime is remarkable.[43] The TPSC approach, however, fails when the temperature is too far below that where the pseudogap appears.

In the TPSC method, the calculation proceeds in two steps. At the first step, spin-spin and charge-charge correlation functions are obtained with irreducible vertices that are determined self-consistently. That is the origin of the name of the approach. At the second level of approximation, a nontrivial self-energy that is consistent with the spin and charge fluctuations and that can explain fluctuation-induced momentum-dependent pseudogaps is then calculated. The charge-charge correlation function at the first level of approximation satisfies the f-sum rule with the Green's function at the same level, but it misses lifetime effects necessary to obtain nontrivial conductivity. What is needed is a calculation of the current-current correlation function that includes the Green's functions dressed at the second level of approximation with the corresponding irreducible vertices. What has been missing up to now is an expression for the corresponding irreducible vertices. Following Baym and Kadanoff,[59,60] here we use a functional derivative approach to obtain irreducible vertices that satisfy conservation laws. We check that the f-sum rule is then satisfied with the Green's function obtained at the second level of approximation. For the conductivity, we show that, not only the MT-type contributions from SDW fluctuations, but also the AL contributions are important. The latter have a dramatic effect in the pseudogap regime.

The paper is structured as follow. The next section contains the details of the methodology and is divided into five subsections: II A, the model; II B, the conductivity in linear response theory; II C, a derivation of the TPSC approach for the spin and charge response functions and the one-particle self-energy; II D, the conductivity in the TPSC approach; and finally II E, a description of the numerical algorithms that were used to calculate the expression given in Sec. II D. Section III presents the results for the system considered, followed by a discussion and a conclusion in Sec. IV and V, respectively. Also, some useful derivations, such as those for the conductivity, the f-sum rule, and Ward identities, are given in the appendices along with details of algorithms that are of more general applicability, such as calculating response functions with fast-Fourier transforms (FFTs) and cubic splines and analytical continuation of numerical data.

II. METHODOLOGY

We first define the model, recall the conductivity formula, and introduce the TPSC method in the functional derivative formalism. This approach allows us, in the fourth subsection, to derive the conductivity formula including vertex corrections. The last subsection briefly describes the numerical algorithms

that we implemented. Those are detailed in the appendices. In this section, we use units where $e = 1$, $\hbar = 1$, and $a = 1$, a being the lattice parameter. In Sec. III, we use both those units and physical units to allow comparison with typical experimental values.

A. Model

Our model is the 2D Hubbard Hamiltonian in the presence of an electromagnetic field that is treated classically. With the usual Peierls substitution, we have

$$H(t) = -\sum_{ij\sigma} t_{ij} c_{i\sigma}^{\dagger} c_{j\sigma} e^{-i \int_i^j d\mathbf{r}_{ij} \cdot \mathbf{A}(\mathbf{r},t)} + U \sum_i n_{i\uparrow} n_{i\downarrow}, \quad (1)$$

where $\mathbf{r}_{ij} = \mathbf{r}_i - \mathbf{r}_j$, t_{ij} are the hopping matrix elements between the sites of the lattice, $c_{j\sigma}$ destroys a particle with spin σ at site j and $c_{i\sigma}^{\dagger}$ creates a particle at site i, $\mathbf{A}(\mathbf{r},t)$ is the vector potential, U is the on-site repulsion energy, and $n_{i\sigma} = c_{i\sigma}^{\dagger} c_{i\sigma}$ is the spin σ particle number operator at site i. Note that it is perfectly general to use only the vector potential to represent the field, since a scalar potential can always be removed using the proper gauge transformation. The form of Eq. (1) for the Hamiltonian is justified by gauge invariance. Further discussion of the Peierls substitution may be found in Ref. 61.

B. Conductivity in linear response theory

This derivation of the linear response result will allow us to set the notation. To obtain the conductivity, we first need the expression for the current operator. In the x direction, for example, it is given by

$$j_x^S(\mathbf{r},t) = -\frac{\delta H}{\delta A_x(\mathbf{r},t)}, \quad (2)$$

where the superscript S indicates that j_x is in Shrödinger representation, despite its dependance on t. If we apply this definition to Eq. (1), keep terms up to linear order in the vector potential, assuming that $\mathbf{A}(\mathbf{r},t) = A_x(\mathbf{r},t)\hat{x}$, with $A_x(\mathbf{r},t)$ varying slowly on the scale of a lattice spacing so that

$$\int_i^j dx_{ij} A_x(\mathbf{r},t) \approx \frac{x_{ij}}{2} (A_x(\mathbf{r}_i,t) + A_x(\mathbf{r}_j,t)), \quad (3)$$

where x_{ij} is the x component of the vector $\mathbf{r}_j - \mathbf{r}_i$, we obtain

$$j_x^S(\mathbf{r}_l,t) = \frac{i}{2} \sum_{\delta\sigma} \delta_x t_\delta \left(c_{l\sigma}^{\dagger} c_{l-\delta,\sigma} + c_{l+\delta,\sigma}^{\dagger} c_{l,\sigma} \right)$$
$$- \frac{1}{2} A_x(\mathbf{r}_l,t) \sum_{\delta\sigma} \delta_x^2 t_\delta \left(c_{l\sigma}^{\dagger} c_{l-\delta,\sigma} + c_{l+\delta,\sigma}^{\dagger} c_{l\sigma} \right) \quad (4)$$

where δ_x is the projection along x of the vector δ between neighbors. t_δ is the corresponding hopping matrix element. For a uniform electric field we can take the vector potential

independent of position, which means that we need only the $\mathbf{q} = 0$ component of the current

$$j_x^S(t) = -\frac{1}{N} \sum_{\mathbf{k}\sigma} \frac{\partial \epsilon_\mathbf{k}}{\partial k_x} c_{\mathbf{k}\sigma}^{\dagger} c_{\mathbf{k},\sigma}$$
$$- A_x(t) \frac{1}{N} \sum_{\mathbf{k}\sigma} \frac{\partial^2 \epsilon_\mathbf{k}}{\partial k_x^2} c_{\mathbf{k}\sigma}^{\dagger} c_{\mathbf{k},\sigma}, \quad (5)$$

where $\epsilon_\mathbf{k}$ is the dispersion relation and N is the number of lattice sites or wave vectors in the Brillouin zone. For the following we need to define the paramagnetic current,

$$j_x^p = -\frac{1}{N} \sum_{\mathbf{k}\sigma} \frac{\partial \epsilon_\mathbf{k}}{\partial k_x} c_{\mathbf{k}\sigma}^{\dagger} c_{\mathbf{k},\sigma}, \quad (6)$$

and the diamagnetic current,

$$j_x^d(t) = -A_x(t) \frac{1}{N} \sum_{\mathbf{k}\sigma} \frac{\partial^2 \epsilon_\mathbf{k}}{\partial k_x^2} c_{\mathbf{k}\sigma}^{\dagger} c_{\mathbf{k},\sigma}, \quad (7)$$

so that $j_x^S(t) = j_x^p + j_x^d(t)$.

According to linear response theory, the frequency-dependent current in response to the field is

$$\langle j_x(\omega) \rangle = \langle \hat{j}_x(\omega) \rangle + \chi_{j_x j_x}(\omega) A_x(\omega), \quad (8)$$

where $j_x(\omega)$ is the Fourier transform of

$$j_x(t) = U^{\dagger}(t, -\infty) j_x^S(t) U(t, -\infty), \quad (9)$$

where $U(t,t')$ is the time-evolution operator for the Hamiltonian $H(t)$, Eq. (1),

$$\chi_{j_x j_x}(\omega) = \frac{i}{N} \int dt \, e^{i\omega(t-t')} \langle [\hat{j}_x^p(t), \hat{j}_x^p(t')] \rangle \theta(t - t') \quad (10)$$

is the *current-current* correlation function, and the notation $\hat{O}(t)$ stands for the interaction representation of the operator O, namely, $\hat{O}(t) = e^{iH_0 t} O e^{-iH_0 t}$, where H_0 is the Hamiltonian in Eq. (1) with $\mathbf{A} = 0$. Also, $\langle \ldots \rangle$ means an equilibrium average, namely in the system H_0.

Since $\langle \hat{j}_x^p(t) \rangle = \langle j_x^p \rangle = 0$, the equilibrium average of the current operator in the interaction representation is given by the diamagnetic term

$$\langle \hat{j}_x(t) \rangle = \langle \hat{j}_x^d(t) \rangle = \langle j_x^d(t) \rangle$$
$$= -A_x(t) \frac{1}{N} \sum_{\mathbf{k}\sigma} \frac{\partial^2 \epsilon_\mathbf{k}}{\partial k_x^2} \langle c_{\mathbf{k}\sigma}^{\dagger} c_{\mathbf{k},\sigma} \rangle. \quad (11)$$

Defining

$$\langle k_x \rangle = -\frac{1}{N} \sum_{\mathbf{k}} \frac{\partial^2 \epsilon_\mathbf{k}}{\partial k_x^2} \langle n_k \rangle, \quad (12)$$

where $n_k = c_{\mathbf{k}\sigma}^{\dagger} c_{\mathbf{k},\sigma}$, we have

$$\langle \hat{j}_x(t) \rangle = \langle k_x \rangle A_x(t), \quad (13)$$

or, in frequency,

$$\langle \hat{j}_x(\omega) \rangle = \langle k_x \rangle A_x(\omega), \quad (14)$$

and Eq. (8) therefore becomes

$$\langle j_x(\omega) \rangle = [\langle k_x \rangle + \chi_{j_x j_x}(\omega)] A_x(\omega). \quad (15)$$

Note that, in the case where the Hamiltonian has only nearest-neighbor hoppings, $\langle k_x \rangle$ is proportional to the local kinetic energy,[8] but in general it cannot be regarded as such, as is clear from Eq. (12).

To find the conductivity, it suffices to relate the electric field to the vector potential through

$$E_x(\omega) = i(\omega + i\eta)A_x(\omega), \tag{16}$$

where η is positive and infinitesimal. Thus the current is related to the electric field by

$$\langle j_x(\omega) \rangle = \frac{\langle k_x \rangle + \chi_{j_x j_x}(\omega)}{i(\omega + i\eta)} E_x(\omega). \tag{17}$$

Finally, since $\langle j_x(\omega) \rangle = \sigma_{xx}(\omega)E_x(\omega)$ by definition, the expression for the optical conductivity in linear response theory is

$$\sigma_{xx}(\omega) = \frac{\langle k_x \rangle + \chi_{j_x j_x}(\omega)}{i(\omega + i\eta)}. \tag{18}$$

In this paper, we calculate only the real part of $\sigma(\omega)$, the dissipative part, and the expression that we use in practice is

$$Re\,\sigma_{xx}(\omega) = \frac{\chi''_{j_x j_x}(\omega)}{\omega}, \tag{19}$$

which is derived in Appendix A from Eqs. (A14)–(A16). If one is interested in the imaginary part, it can be obtained using Kramers–Krönig relations.

C. Two-particle self-consistent approach

In the TPSC approach, one- and two-particle Green's functions for the Hubbard model are calculated in a nonperturbative way. The approach enforces conservation laws, key sum rules, and the Pauli principle. It was shown, from benchmarks with QMC results[36,37,43,56,58,62] to be accurate within a few percent for interaction strengths up to about $U = 6t$. We will derive the TPSC approach below, but the reader can also resort to Refs. 37– 39 for a more detailed discussion of the approach itself and a comparison with other approaches.

In this subsection, we present the key equations for the theory. The following subsection contains details of the derivation. We use the shorthand notation $1 = (\mathbf{r}_1, \tau_1)$ for space and imaginary-time coordinates and $q = (\mathbf{q}, iq_n)$ for reciprocal space and Matsubara frequency coordinates.

The *spin* and *charge* response functions must be computed first from the expressions

$$\chi_{sp}(q) = \frac{1}{N}\int d\tau e^{i\omega_n \tau} \langle T_\tau S^z(\mathbf{q}, \tau)S^z(-\mathbf{q}) \rangle$$
$$= \frac{\chi_0(q)}{1 - \frac{U_{sp}}{2}\chi_0(q)}, \tag{20}$$

$$\chi_{ch}(q) = \frac{1}{N}\int d\tau e^{i\omega_n \tau} \langle T_\tau n(\mathbf{q}, \tau)n(-\mathbf{q}) \rangle - \langle n \rangle^2$$
$$= \frac{\chi_0(q)}{1 + \frac{U_{ch}}{2}\chi_0(q)}, \tag{21}$$

where T_τ is the *imaginary-time-ordering* operator and $\chi_0(q)$ is the Lindhard function, given by

$$\chi_0(q) = -2\frac{T}{N}\sum_k G^{(1)}(k+q)G^{(1)}(k). \tag{22}$$

Here, $G^{(1)}$ corresponds numerically to a noninteracting Green's function because the self-energy Eq. (49) is constant and the chemical potential is adjusted to obtain the correct filling. This point will become clear below. Note that we assume here that the system is paramagnetic so that the spin index will often be omitted and the sum over it replaced by a factor of two, as in Eq. (22). In Eqs. (20) and (21), the parameters U_{sp} and U_{ch} are the spin and charge irreducible vertices, respectively. First, U_{sp} is defined by

$$U_{sp} = U\frac{\langle n_\uparrow(1)n_\downarrow(1) \rangle}{\langle n_\uparrow(1) \rangle \langle n_\downarrow(1) \rangle}, \tag{23}$$

(this definition is used for hole doping, electron doping will be discussed below) so that it can be determined from the fluctuation-dissipation theorem

$$\frac{T}{N}\sum_q \chi_{sp}(q) = \langle S^z S^z \rangle = \langle n \rangle - 2\langle n_\uparrow n_\downarrow \rangle$$
$$= \langle n \rangle - \frac{U_{sp}}{U}\frac{\langle n \rangle^2}{2}, \tag{24}$$

where we have used the Pauli principle $\langle n_\sigma^2 \rangle = \langle n_\sigma \rangle$. Note that all quantities on right-hand side of Eq. (24) are local ones. Then, once the double occupancy is known, U_{ch} can be determined from

$$\frac{T}{N}\sum_q \chi_{ch}(q) = \langle n \rangle + 2\langle n_\uparrow n_\downarrow \rangle - \langle n \rangle^2. \tag{25}$$

We also call Eqs. (24) and (25) the *local spin* and *local charge* sum rules.

Finally, with response functions (20) and (21) we can obtain the one-particle self-energy,

$$\Sigma_\sigma^{(2)}(k) = Un_{-\sigma} + \frac{U}{8}\frac{T}{N}\sum_q [3U_{sp}\chi_{sp}(q) + U_{ch}\chi_{ch}(q)]$$
$$\times G_\sigma^{(1)}(k+q), \tag{26}$$

whose form will be explained below. Expressions (20), (21), and (26) are the basic equations of the TPSC approach.

1. First step: Spin and charge susceptibilities

First let us derive expressions (20) and (21) for the spin and charge susceptibilities. In the following, we use Einstein's convention for the sums (or integrals), namely that an index appearing twice or more in an expression is summed over lattice sites and integrated over imaginary time. An overbar helps clarify which indices are involved. The approach follows the Martin–Schwinger techniques[63] described in Kadanoff and Baym's book.[60]

It is convenient to introduce a "source field" $\phi_\sigma(1,2)$ that couples to one-particle excitations in the system. It allows us to easily obtain correlation functions from functional derivatives. The source field can be set to zero at the end of the calculation. The source-field-dependent Green's function in the grand

canonical ensemble is then given by

$$G_\sigma(1,2;\{\phi\}) = -\frac{\text{Tr}\left[e^{-\beta K} T_\tau e^{-c_{\bar\sigma}^\dagger(\bar1)\phi_{\bar\sigma}(\bar1,\bar2)c_{\bar\sigma}(\bar2)}c_\sigma(1)c_\sigma^\dagger(2)\right]}{\text{Tr}\left[e^{-\beta K} T_\tau e^{-c_{\bar\sigma}^\dagger(\bar1)\phi_{\bar\sigma}(\bar1,\bar2)c_{\bar\sigma}(\bar2)}\right]}$$

$$= -\langle T_\tau c_\sigma(1)c_\sigma^\dagger(2)\rangle_\phi, \quad (27)$$

where $K = H - \mu N$, μ is the chemical potential, and N is the number operator. We have also used the notation $\langle\ldots\rangle_\phi$ which means that the average is taken with the source field turned on. Response functions can be obtained from functional derivatives of G_σ with respect to $\phi_{\sigma'}$ since

$$\frac{\delta G_\sigma(1,2;\{\phi\})}{\delta\phi_{\sigma'}(3,4)} = G_{\sigma'}(4,3;\{\phi\})G_\sigma(1,2;\{\phi\})$$

$$- \langle T_\tau c_{\sigma'}^\dagger(3)c_{\sigma'}(4)c_\sigma^\dagger(2)c_\sigma(1)\rangle_\phi. \quad (28)$$

We also have

$$\chi_{sp}(1,2) = \langle T_\tau S^z(1)S^z(2)\rangle$$
$$= \langle T_\tau[n_\uparrow(1) - n_\downarrow(1)][n_\uparrow(2) - n_\downarrow(2)]\rangle$$
$$= 2(\langle T_\tau n_\uparrow(1)n_\uparrow(2)\rangle - \langle T_\tau n_\uparrow(1)n_\downarrow(2)\rangle), \quad (29)$$

where we have used spin-rotation symmetry to obtain the last line from the previous one. For the charge response function, the corresponding expression is

$$\chi_{ch}(1,2) = \langle n(1)n(2)\rangle - \langle n(1)\rangle\langle n(2)\rangle$$
$$= 2(\langle T_\tau n_\uparrow(1)n_\uparrow(2)\rangle + \langle T_\tau n_\uparrow(1)n_\downarrow(2)\rangle)$$
$$- \langle n(1)\rangle\langle n(2)\rangle. \quad (30)$$

According to Eq. (28), the last two results, Eqs. (29) and (30), can be written as

$$\chi_{ch/sp}(1,2)$$
$$= -2\left(\frac{\delta G_\uparrow(1,1^+;\{\phi\})}{\delta\phi_\uparrow(2^+,2)} \pm \frac{\delta G_\uparrow(1,1^+;\{\phi\})}{\delta\phi_\downarrow(2^+,2)}\right)\Bigg|_{\{\phi\}=0}, \quad (31)$$

where the expressions with the plus and minus sign correspond respectively to the charge and spin response functions. Here, $1^+ = (\mathbf{r}_1, \tau_1 + \epsilon)$, where ϵ is positive and infinitesimal. For the remainder of this section, we implicitly assume that derivatives with respect to ϕ are evaluated at $\{\phi\} = 0$.

To obtain integral equations for the response functions, we begin with

$$G_\sigma(1,\bar1)G_\sigma^{-1}(\bar1,2) = \delta(1-2). \quad (32)$$

Taking the functional derivative of this equation with respect to $\phi_{\sigma'}(3,4)$, taking $2 \to \bar2$, multiplying on the right by $G_\sigma(\bar2,2)$, and summing over $\bar2$, we obtain

$$\frac{\delta G_\sigma(1,2)}{\delta\phi_{\sigma'}(3,4)} = -G_\sigma(1,\bar1)\frac{\delta G_\sigma^{-1}(\bar1,\bar2)}{\delta\phi_{\sigma'}(3,4)}G_\sigma(\bar2,2). \quad (33)$$

On the other hand, Dyson's equation in the presence of the field ϕ reads

$$G_\sigma^{-1}(1,2) = G_\sigma^{(0)-1}(1,2) - \phi_\sigma(1,2) - \Sigma_\sigma(1,2), \quad (34)$$

where $G_\sigma^{(0)}$ is the noninteracting Green's function and Σ_σ is the self-energy, so that

$$\frac{\delta G_\sigma^{-1}(1,2)}{\delta\phi_{\sigma'}(3,4)} = -\delta(1-3)\delta(2-4)\delta_{\sigma\sigma'} - \frac{\delta\Sigma_\sigma(1,2)}{\delta\phi_{\sigma'}(3,4)}, \quad (35)$$

and therefore, from Eq. (33),

$$\frac{\delta G_\sigma(1,2)}{\delta\phi_{\sigma'}(3,4)} = G_\sigma(1,3)G_\sigma(4,2)\delta_{\sigma\sigma'}$$

$$+ G_\sigma(1,\bar1)\frac{\delta\Sigma_\sigma(\bar1,\bar2)}{\delta\phi_{\sigma'}(3,4)}G_\sigma(\bar2,2). \quad (36)$$

Following Luttinger and Ward,[64] Σ_σ is a functional of G_σ and $G_{-\sigma}$, and we find, applying the chain rule, that

$$\frac{\delta G_\sigma(1,2)}{\delta\phi_{\sigma'}(3,4)} = G_\sigma(1,3)G_\sigma(4,2)\delta_{\sigma\sigma'}$$

$$+ G_\sigma(1,\bar1)\frac{\delta\Sigma_\sigma(\bar1,\bar2)}{\delta G_{\bar\sigma}(\bar3,\bar4)}\frac{\delta G_{\bar\sigma}(\bar3,\bar4)}{\delta\phi_{\sigma'}(3,4)}G_\sigma(\bar2,2). \quad (37)$$

This is the analog of the Bethe–Salpeter for the *particle-hole* channel. Defining the *particle-hole* irreducible vertex

$$\Gamma_{\sigma\sigma'}(1,2;3,4) = \frac{\delta\Sigma_\sigma(1,2)}{\delta G_{\sigma'}(3,4)}, \quad (38)$$

Eq. (37) reads

$$\frac{\delta G_\sigma(1,2)}{\delta\phi_{\sigma'}(3,4)} = G_\sigma(1,3)G_\sigma(4,2)\delta_{\sigma\sigma'} + G_\sigma(1,\bar1)$$

$$\times \Gamma_{\sigma\bar\sigma}(\bar1,\bar2;\bar3,\bar4)\frac{\delta G_{\bar\sigma}(\bar3,\bar4)}{\delta\phi_{\sigma'}(3,4)}G_\sigma(\bar2,2). \quad (39)$$

The spin and charge response functions in Eq. (31) are special cases of the more general functions

$$\chi_\pm(1,2;3,4) = -2\left(\frac{\delta G_\uparrow(1,2;\{\phi\})}{\delta\phi_\uparrow(3,4)} \pm \frac{\delta G_\uparrow(1,2;\{\phi\})}{\delta\phi_\downarrow(3,4)}\right). \quad (40)$$

It is straightforward to show, from the Bethe–Salpeter equation, Eq. (39), and spin-rotational invariance, that

$$\chi_\pm(1,2;3,4) = -2G(1,3)G(4,2) \pm \Gamma_{ch/sp}(\bar1,\bar2;\bar3,\bar4)G(1,\bar1)$$
$$\times G(\bar2,2)\chi_\pm(\bar3,\bar4|3,4) \quad (41)$$

where

$$\Gamma_{ch/sp}(\bar1,\bar2;\bar3,\bar4) = \frac{\delta\Sigma_\uparrow(\bar1,\bar2)}{\delta G_\downarrow(\bar3,\bar4)} \pm \frac{\delta\Sigma_\uparrow(\bar1,\bar2)}{\delta G_\uparrow(\bar3,\bar4)} \quad (42)$$

and $G = G_\uparrow = G_\downarrow$.

Up to now, all the results are exact. The first step in the TPSC approach is to obtain a first approximation for the self-energy that will be used to obtain irreducible vertices. First, let us rewrite Dyson's equation, Eq. (34), with zero source field in the form

$$G_\sigma^{(0)-1}(1,\bar3)G_\sigma(\bar3,2) = \delta(1-2) + \Sigma_\sigma(1,\bar3)G_\sigma(\bar3,2). \quad (43)$$

Then, note that the equation of motion for the Green's function reads

$$\sum_l\left[\left(-\frac{\partial}{\partial\tau} + \mu\right)\delta_{il} + t_{il}\right]G_\sigma(l-j,\tau)$$

$$= \delta(\tau)\delta_{ij} - U\langle T_\tau n_{i\bar\sigma}(\tau)c_{i\sigma}(\tau)c_{j\sigma}^\dagger\rangle, \quad (44)$$

or, in compact form,

$$G_\sigma^{(0)-1}(1,\bar3)G_\sigma(\bar3,2) = \delta(1-2) - U\langle T_\tau n_{\bar\sigma}(1)c_\sigma(1)c_\sigma^\dagger(2)\rangle, \quad (45)$$

where $\tilde{\sigma} = -\sigma$. By comparing Eqs. (43) and (45) we conclude that

$$\Sigma_\sigma(1,\bar{3})G_\sigma(\bar{3},2) = -U\langle T_\tau n_{\tilde{\sigma}}(1)c_\sigma(1)c_\sigma^\dagger(2)\rangle. \quad (46)$$

Now comes our first approximation. We replace the last expression of Eq. (46) by

$$\Sigma_\sigma(1,\bar{1})G_\sigma(\bar{1},2) \approx Ug_{\uparrow\downarrow}(1)G_{\tilde{\sigma}}(1,1^+)G_\sigma(1,2), \quad (47)$$

where, for the hole-doped case,

$$g_{\uparrow\downarrow}(1) = \frac{\langle n_\uparrow(1)n_\downarrow(1)\rangle}{\langle n_\uparrow(1)\rangle\langle n_\downarrow(1)\rangle}. \quad (48)$$

For the electron-doped case, we replace n_σ in this expression by $1 - n_\sigma$. Thus, when the lattice is bipartite, particle-hole symetry of the phase diagram is preserved. It also gives a better agreement with QMC results when the lattice is not bipartite. Those two different approximations are equivalent to assuming that approximation (47) is made for holes when the hole density is smaller than the particle density and for particles otherwise. Now, substituting definition (48) into Eq. (47), it is clear that we recover the exact result for the self-energy of Eq. (46) in the special case $2 = 1^+$. The approximation[36,65] is justified if it is correct to assume that the four-point correlation function factorizes only when points 1 and 2 are different.

Within this approximation, the self-energy can be obtained by multiplying Eq. (47) by $G_\sigma^{-1}(2,3)$ from the right and summing over 2 to obtain

$$\Sigma_\sigma^{(1)}(1,2) = Ug_{\uparrow\downarrow}(1)G_{\tilde{\sigma}}(1,1^+)\delta(1-2), \quad (49)$$

which is the self-energy ansatz that is used to define the Green's function $G^{(1)}$ in Lindhard function (22), from which are defined TPSC susceptibilities (20) and (21). Note that once the source field ϕ is turned off and translational invariance is restored, $\Sigma_\sigma^{(1)}(1,2)$ becomes independent of position and its Fourier transform (FT) is simply a constant that can be absorbed in the chemical potential in $G_\sigma^{(1)}(k)$, so that this Green's function is in practice a noninteracting one.

Given the self-energy, as well as the result

$$\frac{\delta g_{\uparrow\downarrow}(1)}{\delta G_\sigma(2,3)} = \frac{\delta g_{\uparrow\downarrow}(1)}{\delta G_{-\sigma}(2,3)}, \quad (50)$$

valid in the paramagnetic phase, and the definition of the spin vertex, Eq. (42), we obtain the spin vertex

$$\Gamma_{sp}(1,2;3,4) = U_{sp}\delta(1-3)\delta(1^+-4)\delta(1^--2), \quad (51)$$

where $U_{sp} = Ug_{\uparrow\downarrow}(1)$. It is possible to obtain an analytical expression for $\delta g_{\uparrow\downarrow}(1)/\delta G_\sigma(3,4)$ to compute the charge vertex from definition (42) and ansatz (49), but to this day the most successful approach has been to approximate this functional derivative as local, i.e., proportional to $\delta(1-3)\delta(1-4)$, which leads to

$$\Gamma_{ch}(1,2;3,4) = U_{ch}\delta(1-3)\delta(1^+-4)\delta(1^--2). \quad (52)$$

Substituting into the Bethe–Salpeter equation for the susceptibilities, Eq. (41), we find the corresponding TPSC expressions for the spin [Eq.(20)] and charge [Eq.(21)] susceptibilities. They suffice to determine also U_{ch}.

2. Second step: Improved self-energy

Collective modes are generally less influenced by details of the single-particle properties than the other way around since collective modes depend more strongly on general principles like conservation laws. We thus wish now to obtain an improved approximation for the self-energy that takes advantage of the fact that we have found accurate approximations for the low-frequency spin and charge fluctuations. We begin from the general definition of the self-energy Eq. (46), obtained from Dyson's equation.

We start with the longitudinal channel (ϕ diagonal in spin indices) and use the corresponding expression for the correlation function in terms of the response function, Eq. (28). In that case, the right-hand side of the general definition of the self-energy, Eq. (46), may be written as

$$\Sigma_\sigma(1,\bar{1})G_\sigma(\bar{1},2)$$
$$= -U\left[\frac{\delta G_\sigma(1,2)}{\delta\phi_{-\sigma}(1^+,1)} - G_{-\sigma}(1,1^+)G_\sigma(1,2)\right]. \quad (53)$$

The last term is the Hartree–Fock contribution, which gives the exact result for the left-hand side in the limit $\omega \to \infty$.[37] The $\delta G_\sigma/\delta\phi_{-\sigma}$ term is thus a contribution to lower frequencies, and it comes from the spin and charge fluctuations. Right-multiplying the last equation by G^{-1}, replacing the lower-energy part $\delta G_\sigma/\delta\phi_{-\sigma}$ by its general expression in terms of irreducible vertices, Eq. (37), and taking Σ and G on the right-hand side to be the first-level approximations $\Sigma^{(1)}$ and $G^{(1)}$, respectively, we find

$$\Sigma_\sigma^{(2)}(1,2) = UG_{-\sigma}^{(1)}(1,1^+)\delta(1-2)$$
$$- UG_\sigma^{(1)}(1,\bar{3})\frac{\delta\Sigma_\sigma^{(1)}(\bar{3},2)}{\delta G_{\tilde{\sigma}}^{(1)}(\bar{4},\bar{5})}\frac{\delta G_{\tilde{\sigma}}^{(1)}(\bar{4},\bar{5})}{\delta\phi_{-\sigma}(1^+,1)}. \quad (54)$$

If we expand the sum over spins on the right-hand side to express the irreducible vertices in terms of their spin and charge versions, Eq. (42), we find, after using the TPSC vertices, Eqs. (51),(52),

$$\Sigma_\sigma^{l(2)}(k) = Un_{-\sigma} + \frac{U}{4}\frac{T}{N}\sum_q [U_{sp}\chi_{sp}(q) + U_{ch}\chi_{ch}(q)]$$
$$\times G_\sigma^{(1)}(k+q). \quad (55)$$

There is, however, an ambiguity in obtaining the self-energy formula. Indeed, we can obtain an expression for the self-energy by using a transverse source field $\phi_{-\sigma\sigma}$ in Eq. (27). By taking functional derivatives of G with respect to this ϕ, we first obtain the transverse spin correlation functions $\chi_{+-}(1,2) = \langle T_\tau S_+(1)S_-(2)\rangle$ and χ_{-+}. Then, using a derivation analogous to that for the longitudinal case,[38] we find

$$\Sigma_\sigma^{t(2)}(k) = Un_{-\sigma} + \frac{U}{2}\frac{T}{N}\sum_k U_{sp}\chi_{sp}(q)G_{-\sigma}^{(1)}(k+q). \quad (56)$$

During the derivation, $\chi_{+-}(1,2) = \chi_{-+}(1,2) = \frac{1}{2}\chi_{sp}(1,2)$ was used, taking spin-rotational invariance into account.

The two previous expressions for the self-energy clearly show that our approximations for the fully reducible vertex do not preserve crossing symmetry, that is, the symmetry under the exchange of two particles or two holes. To improve our approximation and restore crossing symmetry,[43] we average

the two expressions, (55) and (56), which give the final result, Eq. (26), that we use in the rest of this paper. It turns out that this "symmetric" expression of the self-energy gives a better agreement with QMC results.[43] In addition, we verify numerically that the exact sum rule (Appendix A in Ref. [37])

$$-\int \frac{d\omega'}{\pi} \text{Im} \, \Sigma_\sigma^R(\mathbf{k},\omega') = U^2 n_{-\sigma}(1 - n_{-\sigma}), \quad (57)$$

determining the high-frequency behavior of Σ, is satisfied to a higher degree of accuracy with the symmetrized self-energy expression, Eq. (26).

3. Internal accuracy checks

Our final expression for the self-energy $\Sigma^{(2)}$, Eq. (26), is in principle an improvement over the constant self-energy entering the calculation of the susceptibilities. But clearly the approach is not one-particle self-consistent. All the Green's functions entering the right-hand side of Eq. (26) are evaluated with $G^{(1)}$, which has a constant self-energy. The advantage is that all quantities, including the vertices, on the right-hand side of Eq. (26) are computed at the same level of approximation. In fact, one can miss some important physics if this is not the case.[37]

Apart from comparisons with QMC calculations, we can check the accuracy in other ways. For example, the f-sum rule,

$$\int \frac{d\omega}{\pi} \omega \chi_{ch}''(\mathbf{q},\omega) = \frac{1}{N} \sum_{\mathbf{k}\sigma} (\epsilon_{\mathbf{k}+\mathbf{q}} + \epsilon_{\mathbf{k}-\mathbf{q}} - 2\epsilon_{\mathbf{k}}) \langle n_{\mathbf{k}\sigma} \rangle, \quad (58)$$

is exactly satisfied at the first level of approximation (i.e., with $\langle n_{\mathbf{k}\sigma} \rangle^{(1)}$ on the right-hand side) and the charge susceptibility obtained with U_{ch}. Suppose that on the right-hand side of that equation, one uses $\langle n_{\mathbf{k}\sigma} \rangle$ obtained from $G^{(2)}$ instead of the Fermi function. In cases where the agreement with QMC is good, one should find that the right-hand side does not change by more than a few percent.

When we are in the Fermi-liquid regime, another way to verify the accuracy of the approach is to verify if the Fermi surface obtained from $G^{(2)}$ satisfies Luttinger's theorem very closely.

Finally, the consistency relation between one- and two-particle quantities (Σ and $\langle n_\uparrow n_\downarrow \rangle$), Eq. (46), should be satisfied exactly in the Hubbard model. In the special case where $2 = 1^+$, this relation can be written as

$$\frac{1}{2}\text{Tr}(\Sigma G) = \lim_{\tau \to 0^-} \frac{T}{N} \sum_k e^{-ik_n\tau} \Sigma_\sigma(k) G_\sigma(k) = U \langle n_\uparrow n_\downarrow \rangle. \quad (59)$$

In standard many-body books,[66] this expression is encountered in the calculation of the free energy through a coupling-constant integration. In the TPSC approach, it is not difficult to show (Appendix B of Ref. [37]) that the following equation,

$$\frac{1}{2}\text{Tr}(\Sigma^{(2)} G^{(1)}) = U \langle n_\uparrow n_\downarrow \rangle, \quad (60)$$

is satisfied exactly with the self-consistent $U \langle n_\uparrow n_\downarrow \rangle$ obtained from the sum rule of Eq. (24). An internal accuracy check consists of verifying by how much $\frac{1}{2}\text{Tr}(\Sigma^{(2)} G^{(2)})$ differs from $\frac{1}{2}\text{Tr}(\Sigma^{(2)} G^{(1)})$. Again, in regimes where we have agreement with QMC calculations, the difference is only a few percent.

The above relation between Σ and $\langle n_\uparrow n_\downarrow \rangle$ gives us another way to justify our expression for $\Sigma^{(2)}$, Eq. (26). Suppose one starts from Eq. (55) to obtain a self-energy that contains only the longitudinal spin fluctuations and the charge fluctuations, as was done in the first papers on the TPSC method.[36] One finds that the spin part and the charge part each contribute an amount $U \langle n_\uparrow n_\downarrow \rangle/2$ to the consistency relation Eq. (60). Similarly, if we work only in the transverse spin channel,[38,43] we find that each of the two transverse spin components also contributes $U \langle n_\uparrow n_\downarrow \rangle/2$ to $\frac{1}{2}\text{Tr}(\Sigma^{(2)} G^{(1)})$. Hence, averaging the two expressions also preserves rotational invariance since each spin component contributes equally to Eq. (60). Note that Eq. (26) for $\Sigma^{(2)}$ is different from so-called Berk–Schrieffer-type expressions[67] that contain only bare vertices and do not satisfy (Appendix E in Ref. [37]) the consistency condition between one- and two-particle properties, Eq. (59).

D. Conductivity in the two-particle self-consistent approach

To compute Re $\sigma(\omega)$ from the Kubo formula, Eq. (19), we have to obtain the *current-current* correlation function given by Eq. (10), which contains the $\mathbf{q} = 0$ component of the paramagnetic current. From the general expression for the current, Eq. (4), we have

$$j_x^p = \sum_l j_x^p(\mathbf{r}_l) = i \sum_{\delta\sigma} \delta_x t_\delta \sum_l c_{l\sigma}^\dagger c_{l-\delta,\sigma}. \quad (61)$$

Since the actual calculation is done in Matsubara frequency instead of the real-frequency definition of $\chi_{j_x j_x}$, Eq. (10), we use

$$\chi_{j_x j_x}(iq_n) = \frac{1}{N}\int dt \, e^{iq_n(\tau-\tau')} \langle T_\tau \hat{j}_x^p(\tau) \hat{j}_x^p(\tau') \rangle, \quad (62)$$

where $\hat{j}_x^p(\tau) = e^{\tau H_0} j_x^p e^{-\tau H_0}$ and $q_n = 2n\pi T$, with n an integer, is a bosonic Matsubara frequency. Substituting Eq.(61) into this expression gives

$$\langle T_\tau \hat{j}_x^p(\tau) \hat{j}_x^p(\tau') \rangle = - \sum_{il\delta_1\delta_2\sigma_1\sigma_2} \delta_{x1}\delta_{x2} t_{\delta_1} t_{\delta_2}$$
$$\times \langle T_\tau c_{i\sigma}^\dagger(\tau) c_{i-\delta_1,\sigma}(\tau) c_{l\sigma}^\dagger(\tau') c_{l-\delta_2,\sigma}(\tau') \rangle. \quad (63)$$

If we substitute the functional derivative expression for the correlation function, Eq. (28), in this equation, we obtain

$$\langle T_\tau \hat{j}_x^p(\tau_1) \hat{j}_x^p(\tau_2) \rangle = \sum_{\mathbf{r}_1 \mathbf{r}_2 \delta_1 \delta_2 \sigma_1 \sigma_2} \delta_{x1}\delta_{x2} \, t_{\delta1} t_{\delta2} \frac{\delta G_{\sigma_2}(2',2)}{\delta \phi_{\sigma_1}(1,1')}, \quad (64)$$

where have used the notation $1 = (\mathbf{r}_1,\tau_1)$ and $1' = (\mathbf{r}_1 - \delta_1,\tau_1)$. Note that the first term on the right-hand side of Eq. (28) does not contribute to the sum since $\langle j_x^p \rangle = 0$. Now, summing over spin indices and using spin rotational invariance, we obtain

$$\langle T_\tau \hat{j}_x^p(\tau_1) \hat{j}_x^p(\tau_2) \rangle = - \sum_{\mathbf{r}_1 \mathbf{r}_2 \delta_1 \delta_2} \delta_{x1}\delta_{x2} \, t_{\delta1} t_{\delta2} \, \chi_+(2',2; 1,1'), \quad (65)$$

where we have used the definition Eq. (40) for the generalized susceptibility χ_+.

The most general way of thinking about the last result is that it comes from a functional derivative of the current with respect to an applied vector potential representing the electric field. The remaining of the derivation, that we give in the rest of this subsection, is based on the idea that we should evaluate this functional derivative in a systematic way to obtain a conserving approximation, as shown by Baym[59]. We will keep working with the source field ϕ_σ but it is useful to remember that within simple prefactors, it is equivalent to working with the vector potential as the source field.

The susceptibility χ_+ is defined in terms of a functional derivative in Eq. (40). That functional derivative leads to a Bethe-Salpeter like equation (36) that contains two different types of terms

$$
\chi_+(1,2|3,4) = -2G(1,3)G(4,2)
$$
$$
-2G(1,\bar{1})\left(\frac{\delta\Sigma_\sigma(\bar{1},\bar{2})}{\delta\phi_\sigma(3,4)} + \frac{\delta\Sigma_\sigma(\bar{1},\bar{2})}{\delta\phi_{-\sigma}(3,4)}\right)G(\bar{2},2).
$$
$$(66)$$

The product GG comes from the explicit dependence of G^{-1} on the source field while the last one comes from the implicit dependence of the self-energy on that source field. The product GG is what leads to the "bubble" in standard conductivity calculations. The other term is the vertex correction.

Up to now, everything is exact in the present subsection. To work within the TPSC method, it suffices to use everywhere the results obtained at the second level of approximation, namely $G_\sigma^{(2)}$ and $\Sigma_\sigma^{(2)}$, since at the first level of approximation the conductivity is infinite. Our explicit formula for $\Sigma_\sigma^{(2)}$, Eq. (26), is a functional of $G_\sigma^{(1)}$. We can thus write

$$
\frac{\delta\Sigma_\sigma^{(2)}(\bar{1},\bar{2})}{\delta\phi_{\sigma'}(3,4)} = \frac{\delta\Sigma_\sigma^{(2)}(\bar{1},\bar{2})}{\delta G_{\bar{\sigma}}^{(1)}(\bar{3},\bar{4})}\frac{\delta G_{\bar{\sigma}}^{(1)}(\bar{3},\bar{4})}{\delta\phi_{\sigma'}(3,4)}.
$$
$$(67)$$

Expanding the sum over spin, using the chain rule, spin-rotation invariance and the definition of χ_+, Eq. (40), we obtain

$$
\frac{\delta\Sigma_\sigma^{(2)}(\bar{1},\bar{2})}{\delta\phi_\sigma(3,4)} + \frac{\delta\Sigma_\sigma^{(2)}(\bar{1},\bar{2})}{\delta\phi_{-\sigma}(3,4)} = -\frac{1}{2}\left(\frac{\delta\Sigma_\sigma^{(2)}(\bar{1},\bar{2})}{\delta G_\sigma^{(1)}(\bar{3},\bar{4})} + \frac{\delta\Sigma_\sigma^{(2)}(\bar{1},\bar{2})}{\delta G_{-\sigma}^{(1)}(\bar{3},\bar{4})}\right)
$$
$$
\times \chi_+^{(1)}(\bar{3},\bar{4}|3,4) \qquad (68)
$$

where $\chi_+^{(1)}$ is computed with $G_\sigma^{(1)}$. Substituting in the exact expression for χ_+, Eq. (66), we find

$$
\chi_+^{(2)}(1,2|3,4) = -2G^{(2)}(1,3)G^{(2)}(4,2) + G^{(2)}(1,\bar{1})G^{(2)}(\bar{2},2)
$$
$$
\times\left(\frac{\delta\Sigma_\sigma^{(2)}(\bar{1},\bar{2})}{\delta G_\sigma^{(1)}(\bar{3},\bar{4})} + \frac{\delta\Sigma_\sigma^{(2)}(\bar{1},\bar{2})}{\delta G_{-\sigma}^{(1)}(\bar{3},\bar{4})}\right)\chi_+^{(1)}(\bar{3},\bar{4}|3,4).
$$
$$(69)$$

If $\Sigma_\sigma^{(2)}$ had been a functional of $G^{(2)}$ we would have had an infinite series to sum. Instead, here the series ends as we now show. First note that, from Eq. (41) and approximation (52) for the charge vertex,

$$
\chi_+^{(1)}(\bar{3},\bar{4}|3,4) = -2G^{(1)}(\bar{3},3)G^{(1)}(4,\bar{4})
$$
$$
+ G^{(1)}(\bar{3},\bar{5})G^{(1)}(\bar{6},\bar{4})\Gamma_{ch}^{(1)}(\bar{5},\bar{6},\bar{7},\bar{8})\chi_+^{(1)}(\bar{7},\bar{8}|3,4)
$$
$$
= -2G^{(1)}(\bar{3},3)G^{(1)}(4,\bar{4})
$$
$$
+ U_{ch}G^{(1)}(\bar{3},\bar{5})G^{(1)}(\bar{5},\bar{4})\chi_+^{(1)}(\bar{5},\bar{5}^+|3,4). \quad (70)
$$

From this expression, only the first term has to be included in our calculation because the second term will not contribute to the $\mathbf{q} = 0$ current-current correlation function. This is because $\Gamma_{ch}^{(1)}$ is local in space and local vertex corrections do not contribute to the uniform conductivity. To see why, one can represent the correlation function, Eq. (65), as a series of diagrams with current vertices at their ends and vertex functions inserted between them. Whenever a vertex function in a diagram does not depend on $\mathbf{q}$, a bubble is closed with the local vertex on one end and the current vertex on the other. Since a current vertex is an odd function in space and the product of the Green's function is even because the bubble does not carry any momentum, the integral vanishes.

Inserting the first term of $\chi_+^{(1)}$, Eq. (70), into $\chi_+^{(2)}$, Eq. (69), we obtain

$$
\chi_+^{(2)}(1,2|3,4) = -2G^{(2)}(1,3)G^{(2)}(4,2) - 2G^{(2)}(1,\bar{1})G^{(2)}(\bar{2},2)
$$
$$
\times\left(\frac{\delta\Sigma_\sigma^{(2)}(\bar{1},\bar{2})}{\delta G_\sigma^{(1)}(\bar{3},\bar{4})} + \frac{\delta\Sigma_\sigma^{(2)}(\bar{1},\bar{2})}{\delta G_{-\sigma}^{(1)}(\bar{3},\bar{4})}\right)
$$
$$
\times G^{(1)}(\bar{3},3)G^{(1)}(4,\bar{4}). \qquad (71)
$$

The last step is in principle straightforward, but very tedious. We must obtain an expression for the functional derivatives in parenthesis in this expression. The self-energy, Eq. (26), in real space is

$$
\Sigma_\sigma^{(2)}(1,2) = UG_{-\sigma}^{(1)}(1,1^+)\delta(1-2)
$$
$$
+ \frac{U}{8}[3U_{sp}\chi_{sp}(2,1) + U_{ch}\chi_{ch}(2,1)]G_\sigma^{(1)}(1,2),
$$
$$(72)$$

so that

$$
\frac{\delta\Sigma_\sigma^{(2)}(1,2)}{\delta G_{\sigma'}^{(1)}(3,4)} = U\delta(1-2)\delta(1-3)\delta(1^+-4)\delta_{-\sigma,\sigma'}
$$
$$
+ \frac{U}{8}\left[3U_{sp}\chi_{sp}(2,1) + U_{ch}\chi_{ch}(2,1)\right]
$$
$$
\times \delta(1-3)\delta(2-4)\delta_{\sigma\sigma'} + \frac{U}{8}G_\sigma^{(1)}(1,2)
$$
$$
\times \left[3U_{sp}\frac{\delta\chi_{sp}(2,1)}{\delta G_{\sigma'}^{(1)}(3,4)} + U_{ch}\frac{\delta\chi_{ch}(2,1)}{\delta G_{\sigma'}^{(1)}(3,4)}\right].
$$
$$(73)$$

In this expression, the terms involving the functional derivatives of Γ_{sp} and Γ_{ch} have been omitted because they do not contribute to the conductivity. Fundamentally, what is needed is $\frac{\delta\Gamma_{sp/ch}}{\delta A_x}$, where A_x is the vector potential. Since Γ_{sp} and Γ_{ch} are local, this is the correlation function of a local operator that is thus even under parity, and the current operator, that is odd. The $\mathbf{q} = 0$ component of this correlation function that enters the current-current correlation function, Eq. (62), therefore vanishes.

Now, we need an explicit expression for $\delta\chi_{ch/sp}(2,1)/\delta G_{\sigma'}^{(1)}(3,4)$ to know the vertex correction, Eq. (73), completely. Let us start with χ_{ch}. One can obtain an expression for this function by taking $2 = 1^+$ and $3 = 4^+$ in the expressions for $\chi_{+/-}$, Eq. (41). But this expression has been simplified using spin-rotational invariance. If we separate the spin contributions, we have

$$\chi_{ch}(2,1) = -G_\sigma(2,1^+)G_\sigma(1,2^+) - G_{-\sigma}(2,1^+)G_{-\sigma}(1,2^+) + \frac{1}{2}U_{ch}G_\sigma(2,\bar{2}^+)G_\sigma(\bar{2},2^+)\chi_{ch}(\bar{2},1)$$
$$+ \frac{1}{2}U_{ch}G_{-\sigma}(2,\bar{2}^+)G_{-\sigma}(\bar{2},2^+)\chi_{ch}(\bar{2},1), \tag{74}$$

so that

$$\frac{\delta\chi_{ch}(2,1)}{\delta G_{\sigma'}(3,4)} = -\delta(2-3)\delta(1^+-4)G_{\sigma'}(1,2^+) - G_{\sigma'}(2,1^+)\delta(1-3)\delta(2^+-4)$$

$$+ \frac{1}{2}U_{ch}\delta(2-3)G_{\sigma'}(4,2)\chi_{ch}(4,1) + \frac{1}{2}U_{ch}\delta(2-4)G_{\sigma'}(2,3)\chi_{ch}(3,1)$$

$$+ \frac{1}{2}U_{ch}G_\sigma(2,\bar{2}^+)G_\sigma(\bar{2},2^+)\frac{\delta\chi_{ch}(\bar{2},1)}{\delta G_{\sigma'}(3,4)} + \frac{1}{2}U_{ch}G_{-\sigma}(2,\bar{2}^+)G_{-\sigma}(\bar{2},2^+)\frac{\delta\chi_{ch}(\bar{2},1)}{\delta G_{\sigma'}(3,4)}, \tag{75}$$

where, again, the functional derivatives of U_{ch} have been omitted, for the same reason as in Eq. (73). Using again spin-rotational invariance, this gives

$$\frac{\delta\chi_{ch}(2,1)}{\delta G_{\sigma'}(3,4)} = -\delta(2-3)\delta(1^+-4)G(1,2^+) - G(2,1^+)\delta(1-3)\delta(2^+-4)$$

$$+ \frac{1}{2}U_{ch}\delta(2-3)G(4,2)\chi_{ch}(4,1) + \frac{1}{2}U_{ch}\delta(2-4)G(2,3)\chi_{ch}(3,1) + U_{ch}G(2,\bar{2}^+)G(\bar{2},2^+)\frac{\delta\chi_{ch}(\bar{2},1)}{\delta G_{\sigma'}(3,4)}. \tag{76}$$

By Fourier transforming this equation with respect to 2, we obtain an algebraic equation that is trivial to solve. Fourier transforming back the result, we obtain

$$\frac{\delta\chi_{ch}(2,1)}{\delta G_{\sigma'}(3,4)} = \frac{1}{1+\frac{U_{ch}}{2}\chi_0}(2,3)\,G(4,3)\left[-\delta(1-4)+\frac{1}{2}U_{ch}\,\chi_{ch}(4,1)\right]$$

$$+ \frac{1}{1+\frac{U_{ch}}{2}\chi_0}(2,4)\,G(4,3)\left[-\delta(1-3)+\frac{1}{2}U_{ch}\,\chi_{ch}(3,1)\right], \tag{77}$$

where

$$\frac{1}{1+\frac{U_{ch}}{2}\chi_0}(1,2) = \frac{T}{N}\sum_q e^{iq\cdot(1-2)}\frac{1}{1+\frac{U_{ch}}{2}\chi_0(q)}. \tag{78}$$

The expression for $\delta\chi_{sp}(2,1)/\delta G_{\sigma'}(3,4)$ is obtained by simply replacing U_{ch} by $-U_{sp}$ and χ_{ch} by χ_{sp} in the right-hand side of expression (77):

$$\frac{\delta\chi_{sp}(2,1)}{\delta G_{\sigma'}(3,4)} = \frac{1}{1-\frac{U_{sp}}{2}\chi_0}(2,3)\,G(4,3)\left[-\delta(1-4)-\frac{1}{2}U_{sp}\,\chi_{sp}(4,1)\right]$$

$$+ \frac{1}{1-\frac{U_{sp}}{2}\chi_0}(2,4)\,G(4,3)\left[-\delta(1-3)-\frac{1}{2}U_{sp}\,\chi_{sp}(3,1)\right]. \tag{79}$$

Substituting Eqs. (77) and (79) in our expression for the vertex, Eq. (73), we obtain

$$\frac{\delta\Sigma_\sigma^{(2)}(1,2)}{\delta G_{\sigma'}^{(1)}(3,4)} = U\delta(1-2)\delta(1-3)\delta(1^+-4)\delta_{-\sigma,\sigma'} + \frac{U}{8}\left[3U_{sp}\chi_{sp}(2,1)+U_{ch}\chi_{ch}(2,1)\right]\delta(1-3)\delta(2-4)\delta_{\sigma\sigma'} - \frac{U}{8}G^{(1)}(1,2)$$

$$\times G^{(1)}(4,3)\left[3U_{sp}\left(\frac{1}{1-\frac{U_{sp}}{2}\chi_0}(2,3)\left[\delta(1-4)+\frac{1}{2}U_{sp}\,\chi_{sp}(4,1)\right]+\frac{1}{1-\frac{U_{sp}}{2}\chi_0}(2,4)\left[\delta(1-3)+\frac{1}{2}U_{sp}\,\chi_{sp}(3,1)\right]\right)\right.$$

$$\left. + U_{ch}\left(\frac{1}{1+\frac{U_{ch}}{2}\chi_0}(2,3)\left[\delta(1-4)-\frac{1}{2}U_{ch}\,\chi_{ch}(4,1)\right]+\frac{1}{1+\frac{U_{ch}}{2}\chi_0}(2,4)\left[\delta(1-3)-\frac{1}{2}U_{ch}\,\chi_{ch}(3,1)\right]\right)\right], \tag{80}$$

and therefore,

$$\frac{\delta\Sigma_\sigma^{(2)}(\bar{1},\bar{2})}{\delta G_\sigma^{(1)}(\bar{3},\bar{4})} + \frac{\delta\Sigma_\sigma^{(2)}(\bar{1},\bar{2})}{\delta G_{-\sigma}^{(1)}(\bar{3},\bar{4})} = U\delta(\bar{1}-\bar{2})\delta(\bar{1}-\bar{3})\delta(\bar{1}^+-\bar{4}) + \frac{U}{8}[3U_{sp}\chi_{sp}(\bar{2},\bar{1})+U_{ch}\chi_{ch}(\bar{2},\bar{1})]\delta(\bar{1}-\bar{3})\delta(\bar{2}-\bar{4})$$

$$- \frac{U}{4}G^{(1)}(\bar{1},\bar{2})G^{(1)}(\bar{4},\bar{3})\left[3U_{sp}\left(\frac{1}{1-\frac{U_{sp}}{2}\chi_0}(\bar{2},\bar{3})\left[\delta(\bar{1}-\bar{4})+\frac{1}{2}U_{sp}\,\chi_{sp}(\bar{4},\bar{1})\right]+\frac{1}{1-\frac{U_{sp}}{2}\chi_0}(\bar{2},\bar{4})\right.\right.$$

$$\times\left[\delta(\bar{1}-\bar{3})+\frac{1}{2}U_{sp}\,\chi_{sp}(\bar{3},\bar{1})\right]\right) + U_{ch}\left(\frac{1}{1+\frac{U_{ch}}{2}\chi_0}(\bar{2},\bar{3})\left[\delta(\bar{1}-\bar{4})-\frac{1}{2}U_{ch}\,\chi_{ch}(\bar{4},\bar{1})\right]\right.$$

$$\left.\left.+\frac{1}{1+\frac{U_{ch}}{2}\chi_0}(\bar{2},\bar{4})\left[\delta(\bar{1}-\bar{3})-\frac{1}{2}U_{ch}\,\chi_{ch}(\bar{3},\bar{1})\right]\right)\right]. \tag{81}$$

We now have everything to write an explicit form for the susceptibility $\chi_+^{(2)}$ in Eq. (71):

$$
\begin{aligned}
\chi_+^{(2)}(1,2|3,4) = &-2G^{(2)}(1,3)G^{(2)}(4,2) - 2UG^{(2)}(1,\bar{1})G^{(2)}(\bar{1},2)G^{(1)}(\bar{1},3)G^{(1)}(4,\bar{1}^+) \\
&- \frac{U}{4}G^{(2)}(1,\bar{1})G^{(2)}(\bar{2},2)[3U_{sp}\chi_{sp}(\bar{2},\bar{1}) + U_{ch}\chi_{ch}(\bar{2},\bar{1})]G^{(1)}(\bar{1},3)G^{(1)}(4,\bar{2}) \\
&- \frac{U}{2}G^{(2)}(1,\bar{1})G^{(2)}(\bar{2},2)G^{(1)}(\bar{1},\bar{2})G^{(1)}(\bar{4},\bar{3})G^{(1)}(\bar{3},3)G^{(1)}(4,\bar{4}) \\
&\times \left[3U_{sp}\left(\frac{1}{1-\frac{U_{sp}}{2}\chi_0}(\bar{2},\bar{3})\left[-\delta(\bar{1}-\bar{4}) - \frac{1}{2}U_{sp}\,\chi_{sp}(\bar{4},\bar{1})\right] + \frac{1}{1-\frac{U_{sp}}{2}\chi_0}(\bar{2},\bar{4})\left[-\delta(\bar{1}-\bar{3}) - \frac{1}{2}U_{sp}\,\chi_{sp}(\bar{3},\bar{1})\right]\right) \right. \\
&\left. + U_{ch}\left(\frac{1}{1+\frac{U_{ch}}{2}\chi_0}(\bar{2},\bar{3})\left[-\delta(\bar{1}-\bar{4}) + \frac{1}{2}U_{ch}\,\chi_{ch}(\bar{4},\bar{1})\right] + \frac{1}{1+\frac{U_{ch}}{2}\chi_0}(\bar{2},\bar{4})\left[-\delta(\bar{1}-\bar{3}) + \frac{1}{2}U_{ch}\,\chi_{ch}(\bar{3},\bar{1})\right]\right)\right].
\end{aligned}
$$

(82)

To evaluate the current-current correlation function entering the conductivity, it is clearly necessary to go to Fourier space. Inserting then this last result into Eq. (65) for the current-current correlation function and using

$$
\delta_x t_\delta = \frac{i}{N}\sum_{\mathbf{k}} e^{i\mathbf{k}\cdot\delta}\frac{\partial \epsilon_{\mathbf{k}}}{\partial k_x},
$$

(83)

$$
1 + \frac{U_{sp}}{2}\,\chi_{sp}(q) = \frac{1}{1 - \frac{U_{sp}}{2}\chi_0(q)}, \qquad 1 - \frac{U_{ch}}{2}\,\chi_{ch}(q) = \frac{1}{1 + \frac{U_{ch}}{2}\chi_0(q)},
$$

(84)

we finally obtain for the Fourier–Matsubara transformed expression at $\mathbf{q} = 0$,

$$
\begin{aligned}
\chi_{j_x j_x}(iq_n) = &\frac{-2T}{N}\sum_k \left(\frac{\partial \epsilon_{\mathbf{k}}}{\partial k_x}(k)\right)^2 G^{(2)}(k)G^{(2)}(k+iq_n) \\
&- \frac{U}{4}\left(\frac{T}{N}\right)^2 \sum_{k_1 k_2} G^{(2)}(k_1)G^{(2)}(k_1+iq_n)G^{(1)}(k_2)G^{(1)}(k_2+iq_n)\frac{\partial \epsilon_{\mathbf{k}}}{\partial k_x}(k_1)\frac{\partial \epsilon_{\mathbf{k}}}{\partial k_x}(k_2)[3U_{sp}\chi_{sp}(k_2-k_1)+U_{ch}\chi_{ch}(k_2-k_1)] \\
&+ \frac{U}{2}\left(\frac{T}{N}\right)^3 \sum_{k_1,k_2,q_1} \frac{\partial \epsilon_{\mathbf{k}}}{\partial k_x}(k_1)\frac{\partial \epsilon_{\mathbf{k}}}{\partial k_x}(k_2)G^{(2)}(k_1)G^{(2)}(k_1+iq_n)G^{(1)}(k_2)G^{(1)}(k_2+iq_n)[G^{(1)}(k_2+q_1+iq_n)+G^{(1)}(k_2-q_1)] \\
&\times G^{(1)}(k_1+q_1+iq_n)\left(3U_{sp}\frac{1}{1-\frac{U_{sp}}{2}\chi_0(q_1)}\frac{1}{1-\frac{U_{sp}}{2}\chi_0(q_1+iq_n)} + U_{ch}\frac{1}{1+\frac{U_{ch}}{2}\chi_0(q_1)}\frac{1}{1+\frac{U_{ch}}{2}\chi_0(q_1+iq_n)}\right).
\end{aligned}
$$

(85)

In this expression, we use the compact notation $k + iq_n = (\mathbf{k}, ik_m + iq_n)$. Note that the second term on the right-hand side of Eq. (82) does not contribute to $\chi_{j_x j_x}$ because it has a local vertex.

Equation (85) is our final result for the current-current correlation function in Matsubara space, including both bubble and vertex corrections. It is useful for the intuition and to verify the Fourier transforms to represent it schematically, as we have done in Fig. 1. We stress that this representation is not the result of a perturbative calculation. It exists merely because we are working with Green's functions and response functions. This representation helps us note that an analogy can be made between the different contributions to $\chi_{j_x j_x}$ and the diagrams considered in the theory of paraconductivity.[68] In the latter theory, we consider the effect of the superconducting fluctuations on the conductivity of the normal state, while in our case, the bosons exchanged are spin and charge fluctuations. The diagram with a single boson propagator on the first line of Fig. 1 is the analog of the MT contribution,[69–72] while the diagrams on the second and third lines are analogs

of the AL contributions.[73] However, it is important to note that, because our approach is not perturbative, some electron propagators are at the second level of approximation and some are at the first level, and the boson propagators are the susceptibilities computed with the renormalized spin and charge irreducible vertices.

In the system considered in this paper, the relevant collectives modes are magnetic fluctuations with a wave vector close to $\mathbf{Q} = (\pi,\pi)$. First, when those fluctuations become strong, they scatter quasiparticles, which has a dramatic effect on the single-particle spectrum and therefore the conductivity obtained from the bubble alone. But the magnetic fluctuations also lead to important vertex corrections because they correlate the regions of the Fermi surface that are connected by wave vectors close to $\mathbf{Q}$. For the MT diagram in Fig. 1, in the DC limit, the exchange of such a fluctuation between the particle and the hole created by the field causes the pair to be scattered from a region of the Fermi surface where it carries a positive current along the direction of the field to a region where it carries a negative current. This correlation between currents
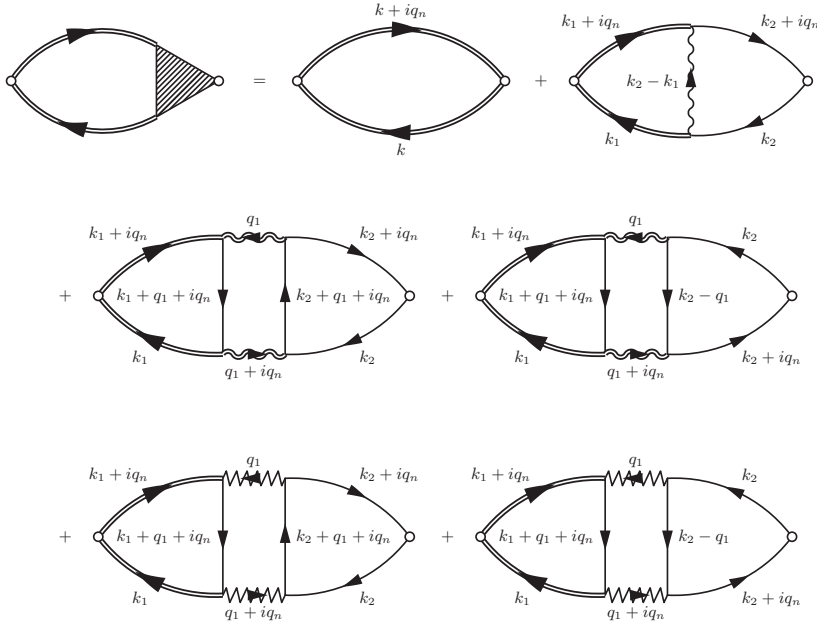
FIG. 1. Schematic representation of the various terms in the current-current correlation function, Eq. (85). Simple fermion lines represent the Green's function $G^{(1)}$ (in practice it has the same form as the bare Green's function), double fermion lines are dressed Green's function $G^{(2)}$, the simple wiggly line in the last diagram on the first line is the function $[3U_{sp}\chi_{sp} + U_{ch}\chi_{ch}]$, the double wiggly lines in the third and fourth diagrams on the right-hand side are the function $1/(1 - U_{sp}\chi_0/2)$, and the zigzag lines in the last two diagrams are the function $1/(1 + U_{ch}\chi_0/2)$. Those diagrams serve only as a graphical representation of Eq. (85); they are not obtained in a perturbative way.

flowing in opposite directions degrades the DC conductivity. In the case of the AL diagrams in Fig. 1, a particle-hole pair creates another one via two magnetic fluctuations. If they have a large correlation length, this will tend to correlate currents on large distances. However, the particle-hole pair created by the fluctuations can carry a current that is either positive or negative. Keeping in mind that when quasiparticles create or absorb magnetic fluctuations, their velocity along the direction of the field changes sign, one finds that the first diagram in the second line of Fig. 1 correlates currents flowing in the same direction, while the second diagram correlates currents in opposite directions. In addition, the former contribution is large if the single-particle spectral density is large below the Fermi level in regions connected by wave vectors around **Q**, while the latter is large if the spectral density is large above the Fermi level. When both processes are summed up, there will therefore be a net effect on the conductivity only if there is an asymmetry in the relevant parts of the density of states.

E. Calculation algorithms

Let us recall that we have used the shorthand notation $k = (\mathbf{k}, ik_n)$, with $\mathbf{k} = (k_x, k_y)$, in the general expression for the current-current correlation function, Eq. (85). Thus, each sum over a trivector k is over the 2D Brillouin zone and over Matsubara frequencies. The second and third sums are therefore six- and nine-dimensional, respectively. The six-dimensional sum would be extremely long to do in a direct way for relevant system sizes and temperatures. For example, for a finite system of 512×512 sites with about 4000 frequencies, which would allow going down to temperatures of about $T = 0.01t$ (without finite-size effects), it would take of the order of 30 years to compute one frequency iq_n, if 10^9 terms are summed per second. Of course, this is using pure brute force, when all wave vectors and frequencies are summed, which is not necessary in practice. In the case of the nine-dimensional sum, it would take about 40 billion years to compute a single frequency in the same conditions. If one was to keep the direct

summation approach, but optimizing the procedure by using a very efficient adaptive scheme, it would still be extremely hard to do the six-dimensional sum to obtain, for example, 100 frequencies in a reasonnable time, namely, of the order of a few days. In the case of the nine-dimensional sum, it is obviously impossible to do this way.

One thus has to resort to a numerical approach completely different from direct summation to succeed in calculating all the terms of Eq. (85) for a useful number of frequencies iq_n. The main tool that we use to make this calculation possible is the *fast Fourier transform (FFT)*, which changes the scaling of Fourier transforms (FTs) from N^2 to $N \log N$. But other mathematical and numerical tricks are also necessary to make the calculation both fast and precise. Precision is critical here since we have to numerically perform the analytical continuation of the computed Matsubara current-current correlation function and numerical analytical continuation is inherently an ill-conditioned problem. For this analytical continuation procedure that produces the real-frequency optical conductivity from the Matsubara current-current correlation function, a maximum entropy algorithm is also developed to maximize the accuracy of the result. The calculation algorithms for $\chi_{j_x j_x}(iq_n)$ and our analytical continuation algorithm are summarized in the next two subsections and detailed in Appendices C–F.

1. Fast Fourier transforms, cubic splines, and asymptotic expansions

The key property that allows us to compute Eq. (85) is that some of its sums are convolutions. Since the convolution of two functions can be written as the FT of the product of their FTs, we can use FFTs to do those convolutions in a very efficient way. However, FFTs are discrete transforms, while some of the transforms we have to do are continuous ones. In the case of the spatial FTs, we can use a finite system with periodic boundary conditions, so that all the transforms are discrete and FFTs can be used directly. Since we work at finite temperature in

two dimensions, all correlation lengths are finite and we can use a system large enough to reach interesting regimes. The system size we use in this paper is 512×512 and the lowest temperature we reach is $0.008t$, which corresponds to 32 K if $t = 0.35$ eV. At this temperature, the thermal de Broglie wavelength is about 100 in lattice units, so that no finite-size effects are seen unless the magnetic correlation length becomes large.

In the case of imaginary time, if it is discretized, then the FT will be periodic in Matsubara frequencies, which is unphysical. In fact, the lowest frequencies will be acceptable, though not very precise, but the precision will decrease rapidly with increasing frequency, so that the high frequencies will be completely wrong. To overcome this problem, we use a cubic spline to interpolate the function between the discrete imaginary-time points and we do a continuous FT on the spline. This technique has already been used in the context of DMFT calculations.[74] However, to our knowledge, it has not been pointed out that, because the spline is only twice continuously differentiable, after integrating by parts three times the Fourier integral, we are left with an expression containing a discrete Fourier transform (DFT) that can be done with a FFT. Using the more general formula derived in Appendix E, the final formula for the FT of the cubic spline of an imaginary-time function $g(\tau)$ is

$$
\begin{aligned}
g(i\omega_n) &= \int_0^\beta d\tau \, g(\tau) e^{i\omega_n \tau} \approx \sum_{j=1}^N \int_{\tau_{j-1}}^{\tau_j} d\tau \, S_j(\tau) e^{i\omega_n \tau} \\
&= -\frac{g(0) - e^{i\omega_n \beta} g(\beta)}{i\omega_n} + \frac{S_1'(0) - e^{i\omega_n \beta} S_N'(\beta)}{(i\omega_n)^2} \\
&\quad - \frac{S_1''(0) - e^{i\omega_n \beta} S_N''(\beta)}{(i\omega_n)^3} \\
&\quad + \frac{1 - e^{i\omega_n \Delta\tau}}{(i\omega_n)^4} \sum_{j=0}^{N-1} S_{j+1}^{(3)} e^{i\omega_n \tau_j} \,,
\end{aligned}
\tag{86}
$$

where N is the number of intervals in the discretized imaginary time between 0 and β, $\Delta\tau$ is the size of an interval, $S_j(\tau)$ is the cubic polynomial in the jth interval, and $S_j'(\tau)$, $S_j''(\tau)$, and $S_j^{(3)}$ are, respectively, the first, second, and third derivatives of $S_j(\tau)$. If g is a fermionic function, $e^{i\omega_n \beta} = -1$, while $e^{i\omega_n \beta} = 1$ if it is bosonic.

When using formula (86), we work explicitly with the high-frequency expansion up to the $1/(i\omega_n)^3$ term, which can be very useful, as will be explained shortly. Up to which term this expansion will be exact depends on how the spline is defined. As shown in Appendix E, there are two conditions defining the spline that can be chosen depending on the information available. If the derivatives at the boundaries $g'(0)$ and $g'(\beta)$ are known, we can fix $S_1'(0)$ and $S_N'(\beta)$ to those values. That is what we do in our calculations. Otherwise, we have to use exact results for the second and third high-frequency coefficients of g, i.e., the second and third moments of its spectral function. Another important point about Eq. (86) is that the last term containing the DFT contributes to only the low frequencies because of its factor $1/(i\omega_n)^4$; therefore the error at high frequency that comes from the discretization of τ rapidly vanishes.

Given the above considerations, it should now be clear that we can compute convolutions both in wave vector and Matsubara frequency using FFTs. Before the calculation of $\chi_{j_x j_x}$, Eq. (85), this technique is used to compute the Lindhard function, Eq. (22), and then the self-energy, Eq. (26). The computation of those functions with FFTs is relatively straightforward to implement, although some care must be taken in the definition of the splines. Those details are given in Appendices C1 and C2. In the case of Eq. (85), we seek only the $\mathbf{q} = 0$ component of $\chi_{j_x j_x}(\mathbf{q}, iq_n)$ so that, in each term, the last sum over the Brillouin zone to be performed is a simple sum and FFTs are not useful there. Regarding the other sums, it is not obvious which one can be put in the form of a convolution, except for the bubble which has the same form as the Lindhard function. In the case of the second term of Eq. (85), represented by the second diagram (MT) on the right-hand side of Fig. 1, it is possible to put all those sums in the form of convolution and thus to compute all of them with FFTs. This means that all the external frequencies iq_n can be obtained at once when the last FFT is performed. The scaling of this calculation with system size and inverse temperature is thus the same as for the bubble. That is not the case however of the last term of Eq. (85), represented by the last four (AL) diagrams in Fig. 1. For this term, each frequency has to be calculated separately, and it is the calculation time of only one frequency that has the same scaling as the bubble. Calculating this term for 100 values of iq_n therefore takes hundreds of times the calculation time of all frequencies of the bubble. The calculation of the bubble is nevertheless very quick, of the order of a few minutes at most for our 512×512 system at low temperatures.

Note, however, that quite a large amount of analytical work is needed to put the last two terms of Eq. (85) in a form suitable for computation with FFTs. This work involves some transformations, and a certain number of sums over Matsubara frequencies must be performed exactly. The details of those transformations and analytical calculations are given in Appendix C3.

Still, it is impossible to calculate the third term of Eq. (85) for thousands of frequencies, namely the number of frequencies below the cutoff used in the calculation. Therefore, to reduce the number of frequencies to be calculated, we have used a nonuniform Matsubara frequency grid in which the frequency spacing increases with frequency magnitude. We give the definition of this grid in Appendix D. We have verified that the function $\chi_{j_x j_x}(iq_n)$ evaluated on this grid has enough information for the analytically continued conductivity $\mathrm{Re}\,\sigma(\omega)$ to be converged.

Using formula (86) for our functions in Matsubara frequencies has the advantage is that we always have at our disposal their high-frequency expansion. Thus if we want the inverse FT (from Matsubara frequencies to imaginary time) of a more complex function, for example the product of two functions of the form of Eq. (86), we can always use the asymptotic form to perform the sum over Matsubara frequencies up to infinity using contour integrals in the complex plane and the residue theorem. In a lot of cases, this is necessary since the sum does not converge otherwise. As will be explained in the next subsection, precision is important in our calculations since we

have to extract Re $\sigma(\omega)$ from the Matsubara function $\chi_{j_x j_x}(iq_n)$ and analytical continuation is a very ill-conditioned problem.

Finally, as one will notice from Appendix C3, the calculation of Eq. (85), especially the second and third terms, contains many steps. The debugging part of the work is therefore considerable. To make sure formula (85) is implemented correctly, we have compared its brute force implementation, term by term, with its fast one given in Appendix C3. Here, brute force means that it is coded exactly as written in Eq. (85), with one exception that will be explained shortly. Therefore, we compare the results of two calculations that are completely different numerically, but mathematically equivalent. Of course, those verifications can be done for only very small systems at very high temperatures, since otherwise the brute force calculation is impossible to do in a reasonable time. But even then, the third term of Eq. (85) takes too much time to compute with brute force. In that case, the procedure is to first verify that the sum over k_2 for some random values of q_n and q_1 gives the same result with the two implementations and then to replace this sum in the brute force version by its fast implementation. After that step we compare this modified brute force implementation with the fast implementation of the whole third term.

2. Analytical continuation

Expression (85) gives the current-current correlation function in Matsubara frequencies while we need it in real frequencies to compute the conductivity from Eq. (18) or Eq. (19). Thus we need a reliable analytical continuation method. To do so, we use a maximum entropy approach. This kind of analytical continuation procedure is often used to extract real-frequency results from imaginary-time QMC data using some information known *a priori* such as sum rules and a default model which contains some known properties of the expected function.[75] This information is included in the algorithm in the form of constraints or in the entropy definition. This kind of approach is well suited for QMC calculations since the results are usually in discretized imaginary time and the amount of noise can be important, so that any additional information is welcome. In our case, the original data are in Matsubara frequencies and the noise level is much lower since it comes only from finite precision rounding errors accumulating throughout the calculation. However, our calculation of $\chi_{j_x j_x}$ contains many steps so that the final result may have an amount of noise such that Padé approximants will not work. Those approximants are very sensitive to noise[76] and their reliability is not very good except at very low temperatures. In any case, we have noticed that they give unstable results as a function of temperature for our data while our maximum entropy procedure is in general stable.

We give here the main features of our approach. The details are given in Appendix F. As usual we minimize the function $\chi^2 - \alpha S$, where S is the entropy, α is a weighting parameter for S, and χ^2 is the quadratic error between $\chi_{j_x j_x}(iq_n)$ and the quantity $\bar{\chi}_{jj}(iq_n)$ computed from the spectral representation of $\chi_{j_x j_x}(iq_n)$ with a trial-real frequency conductivity Re $\sigma(\omega)$. First, an accurate numerical integration scheme has to be chosen to compute $\bar{\chi}_{jj}(iq_n)$ from Re $\sigma(\omega)$ known on a fixed discrete grid in real frequency ω. We use a cubic spline to

approximate Re $\sigma(\omega)$. Since we work in Matsubara frequencies instead of imaginary time, the spectral form is simple and can be integrated analytically if Re $\sigma(\omega)$ is approximated by a piecewise cubic polynomial function. Also, because we want to integrate Re $\sigma(\omega)$ in the interval $[0,\infty[$, we integrate the low-frequency part with respect to ω and the high-frequency part with respect to $1/\omega$. To do so, we use a spline cubic in ω for low frequencies and cubic in $1/\omega$ for high frequencies. As for the choice of grid, we take it to be uniform in ω for the low-frequency part and uniform in $1/\omega$ for high frequencies. This choice of grid ensures that the matrix for the spline linear system is well conditioned and keeps the number of values Re $\sigma(\omega_j)$ reasonable, so that the minimization procedure is not too heavy. The integration using the spline turns out to be very accurate compared with a simple piecewise linear approximation. In our tests with a well-defined analytical form for Re $\sigma(\omega)$ for which $\chi_{j_x j_x}(iq_n)$ could be computed very accurately with an adaptive integration routine, the relative precision was typically five orders of magnitude smaller with the spline than the piecewise linear approximation. The reason we have to use a very accurate integration method is that the relative difference between $\bar{\chi}_{jj}(iq_n)$ and $\chi_{j_x j_x}(iq_n)$ has to be very small, typically $< 10^{-5}$ in our calculation, for Re $\sigma(\omega)$ to be converged in the optimization procedure. The precision of the numerical integral for a given Re $\sigma(\omega)$ clearly has to be smaller than this required relative error on $\bar{\chi}_{jj}(iq_n)$ for the result to be reliable.

The fact that the spline is integrated analytically has the great advantage that low temperatures are not more difficult to handle, while it is the case with standard numerical integration because the integrand becomes sharper as temperature decreases. Note that all those precision issues are important if one is interested in quantitative results. For instance, we want to obtain the resistivity as a function of temperature, but since the results at different temperatures are numerically completely independent, the quantitative aspect becomes crucial. If one is interested only in the shape of Re $\sigma(\omega)$ at a given temperature, simpler and cruder approximations can be sufficient.

III. NUMERICAL RESULTS

Before we show the results of this paper, let us recall some important former results of the TPSC approach. First, the theory respects the Mermin–Wagner theorem, so that no phase transition occur at finite temperatures. However, with proper values of U and hopping parameters, antiferromagnetic correlations are present up to very high temperatures around half-filling. For example, with $U = 6t$ and nearest-neighbor hopping only, for dopings smaller than $p_c = 0.205$ a crossover to a renormalized classical regime appears. This regime appears when $k_B T \gg \hbar \omega_{sp}$, where ω_{sp} is the characteristic frequency of the antiferromagnetic fluctuations, i.e., the frequency at which the imaginary part of the spin correlation function $\chi''_{sp}(\omega)$ is maximum. In this regime, the antiferromagnetic correlation length has the form $\xi_{sp} \propto \exp(C/T)$, where C has a very weak temperature dependence. Therefore, at a certain temperature T^*, ξ_{sp} becomes larger than the single-particle thermal de Broglie wavelength $\xi_{th} = \hbar v_F/(\pi k_B T)$. When this happens, the parts of the Fermi surface that are connected by the antiferromagnetic wave vector, called the

hot spots, are strongly scattered by the magnetic fluctuations and eventually destroyed, producing a gap in those regions of the Brillouin zone.[37,62] However, before the correlation length becomes infinite, which is the case only at $T = 0$ in two dimensions, there is still spectral weight at the Fermi level and thus no real gap exits, but what is observed instead is a pseudogap, namely, a depression of the density of states at the Fermi level. Therefore, the crossover temperature to the renormalized classical regime T^* can also be called a pseudogap temperature. When $T = 0$, long-range SDW order exists for $p < p_c$ and thus p_c is a QCP. Depending on band parameters and doping, this SDW state can be commensurate or incommensurate. Usually it is commensurate close to half-filling and a transition to incommensurate appears at a certain doping.[77]

Benchmarks of TPSC results were made against QMC results for quantities such as the spin and charge structure factors,[36] the quasiparticle renormalization factor and the imaginary time Green's function,[62] the finite frequency spin susceptibility, the double occupancy and the one-particle occupation number,[37] and finally, the one-particle spectral weight.[43] Those benchmarks were made in the weak to intermediate coupling regime for a large range of doping around half-filling and for temperatures where no finite-size effects are seen in the QMC results and, at finite doping, when the sign problem is not too strong. In general, a good quantitative agreement is obtained for all quantities at a coupling $U = 4t$. For some quantities such as the spin structure factor, the agreement is almost perfect above T^* for couplings up to $U = 8t$. Since the TPSC method has some mean-field aspects[78] coming from the ansatz, Eq. (49), it slightly overestimates T^* (see Fig. 7 of Ref. 37), but the qualitative behavior just below T^*, when the spin correlation length grows exponentially, is still very well reproduced. The spectral weight at half-filing in this regime is also very well reproduced by the TPSC method.[43] This is the regime where precursors of the antiferromagnetic bands are formed and a pseudogap appears in the spectral weight.

The results we present in this section are for the one-band Hubbard model with nearest-neighbor hopping only. All numerical examples are for $U = 6t$ and various dopings and temperatures. We begin by showing the accuracy with which the f-sum rule is satisfied. We then give a few typical examples of the frequency-dependent conductivity. The last subsection will focus on the temperature-dependent resistivity for various dopings.

A. f-sum rule

Although our expression for the conductivity, Eq. (85), was obtained from functional derivative methods that lead to results that satisfy conservation laws,[59] usually this method is applied to perturbative one-particle self-consistent schemes. In the TPSC method, all the functional dependence on vector potential is in $G^{(1)}$. One may question whether this preserves conservation laws. The full Ward identity is derived in Appendix B where one also finds comments on why it cannot be used to find the vertex corrections in the limiting case we are interested in. Given the difficulty of computing the current-current correlation function alone for only the wave vector $\mathbf{q} = 0$, it will be clear why the full Ward identity cannot be verified. As a test of particle conservation, we focus
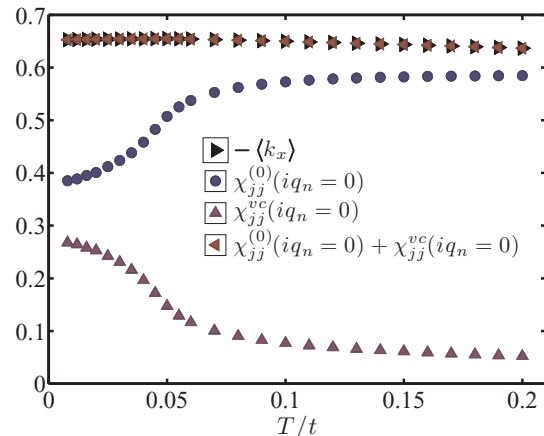

FIG. 2. Contributions to the zero-Matsubara-frequency value of the current-current correlation function compared with the sum-rule value $-\langle k_x \rangle$ for $p = 0.17$.

instead on how accurately the f-sum rule, Eq. (A19) derived in Appendix A,

$$\chi_{j_x j_x}(iq_n = 0) = \frac{1}{N} \sum_{\mathbf{k}\sigma} \frac{\partial^2 \epsilon_{\mathbf{k}}}{\partial k_x^2} \langle n_{\mathbf{k}\sigma} \rangle , \qquad (87)$$

is satisfied numerically. In this equation, the occupation probability $\langle n_{\mathbf{k}\sigma} \rangle$ is computed with $G^{(2)}$, while the left-hand side is the zero-Matsubara-frequency current-current correlation function $\chi_{j_x j_x}$, Eq. (85), obtained with the functional derivative approach that gives us $\partial \Sigma^{(2)} / \partial G^{(1)}$ as an irreducible vertex.

Typically, using $500t$ as the cutoff Matsubara frequency, i.e., about 60 times the bandwidth, the above equation is satisfied to a relative accuracy of 10^{-7}. By increasing the cutoff, the accuracy can be increased at will. We have reached an accuracy of 10^{-10}. The separate contributions of the different terms of expression (85), also represented schematically in Fig. 1, are shown in Fig. 2 as functions of temperature for 17% doping, i.e., on the left-hand side of the QCP. As one would expect, the bubble contribution is dominant at high temperatures, although the first vertex correction is not negligible. At low temperatures, in the renormalized classical regime, the two terms give comparable contributions. The contribution of the third term in Eq. (85), the AL-like diagrams in Fig. 1, vanishes at all temperatures. This is discussed further at the end of Appendix B. As will be seen in the next subsections, despite this vanishing contribution of this term to $\chi_{j_x j_x}(iq_n = 0)$, i.e., to the integral of the real part of the conductivity, this term contributes in a nontrivial way both to the DC and the finite frequency conductivity.

B. Optical conductivity

The optical conductivity and the effect of the vertex corrections are different depending on which side of the QCP the system is and on the temperature. On the left-hand side of the critical point, the conductivity changes qualitatively as the temperature approaches the crossover temperature to the renormalized classical regime T^*. Here T^* is defined as the temperature at which $\xi_{sp} = \xi_{th}$. As shown in Fig. 3(a), at high temperatures it has a Lorentzian-like shape at low frequencies,
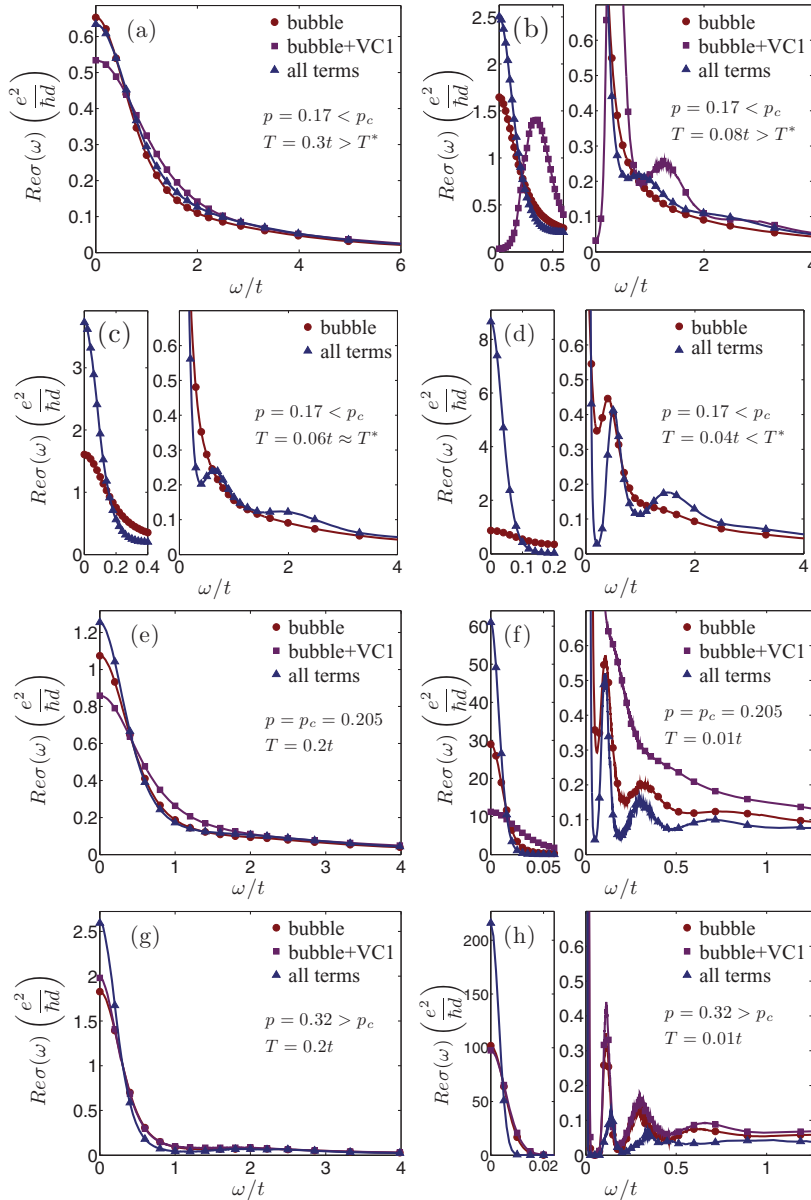
FIG. 3. Optical conductivity with and without vertex corrections at different dopings and temperatures. From (a) to (d) the doping is $p = 0.17 < p_c$ and the temperatures are (a) $T = 0.3t > T^*$, (b) $T = 0.08t > T^*$, (c) $T = 0.06 \approx T^*$, and (d) $T = 0.04t < T^*$. The other dopings are $p = 0.205 = p_c$ at temperatures (e) $T = 0.2t$ and (f) $T = 0.01t$ and $p = 0.32 > p_c$ at (g) $T = 0.2t$ and (h) $T = 0.2t$. All panels on the right-hand side contain a blowup of the low-frequency region of the rightmost plot. The symbols are shown for only a small fraction of the total number of points in the grids.

whether we look at the bubble alone, the bubble with the first vertex correction, or with both vertex corrections. In this region of the phase diagram, the low-frequency conductivity is smaller if the vertex corrections are included. Then, as seen in the left-hand part of Fig. 3(b), as T is lowered toward T^* but still above it, the effect of the first vertex correction is to strongly decrease the low-frequency conductivity, while the second correction does not just compensate for this effect, but makes the total even higher than the bubble alone. At higher frequencies, in the right-hand part of Fig. 3(b), a hump, not present without vertex corrections, appears in the total conductivity. Note that, at this temperature, the spin fluctuation frequency ω_{sp} is about $T/2$. When T is around T^*, in Fig. 3(c), the hump is more pronounced, and finally, when $T < T^*$, in Fig. 3(d), it becomes a very distinct peak. At this temperature, a hump similar to the one seen with vertex corrections at higher temperatures appears in the bubble term alone. At this temperature, $T \approx 600\omega_{sp}$ and $\xi_{sp} = 147 \approx 6\xi_{th}$. If we were to

compare our result with experiments, assuming an energy scale $t = 350$ meV, the hump seen around $0.5t$ would correspond to the feature observed in the mid-infrared frequency range in the optical conductivity of electron-doped cuprates.[79,80] Note that another clear hump appears in the conductivity with vertex corrections in Fig. 3(d). At this doping and temperature, the spin fluctuations are incommensurate; hence their effect on the spectral weight at finite energies can be quite complex. This additional structure in the conductivity may be a consequence of this incommensurability.

At the critical doping, Figs. 3(e) and 3(f), the low-frequency conductivity is lower than the bubble result when only the first vertex correction is taken into account, while it is higher with both corrections. This effect is much more pronounced at low temperatures in Fig. 3(f). New secondary peaks also appear at low temperatures. Those peaks are at frequencies considerably smaller than the peak seen at $p = 0.17$ below T^* and, as will be clear from the DC resistivity results in the next subsection,

there is no pseudogap regime at this doping. Those peaks may nevertheless be caused by correlations that are present far beyond the critical doping, at least at finite temperatures. The effects of those correlations are also clear in the resistivity results in the following subsection.

Finally, at a doping higher than the critical doping, in Figs. 3(g) and 3(h), the conductivity with the first vertex correction can be almost the same as the bubble result at low frequencies both at high and low temperatures, although this correction does not vanish in Matsubara frequency [at $T = 0.01t$, $\chi_{j_x j_x}^{vc1}(0)$ is about 7% of $\chi_{j_x j_x}^{(0)}(0)$ and $\chi_{j_x j_x}^{vc1}(i2\pi T)$ is about 14% of $\chi_{j_x j_x}^{(0)}(i2\pi T)$]. Adding the other correction makes the low-frequency conductivity increase substantially. However, while the finite frequency conductivity stays finite when the doping is closer to p_c or smaller, at low temperatures, in Fig. 3(h), it vanishes completely just after the main low-frequency peak when both vertex corrections are included. This peak is also sharper and higher at high doping (not shown). As will be confirmed in the next subsection, this means that the system becomes closer to a Fermi liquid, although it has not yet reached this regime at this doping. When it does, the DC conductivity will be inversely proportional to T^2 at low-temperatures so that, to conserve the weight which is roughly constant with respect to temperature, i.e. to respect the f-sum rule, the width has to be proportional to T^2. At zero temperature, since there is no impurity scattering in our model, the low-frequency part becomes a delta function. Note that an absoption band remains at finite frequency at the highest doping since there is still an incoherent part in the one particle spectrum. However, one must also note that the highest values of the conductivity in that band are about a thousand times smaller than the DC value and that the total optical weight of this band is about 10 times smaller than the weight of the low-frequency peak.

The frequency region where the effect of vertex corrections is important becomes smaller as the doping increases. For $p = 0.17$, the difference between the different results vanishes around $\omega = 4t$, at the critical point, this happens around $\omega = 2t$, and at $p = 0.32$, around $\omega = 1.5t$.

As the doping increases, the conductivity at low temperatures becomes extremely sharp and it becomes very hard to do the maximum entropy analytical continuation. That is because a very fine grid must be used at low frequency, while one still needs a cutoff larger that the bandwidth. This makes the number of points in the real-frequency grid explode, as well as the time for the optimization process.

C. DC resistivity as a function of temperature and doping close to the quantum critical point

Figure 4 shows five interesting doping regimes for the DC resistivity. The left vertical axis is in units of the Ioffe–Regel maximum metallic resistivity. The right vertical axis translates the result in micro-ohms-centimeters by taking $d = 5$ Å as the interplane lattice constant. For the temperature scale, we use $t = 350$ meV. The resistivity without vertex corrections (bubble) appears as red circles, with the first correction, namely the second term in expression (85) or the MT-like diagram in Fig. 1, in purple squares (bubble + VC1) and the total
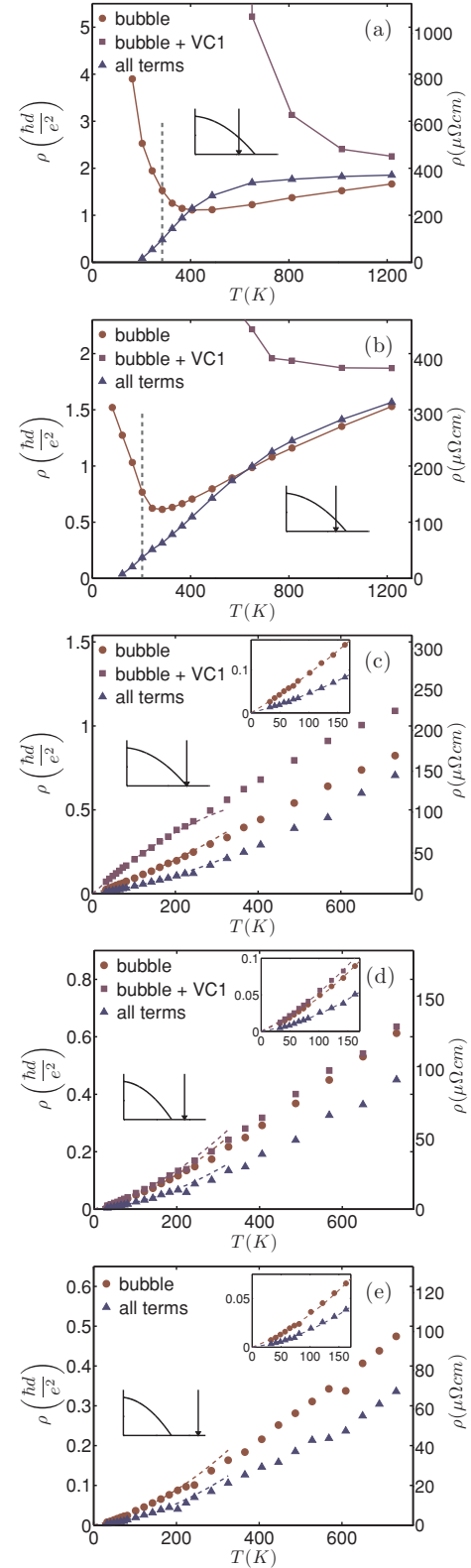

FIG. 4. (Color online) Resistivity as a function of temperature for (a) $p = 0.15$ (b) $p = 0.17$ (c) $p = 0.205$ (critical doping) (d) $p = 0.26$ and (e) $p = 0.32$. The dashed vertical line in (a) and (b) indicates the temperature at which the internal accuracy starts failing as T decreases. Dashed curves in (c), (d), and (e) are the results of fits of the low-T resistivity to the form $AT + BT^2$.

resistivity appears as blue triangles. The insets of the last three figures display the low temperature behavior. The position of each doping is indicated by an arrow for each figure on a schematic "phase diagrams" with the quantum critical point and the crossover line.

At the smallest doping, $p = 0.15$ in Fig. 4(a), one observes at high temperature the expected Ioffe-Regel maximum metallic resistivity saturation. The value is about $2\hbar d/e^2$. The resistivity is higher when vertex corrections are included at high temperature. Without vertex corrections, it increases with decreasing temperature below the crossover temperature to the renormalized classical regime T^*, which is about 400 K ($0.1t$) at this doping. The effect of vertex corrections is dramatic at low temperatures, essentially changing the resistivity from insulating to metallic. An important point is that this effect can be obtained only when both corrections are included. When only the first correction is included, the scattering effect of magnetic correlations is largely overestimated and the resistive behavior thus amplified. At $p = 0.17$, closer to the QCP, Fig. 4(b) exhibits essentially the same behavior except that, given the overall smaller resistivity, the saturation at high temperatures occurs beyond the range displayed. At low temperatures in Figs. 4(a) and 4(b), the resistivity with vertex corrections seems to extrapolate to negative values. However, as indicated by the vertical dashed lines in those figures, this happens in a region where the TPSC result is no longer quantitatively reliable because the internal accuracy check starts to fail when the magnetic correlation length becomes too large compared with the thermal de Broglie wavelength. The results at those temperatures and dopings, namely, deep in the peudogap regime, can thus at most be considered as qualitative tendencies.

At the QCP, $p = 0.205$, one observes in Fig. 4(c) that, without vertex corrections, the resistivity is quite linear at low temperatures, as found previously in spin fluctuation theories.[21,81] When all the corrections are included, the most obvious effect is that the resistivity decreases at all temperatures. The linear behavior remains at low temperatures, but the vertex corrections tend to reduce the linear contribution and a T^2 behavior appears at a lower temperature than that without vertex corrections. Note that, with only the first correction, there is a change in curvature. Also, the resistivity is larger than the bubble result at all temperatures instead of smaller as found when all vertex corrections are included.

As the doping becomes larger than the quantum critical doping, Figs. 4(d) and 4(e) show that a linear T behavior is still present at the lowest temperatures, but gradually disappears as the doping increases and the Fermi-liquid-like T^2 behavior becomes dominant. The resistivity with the first vertex correction only is omitted in Fig. 4(e) because it is almost equal to the bubble result at all temperatures.

The result of fits of the temperature dependence of the resistivity to the functional form $AT + BT^2$ over the range $0.008t < T < 0.05t$ (30K $< T <$ 200K) is illustrated in Figs. 5(a) and 5(b). Those fits were done using two other resistivity curves in addition to those shown in Fig. 4, namely, at $p = 0.22$ and $p = 0.24$. The linear coefficient A decreases as one moves away from the QCP. This decrease is correlated with the superconducting transition temperature, shown in the inset, estimated from TPSC calculations of the $d_{x^2-y^2}$-wave
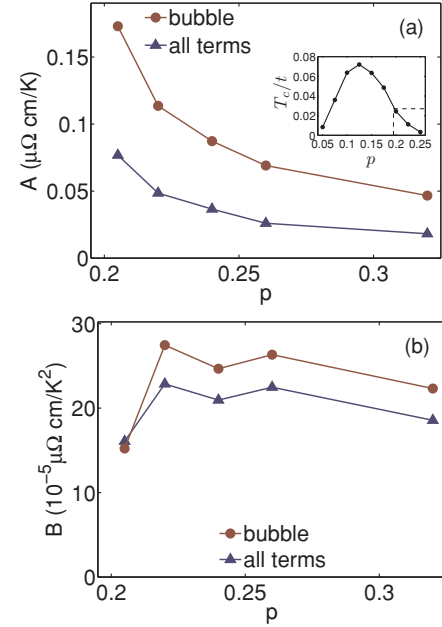

FIG. 5. Coefficients (a) A and (b) B in the fit of the form $AT + BT^2$ to the resistivity, as a function of doping, starting at the QCP. The inset in (a) shows the superconducting transition temperature as a function of doping estimated with the TPSC approach, from Ref. 82. The doping region relevant for our fits is indicated with dashed lines in this inset.

susceptibility.[82] As for the coefficient B, it seems to have a rapid increase as we move away from the QCP and then to remain roughly constant as the doping increases. Note, however, that this coefficient is hard to obtain precisely close to the QCP. For example, if we change the number of points used in the fit, the value of B in this doping region can change by about 20%. This is because, at low temperatures, the region of interest here, the quadratic term has a very small contribution compared with the linear term close to the QCP. Also, there is always some noise in the resistivity, a consequence of the fact that those results are obtained by analytical continuation of Matsubara response functions, a procedure very sensitive to finite precision noise in these response functions. Therefore, the values of B for the two smallest dopings in Fig. 5(b) are rough estimations. However, as the doping increases, the quadratic contribution becomes more important and thus B is more accurate.

IV. DISCUSSION

Starting with the self-energy at the second level of approximation, Eq. (72), the only nonstraightforward part of the derivation is the neglect of the functional derivatives of the irreducibles vertices Γ_{sp} and Γ_{ch} in the derivative of $\Sigma^{(2)}$ with respect to the field or with respect to $G^{(1)}$. However, as was explained in Sec. II D, following Eq. (73), the vanishing of those contributions to the conductivity is exact. Therefore, starting from approximation (26) for the self-energy that contains the local spin and charge irreducible vertices Γ_{sp} and Γ_{ch}, Eqs. (51) and (52), the rest of the calculation is exact.

In fact, purely from our numerical results, with the Green's function at the second level of approximation and the irreducible vertex generated from the corresponding self-energy, we would have strong reasons to suggest that the f-sum rule is satisfied exactly in our approach. At all dopings and temperatures, that sum rule is satisfied with very high accuracy and the precision increases with the cutoff Matsubara frequency. Since the f-sum rule is a consequence of particle conservation (see Appendix A), this means that our approach is consistent with particle number conservation. This result is a consequence of our use of functional derivatives to calculate the Green's function and correlation functions, as in conserving approximations.[59] However, unlike in those approaches, there is no self-consistency at the one-particle level, i.e., our self-energy $\Sigma^{(2)}$ is calculated with $G^{(1)}$ and not $G^{(2)}$. Thus one-particle self-consistency is not necessary to ensure particle conservation.

The saturation of the resistivity to the Ioffe–Regel maximum value at high temperatures is a general constraint, this time based on general physical considerations, that is satisfied by our approach and not by Boltzmann-based approaches. At high doping the Fermi-liquid T^2 resistivity is also recovered, as expected.

From the fact that the first vertex correction, the MT-like diagram in Fig. 1, is sufficient to respect the sum rule, one would be tempted to assume that the other type of vertex corrections will not contribute, as was done in previous calculations.[27] It is clear from our results that this is not the case. In the pseudogap regime, the AL-like contribution has a drastic effect on the DC resistivity, making the system metallic instead of insulating. If only the first correction is included, we would wrongly assume that the system is even more insulating than without any correction. On the right-hand side of the QCP, it is also very important to include both vertex corrections since their total effect is to reduce the resistivity, while it would increase, for a large range of doping, if only the first correction was taken into account. Also, when both corrections are included, the T^2 Fermi-liquid resistivity is recovered at a lower doping. The importance of including both corrections is also very clear in the optical conductivity, especially on the left of the QCP, where the result is qualitatively very different with only the first vertex correction.

One may ask whether it is enough to include only those two vertex corrections. To answer that question we recall that our expression for the current-current response function Eq. (85), is not derived perturbatively, but using functional derivatives. Since the calculation of $\chi_{j_x j_x}$ is exact starting from the TPSC self-energy, Eq. (49), as long as the TPSC calculation is valid, all the terms needed are the ones that we have used. The region of the phase diagram where the TPSC calculation breaks down is deep in the pseudogap regime, when some parts of the Fermi surface are destroyed and, thus, the one-particle spectrum is dramatically different from the noninteracting one. Therefore, in this regime, the TPSC results should be regarded as more qualitative than quantitative.

Since we have not used realistic band parameters, we cannot directly compare our results with any real material. However, some tendencies can help us understand experiments and provide some hints on what would be interesting to investigate using more realistic band structures.

First, there is a pseudogap in the TPSC approach. For electron-doped cuprates, it was shown that the pseudogap has properties predicted by this approach, namely it appears when the antiferromagnetic correlation length becomes larger than the single-particle de Broglie wavelength or the mean free path.[55] The hump around $\omega = 0.5t$, seen in Figs. 3(b), 3(c), and 3(d), thus corresponds to the analogous feature seen, for example, in $Nd_{2-x}Ce_xCuO_4$ in the mid-infrared energy range.[79,80] If we use $t = 0.35$ eV, the location in energy of this structure is also in the correct energy range. Those optical conductivity results and previous comparison of TPSC spectral weights with photoemission experiments on electron-doped cuprates add to the evidence that those materials are well described by the accurate solutions of the Hubbard model provided by the TPSC approach at intermediate coupling.[44,83]

An interesting aspect of our results is the linear low-temperature resistivity observed at the quantum critical doping. As mentioned in Sec. III C, linear T resistivity has already been obtained in spin fluctuation theory within the so-called *self-consistent renormalization* approach.[21,81] This is discussed in the review in Ref. 24. However, this theory is based on the variational approach to the Boltzmann equation. It has been shown with a better variational ansatz that the resistivity should be in T^2.[22] That variational ansatz is better because it takes into account that hot regions on the Fermi surface that are strongly influenced by spin scattering should be short circuited by the cold regions. Indeed, it is the conductivities of the different Fermi surface regions that are integrated and not the resistivities. Thus, like parallel resistors, the total resistivity depends on only the more conductive regions. In our results, vertex corrections tend to make the resistivity more quadratic, but a linear term remains at low temperatures. This result tells us that, at least for the parameters used in this paper, the region of the Fermi surface with the lowest resistivity has linear T resitivity. This is coherent with our observation, from spectral density calculations (not shown), that the whole Fermi surface seems incoherent, or hot, over a range of dopings that extends beyond the QCP at the temperatures considered.[84]

Another important question is whether, in the quantum critical region above the QCP, the whole Fermi surface is always incoherent, as suggested by some experiments.[85,86] This is possible because what characterizes this region is that the magnetic fluctuations are strong, but not yet strong enough to destroy any part of the Fermi surface. In other words, instead of having spin excitations that are well defined, they are broad in energy and wave vector, which means that they affect large parts of the Fermi surface and possibly all of it. To understand the transport, it is important to make the distinction between this regime and the pseudogap regime, where the well-defined hot spots appear. This distinction is not made in Ref. 22. In the present paper, the incoherence of the whole Fermi surface may come, however, from the fact that we have included only nearest-neighbor hoppings and that large parts of the Fermi surface are almost nested. More calculations of the conductivity using second and third nearest-neighbor hoppings will be necessary to verify if this global incoherence of the Fermi surface in the quantum critical region is universal. Note that this is a subtle question that cannot be answered using

approaches with adjustable parameters, like those of Refs. 21 and 22, which can give qualitatively different results depending on how those parameters are chosen.

Another interesting point about the linear term in the resistivity is its correlation with the superconducting transition temperature T_c. This correlation seems to be present in all the unconventional superconductors. It has been observed in the cuprates, the pnictides, and the organics.[87–90] In those materials, it seems that the linear coefficient A disappears exactly at the end of the superconducting dome on the overdoped side, which strongly suggests a common origin for linear resistivity and superconductivity. In the Hubbard model, in the weak to intermediate coupling regime, the TPSC approach finds that superconductivity and linear resistivity also have the same origin, namely the interaction of quasiparticles with antiferromagnetic fluctuations. However, from Fig. 5, it does not seem that A disappears completely with T_c, which vanishes at around $p = 0.25$, as shown in the inset of the figure. Note that there is some uncertainty in the values of A that could come from a small systematic error in the resistivity. This is possible because it is difficult to obtain very precise analytically continued results. Nevertheless, it is clear that the most important drop in A is before T_c vanishes.

One striking result we obtain in the pseudogap regime on the left-hand side of the QCP is the change of the resistivity from an insulating to a metallic behavior when the vertex corrections are taken into account. This is an effect of the AL-like contribution which, as mentioned at the end of Sec. II D, gives a positive contribution to the conductivity when the density of states below the Fermi level is larger than above. In the present case the Fermi level is just above the Van Hove singularity. The density of states is therefore extremely asymmetric at the Fermi level, and that explains why the AL term is so large that it counters both the effect of the one-particle self-energy that makes the bubble result insulating and the effect of the MT-like term that tends to make the system even more insulating. From preliminary results with second and third nearest neighbor hoppings t' and t'', we notice that the second vertex corrections cannot always compensate for the first correction and the resistivity for $p < p_c$ can be higher than the bubble result even with both vertex corrections. This happens when the Fermi level is farther from the Van Hove singularity, so that the density of states is much less asymmetric around $\omega = 0$ and thus the AL term is weaker. Those results tell us that the behavior observed in the pseudogap regime on the left-hand side of the QCP in Figs. 4(a) and 4(b) is not universal. However, on the right-hand side of the QCP, the results should be qualitatively the same since eventually Fermi-liquid physics dominates. That is effectively what we observe so far.

Another interesting question is the effect of disorder on the importance of vertex corrections. In our case, as mentioned in Sec. II D, if the vertices do not depend on the wave vector, i.e., they are isotropic, they have no effect on the conductivity. Adding disorder would probably make the vertices more isotropic, and therefore their effect should be smaller. It would be very interesting to see if, by adding enough disorder, we could reduce the effect of vertex corrections to the point where the resistivity recovers its insulating behavior in the pseudogap

region. This would also provide one possible explanation for the fact that, in less clean cuprates, such as $La_{2-x}Sr_xCu_2O_4$ the resistivity increases below T^*, while it increases in cleaner systems such as $YBa_2Cu_3O_{7-y}$. That contrasting behavior can be seen in Ref. 91 when, for the latter compound, we take the pseudogap line to end at optimal doping. However, from our preliminary results with hoppings t' and t'' relevant for cuprates, we have noticed that, on the hole-doped side, the qualitative behavior with and without vertex corrections can be inverted with respect to the results of Figs. 4(a) and 4(b). That is, the resistivity without vertex corrections decreases below T^*, while it increases with vertex corrections. By changing the band parameters and the doping we can therefore change dramatically the transport properties in the pseudogap regime.

V. CONCLUSION

To satisfy current conservation, conductivity calculations must include vertex corrections that are consistent with the self-energy. A systematic way of achieving this proceeds with functional derivatives with respect to the vector potential. We have shown how this approach can be generalized to the nonperturbative TPSC approach. The various terms of the resulting algebraic expression, Eq. (85), have the physical interpretation illustrated schematically in Fig. 1. One type of vertex correction has the structure of the MT term in fluctuation superconductivity, while the other has the structure of the AL term. These diagrams contain many elements that are not computed perturbatively, as for example the irreducible spin and charge vertices and the vertex corrections. With this approach, the f-sum-rule is satisfied in principle exactly. We verified the agreement to the accuracy of the numerical calculations (a typical relative precision of 10^{-7}).

The numerical evaluation of the conductivity with vertex corrections can be done only if FFTs and other advanced numerical algorithms are employed. Brute force calculations are impossible with any kind of computing resource currently available. Analytical continuation is performed with a specialized maximum entropy technique that we have described in detail in the appendices, along with all other algorithms.

We have shown that our approach allows us to compute the optical conductivity and DC resistivity of the nearest-neighbor 2D one-band Hubbard model in a variety of regimes, without adjustable parameters or phenomenological assumptions. There is no need to assume the existence of quasiparticles, as is the case in Boltzmann equation approaches.

For illustrative purposes, we have presented the results of calculations for $U = 6t$ and nearest-neighbor hoppings only. For the DC resistivity, we find at high temperatures that it saturates at the Ioffe–Regel value, namely when the mean free path is of the order of the interlattice spacing. The existence of this Ioffe–Regel limit is usually assumed on phenomenological grounds. Here we have demonstrated it. That limit may be exceeded in strong coupling,[92,93] but that is beyond the TPSC approach. Vertex corrections have a dramatic influence for dopings smaller than the quantum critical doping. They can

change the temperature dependence of the resistivity from insulating to metallic when the antiferromagnetic correlation length becomes larger than the thermal de Broglie wavelength, namely in the pseudogap regime. At the QCP, the resistivity is linear at low temperatures, although vertex corrections tend to reduce the temperature range of the linearity compared with the calculation with the bubble only. At low temperatures, the linear term persists at dopings larger than the QCP, although we cannot exclude that it disappears at temperatures lower than those accessible to us. The coefficient of this linear term is also correlated with the vanishing of the superconducting T_c obtained with the TPSC method, in qualitative agreement with experimental results on the cuprates, the pnictides, and the organics.[88,89] For dopings equal to or greater than the critical doping, the resistivity with all vertex corrections is always smaller than the simple bubble result. In general, for most of the dopings and temperatures considered, the first vertex correction has the tendency to increase the resistivity, while the second has the opposite effect. Therefore the results of each type of term are always very different and one cannot neglect the AL-like contribution in those regimes. The latter contribution vanishes only when there is exact particle-hole symmetry.

We observe in the optical conductivity that vertex corrections are important at all the dopings considered and that no term can be neglected. The effect is the strongest for dopings smaller than the critical doping near and below the pseudogap temperature. We also observe that the frequency at which the results with and without vertex corrections cease to differ decrease with increasing doping. The hump structure in the mid-infrared frequency range, related to the pseudogap, is observed both with and without vertex corrections, but with different amplitudes at a given temperature. At the quantum critical point and beyond, the effect is important both at high and low temperatures, though more important at low temperatures. The low-frequency part of the conductivity is higher with the vertex corrections and increases quite rapidly with doping.

This work is currently being extended in several directions. For example, one can study more realistic band parameters for high-temperature superconductors and investigate the connection between the single-particle scattering rate along the Fermi surface and the temperature dependence of the resistivity. The sensitivity of the resistivity to the details of the model in the pseudogap regime would also be interesting to investigate. Using a similar approach, one can also envisage calculating the thermopower and other transport properties.

APPENDIX A: f-SUM RULE FOR THE CONDUCTIVITY

In this appendix, we derive the general expression for the real part of the conductivity, Eq. (19), and we show that the zero-Matsubara-frequency value of the current-current correlation function suffices to check numerically the validity of the f-sum rule. We begin from the continuity equation,

$$\frac{\partial \rho(\mathbf{r},t)}{\partial t} + \nabla \cdot \mathbf{j}(\mathbf{r},t) = 0, \quad (A1)$$

which, in Fourier space, reads

$$-\omega\rho(\mathbf{q},\omega) + \mathbf{q}\cdot\mathbf{j}(\mathbf{q},\omega) = 0. \quad (A2)$$

If $\mathbf{j}(\mathbf{q},\omega) = j_x(\mathbf{q},\omega)\hat{x}$, we have

$$q_x j_x(\mathbf{q},\omega) = \omega\rho(\mathbf{q},\omega). \quad (A3)$$

Using space translational invariance, the two-particle spectral function corresponding to an observable A can be written formally as

$$\chi''_{AA}(\mathbf{q},\omega) = \frac{1}{N\top}\langle[A(\mathbf{q},\omega),A(-\mathbf{q},-\omega)]\rangle, \quad (A4)$$

with $\top \to \infty$, so that, from continuity equation (A3), we have the relation between current and charge correlation functions,

$$\chi''_{j_x j_x}(\mathbf{q},\omega) = \frac{\omega^2}{q_x^2}\chi''_{\rho\rho}(\mathbf{q},\omega), \quad (A5)$$

and thus,

$$\int\frac{d\omega}{\pi}\frac{\chi''_{j_x j_x}(\mathbf{q},\omega)}{\omega} = \frac{1}{q_x^2}\int\frac{d\omega}{\pi}\omega\chi''_{\rho\rho}(\mathbf{q},\omega). \quad (A6)$$

The right-hand side can be obtained from equal-time commutators since

$$\int\frac{d\omega}{\pi}\omega\chi''_{\rho\rho}(\mathbf{q},\omega) = \left(i\frac{\partial}{\partial t}\int\frac{d\omega}{2\pi}e^{-i\omega t}2\chi''_{\rho\rho}(\mathbf{q},\omega)\right)\Big|_{t=0}, \quad (A7)$$

and, by definition,

$$\int\frac{d\omega}{2\pi}e^{-i\omega t}2\chi''_{\rho\rho}(\mathbf{q},\omega) = \frac{1}{N}\langle[\rho(\mathbf{q},t),\rho(-\mathbf{q},0)]\rangle, \quad (A8)$$

so that

$$\int\frac{d\omega}{\pi}\frac{\chi''_{j_x j_x}(\mathbf{q},\omega)}{\omega} = \frac{1}{q_x^2}\frac{1}{N}\left\langle\left[i\frac{\partial}{\partial t}\rho(\mathbf{q},t),\rho(-\mathbf{q},0)\right]\right\rangle\Big|_{t=0}$$
$$= \frac{1}{q_x^2}\frac{1}{N}\left\langle\left[[\rho(\mathbf{q}),H](t),\rho(-\mathbf{q},0)\right]\right\rangle\Big|_{t=0}. \quad (A9)$$

Taking for H the Hubbard Hamiltonian and calculating the commutators, we get

$$\int\frac{d\omega}{\pi}\frac{\chi''_{j_x j_x}(\mathbf{q},\omega)}{\omega} = \frac{1}{q_x^2}\frac{1}{N}\sum_{\mathbf{k}\sigma}(\epsilon_{\mathbf{k+q}} + \epsilon_{\mathbf{k-q}} - 2\epsilon_{\mathbf{k}})\langle n_{\mathbf{k}\sigma}\rangle, \quad (A10)$$

We are interested in the long wavelength limit, namely $\mathbf{q} \to 0$, so that

$$\epsilon_{\mathbf{k+q}} \approx \epsilon_{\mathbf{k}} + \frac{\partial\epsilon_{\mathbf{k}}}{\partial k_x}q_x + \frac{\partial\epsilon_{\mathbf{k}}}{\partial k_y}q_y + \frac{1}{2}\frac{\partial^2\epsilon_{\mathbf{k}}}{\partial k_x^2}q_x^2$$
$$+ \frac{1}{2}\frac{\partial^2\epsilon_{\mathbf{k}}}{\partial k_y^2}q_y^2 + \frac{\partial^2\epsilon_{\mathbf{k}}}{\partial k_x \partial k_y}q_x q_y, \quad (A11)$$

and, if we consider the longitudinal conductivity $\mathbf{q} = q_x \hat{x}$, we obtain

$$\int \frac{d\omega}{\pi} \frac{\chi''_{j_x j_x}(q_x, \omega)}{\omega} = \frac{1}{N} \sum_{\mathbf{k}\sigma} \frac{\partial^2 \epsilon_{\mathbf{k}}}{\partial k_x^2} \langle n_{\mathbf{k}\sigma} \rangle = -\langle k_x \rangle, \quad (A12)$$

using the earlier definition, Eq. (12).

To derive the general results for the real part of the conductivity, Eq. (19), we begin with the spectral form for $\chi_{j_x j_x}(q_x, \omega)$ that reads

$$\chi_{j_x j_x}(q_x, \omega) = \int \frac{d\omega'}{\pi} \frac{\chi''_{j_x j_x}(q_x, \omega)}{\omega' - \omega - i\eta}, \quad (A13)$$

so that, from Eqs. (18) and (A12), we have

$$\begin{aligned}
\sigma_{xx}(q_x, \omega) &= \frac{\langle k_x \rangle + \chi_{j_x j_x}(\omega)}{i(\omega + i\eta)} \\
&= \frac{1}{i(\omega + i\eta)} \left(-\int \frac{d\omega'}{\pi} \frac{\chi''_{j_x j_x}(q_x, \omega')}{\omega'} \right. \\
&\quad \left. + \int \frac{d\omega'}{\pi} \frac{\chi''_{j_x j_x}(q_x, \omega')}{\omega' - \omega - i\eta} \right) \\
&= \frac{1}{i(\omega + i\eta)} \int \frac{d\omega'}{\pi} \frac{(\omega + i\eta)\chi''_{j_x j_x}(q_x, \omega')}{\omega'(\omega' - \omega - i\eta)} \\
&= \frac{1}{i} \int \frac{d\omega'}{\pi} \frac{\chi''_{j_x j_x}(q_x, \omega')}{\omega'(\omega' - \omega - i\eta)}, \quad (A14)
\end{aligned}$$

and since

$$\frac{1}{\omega' - \omega - i\eta} = P \frac{1}{\omega' - \omega} + i\pi \delta(\omega' - \omega), \quad (A15)$$

we obtain the desired result:

$$Re\, \sigma_{xx}(q_x, \omega) = \frac{\chi''_{j_x j_x}(q_x, \omega)}{\omega}. \quad (A16)$$

Substituting in the form found earlier, Eq. (A12), the f-sum rule for the conductivity is

$$\int_{-\infty}^{\infty} \frac{d\omega}{\pi} Re\, \sigma_{xx}(q_x, \omega) = \frac{1}{N} \sum_{\mathbf{k}\sigma} \frac{\partial^2 \epsilon_{\mathbf{k}}}{\partial k_x^2} \langle n_{\mathbf{k}\sigma} \rangle \quad (A17)$$

for $q_x \to 0$. Since the spectral form for $\chi_{j_x j_x}(q_x, iq_n)$ is

$$\chi_{j_x j_x}(q_x, iq_n) = \int_{-\infty}^{\infty} \frac{d\omega}{\pi} \frac{\chi''_{j_x j_x}(q_x, \omega)}{\omega - iq_n}, \quad (A18)$$

we have the desired result:

$$\chi_{j_x j_x}(q_x, iq_n = 0) = \frac{1}{N} \sum_{\mathbf{k}\sigma} \frac{\partial^2 \epsilon_{\mathbf{k}}}{\partial k_x^2} \langle n_{\mathbf{k}\sigma} \rangle. \quad (A19)$$

It is thus sufficient to look at the zero-Matsubara-frequency value of $\chi_{j_x j_x}$ to check whether the sum rule is satisfied (assuming that $\langle k_x \rangle$ has been calculated).

Since the results in Eq. (A17), or equivalently Eq. (A19), are a consequence of the continuity equation, it means this sum rule must be respected when there is conservation of particle number.

APPENDIX B: WARD IDENTITY

In this appendix, we derive the general Ward identity that follows from charge conservation. It is far too complicated to

be verified in full generality numerically within our approach. We also indicate that the Ward identity suffices to find the vertex correction simply in cases where frequency and momentum variations are smooth. These assumptions are not fulfilled in our case; hence these simplifications cannot be used.

We begin from linear response theory in imaginary time. We omit the diamagnetic term, which is not relevant for the present discussion. We find

$$\langle \mathbf{j}_{\mathbf{q}}(\tau) \rangle = \int_0^{\beta} d\tau' \langle T_{\tau} \hat{\mathbf{j}}_{\mathbf{q}}(\tau) \hat{\mathbf{j}}_{-\mathbf{q}}(\tau') \rangle \cdot \mathbf{A}_{\mathbf{q}}(\tau'), \quad (B1)$$

where $\hat{\mathbf{j}}$ is the paramagnetic current in the interaction representation. Take a single (bosonic) Matsubara frequency for the vector potential

$$\mathbf{A}_{\mathbf{q}}(\tau') = T\mathbf{A}_{\mathbf{q}}(q_m) e^{-iq_m \tau'} \quad (B2)$$

and extract the corresponding Matsubara frequency for the current; then the quantity to evaluate is

$$\begin{aligned}
\langle \mathbf{j}_{\mathbf{q}}(q_m) \rangle &= T \int_0^{\beta} d\tau \int_0^{\beta} d\tau' e^{iq_m(\tau - \tau')} \langle T_{\tau} \hat{\mathbf{j}}_{\mathbf{q}}(\tau) \hat{\mathbf{j}}_{-\mathbf{q}}(\tau') \rangle \cdot \mathbf{A}_{\mathbf{q}}(q_m) \\
&= T \int_0^{\beta} d\tau \int_0^{\beta} d\tau' e^{iq_m(\tau - \tau')} \frac{1}{N} \sum_{\mathbf{k},\sigma} \sum_{\mathbf{k}'} \nabla_{\mathbf{k}} \varepsilon_{\mathbf{k}} \\
&\quad \times \langle T_{\tau} c^{\dagger}_{\mathbf{k}\sigma}(\tau) c_{\mathbf{k}+\mathbf{q}\sigma}(\tau) c^{\dagger}_{\mathbf{k}'+\mathbf{q}\sigma}(\tau') c_{\mathbf{k}'\sigma}(\tau') \rangle \\
&\quad \times \nabla_{\mathbf{k}'} \varepsilon_{\mathbf{k}'} \cdot \mathbf{A}_{\mathbf{q}}(q_m) \quad (B3)
\end{aligned}$$

where, in the last equality, we have also used spin conservation with the fact that only the connected piece will contribute because the average current in equilibrium vanishes.

The Ward identity that we need can be obtained from the single-spin-component version of following equality that can be derived from current conservation:[94]

$$\begin{aligned}
\sum_{\mathbf{k}} \left[\frac{\partial}{\partial \tau} + (\varepsilon_{\mathbf{k}+\mathbf{q}} - \varepsilon_{\mathbf{k}}) \right] \langle T_{\tau} c^{\dagger}_{\mathbf{k}\sigma}(\tau) c_{\mathbf{k}+\mathbf{q}\sigma}(\tau) c^{\dagger}_{\mathbf{k}'+\mathbf{q}\sigma}(\tau_1) c_{\mathbf{k}'\sigma}(\tau_2) \rangle \\
= \delta(\tau - \tau_1) G_{\mathbf{k}'\sigma}(\tau_2 - \tau) - \delta(\tau - \tau_2) G_{\mathbf{k}'+\mathbf{q}\sigma}(\tau - \tau_1). \quad (B4)
\end{aligned}$$

Current conservation, which we saw in the first two equations of Appendix A, would give a vanishing right-hand side were it not for the theta functions whose derivatives give delta functions and ultimately equal-time commutators that can be evaluated. Define the fermionic Matsubara frequency four-point correlation function:

$$\begin{aligned}
&\Lambda_{\sigma}(\mathbf{k}, \mathbf{k} + \mathbf{q}; k_m, \mathbf{k}' + \mathbf{q}; k'_n, \mathbf{k}') \\
&\equiv \int_0^{\beta} d\tau_1 \int_0^{\beta} d\tau_2 e^{ik_m(\tau - \tau_1)} e^{ik'_n(\tau_2 - \tau)} \\
&\quad \times \langle T_{\tau} c^{\dagger}_{\mathbf{k}\sigma}(\tau) c_{\mathbf{k}+\mathbf{q}\sigma}(\tau) c^{\dagger}_{\mathbf{k}'+\mathbf{q}\sigma}(\tau_1) c_{\mathbf{k}'\sigma}(\tau_2) \rangle. \quad (B5)
\end{aligned}$$

Then, taking the same fermionic components of the Ward identity and integrating by parts, it takes the form

$$\begin{aligned}
&\sum_{\mathbf{k}} [(-ik_m + ik'_n) + (\varepsilon_{\mathbf{k}+\mathbf{q}} - \varepsilon_{\mathbf{k}})] \Lambda_{\sigma}(\mathbf{k}, \mathbf{k} + \mathbf{q}; k_m, \mathbf{k}' + \mathbf{q}; k'_n, \mathbf{k}') \\
&= G_{\mathbf{k}'\sigma}(k'_n) - G_{\mathbf{k}'+\mathbf{q}\sigma}(k_m). \quad (B6)
\end{aligned}$$

We need the amputated function that is summed over all wave vectors to compute the current-current correlation function. So let us define the charge and current three-point vertices (for a single-spin component), valid in the small $\mathbf{q}$ limit:

$$
\Gamma_\rho(k_m, \mathbf{k}' + \mathbf{q}; k'_n, \mathbf{k}')
$$
$$
= -\sum_{\mathbf{k}} \Lambda_\sigma(\mathbf{k}, \mathbf{k} + \mathbf{q}; k_m, \mathbf{k}' + \mathbf{q}; k'_n, \mathbf{k}') G^{-1}_{\mathbf{k}'\sigma}(k'_n) G^{-1}_{\mathbf{k}'+\mathbf{q}\sigma}(k_m),
$$
$$
\text{(B7)}
$$

$$
\mathbf{q} \cdot \Gamma_J(k_m, \mathbf{k}' + \mathbf{q}; k'_n, \mathbf{k}')
$$
$$
= -\mathbf{q} \cdot \sum_{\mathbf{k}} \nabla_{\mathbf{k}} \varepsilon_{\mathbf{k}} \Lambda_\sigma(\mathbf{k}, \mathbf{k} + \mathbf{q}; k_m, \mathbf{k}' + \mathbf{q}; k'_n, \mathbf{k}')
$$
$$
\times G^{-1}_{\mathbf{k}'\sigma}(k'_n) G^{-1}_{\mathbf{k}'+\mathbf{q}\sigma}(k_m). \quad \text{(B8)}
$$

Then, in the long wavelength limit, the general Ward identity, Eq. (B6), can be rewritten for the three-point functions as follows:

$$
(ik_m - ik'_n)\Gamma_\rho - \mathbf{q} \cdot \Gamma_J = G^{-1}_{\mathbf{k}'+\mathbf{q}\sigma}(k_m) - G^{-1}_{\mathbf{k}'\sigma}(k'_n)
$$
$$
= (ik_m - ik'_n) - \mathbf{q} \cdot \nabla_{\mathbf{k}'} \varepsilon_{\mathbf{k}'}
$$
$$
- \Sigma_{\mathbf{k}'+\mathbf{q}\sigma}(k_m) + \Sigma_{\mathbf{k}'\sigma}(k'_n) \quad \text{(B9)}
$$

We can obtain the four-point function that we need in the expression for the current, Eq. (B3), from the fermionic Matsubara expression, Eq. (B5), for the four-point function at $\tau_1 = \tau_2 = \tau'$ as follows:

$$
\langle \mathbf{j}_{\mathbf{q}}(q_m) \rangle = T \int_0^\beta d\tau \int_0^\beta d\tau' e^{iq_m(\tau-\tau')}
$$
$$
\times \frac{1}{N} \sum_{\mathbf{k},\sigma} \sum_{\mathbf{k}'} T \sum_{k_m} T \sum_{k'_n} e^{-ik_m(\tau-\tau')} e^{-ik'_n(\tau'-\tau)}
$$
$$
\times \nabla_{\mathbf{k}} \varepsilon_{\mathbf{k}} \Lambda_\sigma(\mathbf{k}, \mathbf{k}+\mathbf{q}; k_m, \mathbf{k}'+\mathbf{q}; k'_n, \mathbf{k}') \nabla_{\mathbf{k}'} \varepsilon_{\mathbf{k}'} \cdot \mathbf{A}_{\mathbf{q}}(q_m)
$$
$$
= \frac{1}{N} \sum_{\mathbf{k},\sigma} \sum_{\mathbf{k}'} T \sum_{k'_n} \nabla_{\mathbf{k}} \varepsilon_{\mathbf{k}}
$$
$$
\times \Lambda_\sigma(\mathbf{k}, \mathbf{k}+\mathbf{q}; k'_n+q_m, \mathbf{k}'+\mathbf{q}; k'_n, \mathbf{k}') \nabla_{\mathbf{k}'} \varepsilon_{\mathbf{k}'} \cdot \mathbf{A}_{\mathbf{q}}(q_m).
$$
$$
\text{(B10)}
$$

The sum over wave vectors $\mathbf{k}$ allows one to rewrite the latter in terms of the current vertex defined in Eq. (B8)

$$
\langle \mathbf{j}_{\mathbf{q}=\mathbf{0}}(q_m) \rangle = -\frac{2}{N} \sum_{\mathbf{k}'} T \sum_{k'_n} \Gamma_J(k'_n + q_m, \mathbf{k}'; k'_n, \mathbf{k}')
$$
$$
\times G_{\mathbf{k}'}(k'_n) G_{\mathbf{k}'}(k'_n + q_m) \nabla_{\mathbf{k}'} \varepsilon_{\mathbf{k}'} \cdot \mathbf{A}_{\mathbf{q}=\mathbf{0}}(q_m).
$$
$$
\text{(B11)}
$$

We have performed the sum over spins, which explains the factor of two, and taken the $\mathbf{q} = \mathbf{0}$ limit first to represent a constant electric field.

There is a simple case where the Ward identity suffices to find the vertex correction. Consider the Ward identity for the three-point function, Eq. (B9). The rest of this appendix is correct only if we can assume that in the $\mathbf{q} \to \mathbf{0}$ finite frequency $ik_m - ik'_n$ limit, the charge vertex $\Gamma_\rho(k_m, \mathbf{k}' + \mathbf{q}; k'_n, \mathbf{k}')$ and current vertex $\Gamma_J(k_m, \mathbf{k}' + \mathbf{q}; k'_n, \mathbf{k}')$ are analytical in $\mathbf{q}$ and have a finite limit at $\mathbf{q} = \mathbf{0}$. It can be checked that this is the case for the noninteracting system. In that case, all the nonanalyticities are contained in the product of the Green's

functions appearing in our last expression for $\langle \mathbf{j}_{\mathbf{q}=\mathbf{0}}(q_m) \rangle$. While these kinds of analytic properties can be assumed for Fermi liquids, this is *not* appropriate in our case, which is more singular in the presence of strong antiferromagnetic fluctuations.

In the case where we can assume analyticity, the expansion for Γ_ρ in powers of $\mathbf{q}$ must begin at order q^2 because it is a scalar. Then, the long wavelength limit of the vertices can be found by identifying the coefficients of the $(ik_m - ik'_n)$ and of the $\mathbf{q}$ on the left- and right-hand sides of the Ward identity for the three-point function, Eq. (B9). For the charge three-point function we thus find

$$
\Gamma_\rho(k_m, \mathbf{k}'; k'_n, \mathbf{k}') = 1 - \frac{\Sigma_{\mathbf{k}'\sigma}(k_m) - \Sigma_{\mathbf{k}'\sigma}(k'_n)}{(ik_m - ik'_n)}, \quad \text{(B12)}
$$

while for the current vertex, taking the $\mathbf{q} \to \mathbf{0}$ limit, we obtain

$$
\Gamma_J(k_m, \mathbf{k}'; k'_n, \mathbf{k}') = \nabla_{\mathbf{k}'} \varepsilon_{\mathbf{k}'} + \nabla_{\mathbf{k}'} \Sigma_{\mathbf{k}'\sigma}(k_m). \quad \text{(B13)}
$$

The first term in the last two equations is the bare vertex and the last term the vertex correction. These results for the vertex corrections are valid, for example, for impurity scattering or electron-phonon interactions where the assumptions on which they were derived are valid,[95] but not in our case where the gradient of the self-energy with respect to wave vector can be very large, for example near hot spots. The above two equations by themselves are often called the Ward identities.[95]

Note that at zero external Matsubara frequency, as long as the charge vertex does not diverge, Eq. (B13) becomes exact for $k_m = k'_n$. This form for the vertex generates ladder diagrams only, demonstrating that the Aslamasov-Larkin contribution vanishes, as found numerically in Sec. III A.

APPENDIX C: FAST FOURIER TRANSFORMS, CUBIC SPLINES, AND ASYMPTOTIC EXPANSIONS

The use of FFTs is absolutely essential for this calculation. We begin by describing their use for obtaining the Lindhard function, Eq. (22), and the self-energy, where the convolutions that render the use of FFTs possible are apparent. The convolutions are not so apparent in the case of the conductivity, particularly the AL-like terms, that require an elaborate discussion in the third subsection.

A. The Lindhard function

The Lindhard function, Eq. (22), is needed to compute the spin and charge susceptibilities, Eqs. (20), and (21), which is defined in a more explicit way as

$$
\chi_0(\mathbf{q}, iq_n) = -2\frac{T}{N} \sum_{k, ik_n} G^{(1)}(\mathbf{k} + \mathbf{q}, ik_n + iq_n) G^{(1)}(\mathbf{k}, ik_n),
$$
$$
\text{(C1)}
$$

with

$$
G^{(1)}(\mathbf{k}, ik_n) = \frac{1}{ik_n - \epsilon_{\mathbf{k}} + \mu_0}, \quad \text{(C2)}
$$

where $\epsilon_{\mathbf{k}}$ is the bare particle dispersion relation, $k_n = (2n + 1)\pi T$ is a fermionic Matsubara frequency and μ_0 is the bare chemical potential. Expression (C1) could be calculated

by first performing analytically the sum over Matsubara frequencies to obtain

$$\chi_0(\mathbf{q},iq_n) = -\frac{2}{N}\sum_{\mathbf{k}}\frac{f(\xi_{\mathbf{k}}) - f(\xi_{\mathbf{k+q}})}{iq_n + \xi_{\mathbf{k}} - \xi_{\mathbf{k+q}}}, \qquad \text{(C3)}$$

where $\xi_{\mathbf{k}} = \epsilon_{\mathbf{k}} - \mu_0$ and $f(\xi_{\mathbf{k}})$ is the Fermi–Dirac distribution, and then integrating numerically over $\mathbf{k}$ for each value of $(\mathbf{q},iq_n)$. While it may seem that we have saved some work by doing exactly the Matsubara sum, by doing so we do not use a property of Eq. (C1) that can make our calculation much easier. This is the fact that this expression is a convolution, and convolutions can be calculated in a very efficient way using FFTs. For instance, Eq.(C1) can be written as

$$\chi_0(\mathbf{q},iq_n) = -2\int_0^\beta d\tau\, e^{iq_n\tau}\sum_{\mathbf{r}}e^{-i\mathbf{q}\cdot\mathbf{r}}G^{(1)}(\mathbf{r},\tau)G^{(1)}(-\mathbf{r},-\tau),$$

$$\text{(C4)}$$

where $\beta = T^{-1}$.

To compute $\chi_0(\mathbf{q},iq_n)$ on a grid of size $N_{\mathbf{q}}N_{q_n}$ using the form where Matsubara sums have been done, Eq. (C3), one needs to do this number of integrals over the Brillouin zone, a number of operations that scales like $N_{\mathbf{q}}^2N_{q_n}$ if we consider that each integral scales like $N_{\mathbf{q}}$. On the other hand, using the convolution form, Eq. (C4), we need to do a 2D FFT on $G^{(1)}(\mathbf{k},\tau)$ to obtain $G^{(1)}(\mathbf{r},\tau)$ [here, $G^{(1)}(\mathbf{k},\tau)$ is known analytically], a task that scales like $N_{\mathbf{q}}N_{q_n}\log N_{\mathbf{q}}$, and then the three-dimensional FFT in Eq. (C4) that scales like $N_{\mathbf{q}}N_{q_n}\log N_{\mathbf{q}}N_{q_n}$. We therefore have a gain proportional to $N_{\mathbf{q}}/\log N_{\mathbf{q}}N_{q_n}$.

There is one delicate point. Equation (C4) contains a continuous FT on the imaginary time τ while FFTs are discrete transforms. The simplest thing to do would be to discretize τ and perform an ordinary FFT. This would give acceptable results for the low Matsubara frequencies but the high frequencies would be completely wrong since $\chi_0(\mathbf{q},iq_n)$ would be periodic in q_n while it has to decrease as a series in even powers of $1/q_n$. To solve this problem we make use of cubic splines to approximate the integrand between the discrete imaginary-time points and perform a continuous FT on this spline. In Appendix E, we show how to compute the continuous FT of a cubic spline using in fact only a DFT. Let us consider first the imaginary-time FT in Eq. (C4). Using the form of Eq.(E7) given in Appendix E, we obtain

$$\chi_0(\mathbf{r},iq_n) = \frac{\chi_0'(\mathbf{r},\tau=\beta) - \chi_0'(\mathbf{r},\tau=0)}{q_n^2}$$

$$+\frac{1-e^{iq_n\Delta\tau}}{q_n^4}\sum_{j=0}^{N-1}S_{j+1}^{(3)}(\mathbf{r})e^{iq_n\tau_j}, \qquad \text{(C5)}$$

where N is the number of intervals in the imaginary time grid, $\Delta\tau$ is the size of an interval, $S_j(\mathbf{r},\tau)$ is the cubic polynomial in the jth interval and $S_j^{(3)}(\mathbf{r})$ is the third derivative of $S_j(\mathbf{r},\tau)$.

Notice that Eq. (C5) contains the discrete Fourier transform of $S_j^{(3)}(\mathbf{r})$, so that the result of this transform itself will be periodic in q_n. But the factor $1/(q_n^4)$ in front makes this term important for only low frequencies. Expression (C5) contains the derivatives of $\chi_0(\mathbf{r},\tau)$ with respect to τ at the boundaries. It is explained in Appendix E how those derivatives are used

to complete the linear system that must be solved to obtain the spline coefficients. They thus have to be calculated before the spline and must be known when Eq. (C5) is used. Here since $\chi_0(\mathbf{r},\tau) = -2G^{(1)}(\mathbf{r},\tau)G^{(1)}(-\mathbf{r},-\tau)$, and we have analytical expressions for $G^{(1)}(\mathbf{k},\tau)$, it is straightforward to calculate this derivative. For $0 < \tau < \beta$, we have

$$G^{(1)}(\mathbf{k},\tau) = -e^{-\xi_{\mathbf{k}}\tau}f(-\xi_{\mathbf{k}}) = -e^{\xi_{\mathbf{k}}(\beta-\tau)}f(\xi_{\mathbf{k}}), \qquad \text{(C6)}$$

so that

$$\frac{\partial G^{(1)}(\mathbf{r},\tau)}{\partial\tau} = \frac{1}{N}\sum_{\mathbf{k}}e^{i\mathbf{k}\cdot\mathbf{r}}\xi_{\mathbf{k}}\,e^{-\xi_{\mathbf{k}}\tau}f(-\xi_{\mathbf{k}})$$

$$= \frac{1}{N}\sum_{\mathbf{k}}e^{i\mathbf{k}\cdot\mathbf{r}}\xi_{\mathbf{k}}\,e^{\xi_{\mathbf{k}}(\beta-\tau)}f(\xi_{\mathbf{k}}). \qquad \text{(C7)}$$

Then, still for $0 < \tau < \beta$,

$$G^{(1)}(\mathbf{k},-\tau) = e^{\xi_{\mathbf{k}}\tau}f(\xi_{\mathbf{k}}), \qquad \text{(C8)}$$

and, therefore,

$$\frac{\partial G^{(1)}(-\mathbf{r},-\tau)}{\partial\tau} = \frac{1}{N}\sum_{\mathbf{k}}e^{-i\mathbf{k}\cdot\mathbf{r}}\xi_{\mathbf{k}}e^{\xi_{\mathbf{k}}\tau}f(\xi_{\mathbf{k}}). \qquad \text{(C9)}$$

If we have inversion symmetry,

$$G^{(1)}(-\mathbf{r},-\tau) = G^{(1)}(\mathbf{r},-\tau), \qquad \text{(C10)}$$

then

$$\frac{\partial G^{(1)}(-\mathbf{r},-\tau)}{\partial\tau} = \frac{1}{N}\sum_{\mathbf{k}}e^{i\mathbf{k}\cdot\mathbf{r}}\xi_{\mathbf{k}}e^{\xi_{\mathbf{k}}\tau}f(\xi_{\mathbf{k}}), \qquad \text{(C11)}$$

and we have

$$\frac{\partial G^{(1)}(-\mathbf{r},-\tau)}{\partial\tau} = -\frac{\partial G^{(1)}(\mathbf{r},\beta-\tau)}{\partial\tau}. \qquad \text{(C12)}$$

B. The self-energy

The next function we can calculate using FFTs is the self-energy, Eq. (26), that can be written as

$$\Sigma_\sigma^{(2)}(\mathbf{k},ik_n) = Un_{-\sigma} + \int d\tau\, e^{ik_n\tau}\sum_{\mathbf{r}}e^{-i\mathbf{k}\cdot\mathbf{r}}V(-\mathbf{r},-\tau)G_\sigma^{(1)}(\mathbf{r},\tau),$$

$$\text{(C13)}$$

where

$$V(\mathbf{r},\tau) = \frac{U}{8}[3U_{sp}\chi_{sp}(\mathbf{r},\tau) + U_{ch}\chi_{ch}(\mathbf{r},\tau)]. \qquad \text{(C14)}$$

To calculate $V(\mathbf{r},\tau)$ accurately, we can use the fact that $\chi_{sp}(\mathbf{q},iq_n)$ and $\chi_{ch}(\mathbf{q},iq_n)$ approach asymptotically $\chi_0(\mathbf{q},iq_n)$ as q_n increases and that $\chi_0(\mathbf{r},\tau)$ is known once $G_\sigma^{(1)}(\mathbf{r},\tau)$ is. Then $V(\mathbf{r},\tau)$ is computed from

$$V(\mathbf{r},\tau) = \frac{U}{8}\frac{T}{N}\sum_{\mathbf{q},iq_n}e^{i\mathbf{q}\cdot\mathbf{r}}e^{-iq_n\tau}[3U_{sp}\chi_{sp}(\mathbf{q},iq_n) + U_{ch}\chi_{ch}(\mathbf{q},iq_n)$$

$$-(3U_{sp} + U_{ch})\chi_0(\mathbf{q},iq_n)]$$

$$+\frac{U}{8}(3U_{sp} + U_{ch})\chi_0(\mathbf{r},\tau), \qquad \text{(C15)}$$

where $\chi_0(\mathbf{r},\tau) = -2G_\sigma^{(1)}(\mathbf{r},\tau)G_\sigma^{(1)}(-\mathbf{r},-\tau)$. Because the asymptotic part is removed in the FT, it converges as the

transform of $1/(q_n^4)$ instead of $1/(q_n^2)$, so that a smaller cutoff can be used.

In Eq. (C13), there is a continuous FT so that we have to use cubic splines to represent the τ dependence of the integrand. To compute the splines and then use formula (E7) we need to compute the derivatives of $V(-\mathbf{r}, -\tau)G_\sigma^{(1)}(\mathbf{r},\tau)$ at $\tau = 0$ and $\tau = \beta$, i.e., those derivatives of $V(-\mathbf{r}, -\tau)$ and $G_\sigma^{(1)}(\mathbf{r},\tau)$. The latter were already computed using Eq. (C7) to calculate χ_0. For $V(-\mathbf{r}, -\tau)$, since this function is symmetric with respect to $\tau = \beta/2$, we only need the derivative at $\tau = 0$. If we differentiate expression (C15) with respect to τ and set $\tau = 0$, we notice that the sum disapears since $\chi_{sp}(\mathbf{q},iq_n)$ and $\chi_{ch}(\mathbf{q},iq_n)$ are even functions of q_n while the derivative makes a factor q_n appear in the sum. In other words, at $\tau = 0$ (and thus $\tau = \beta$), the derivatives of $\chi_{sp}(\tau)$, $\chi_{ch}(\tau)$, and $\chi_0(\tau)$ are equal, which comes from the fact that they have the same asymptotic limit as can be seen from Eq. (E7) (with $k = q_n$), considering that there are no odd terms for those functions. Therefore, we have

$$\left.\frac{\partial V(\mathbf{r},\tau)}{\partial \tau}\right|_{\tau=0} = \frac{U}{8}(3U_{sp} + U_{ch})\left.\frac{\partial \chi_0(\mathbf{r},\tau)}{\partial \tau}\right|_{\tau=0}. \quad \text{(C16)}$$

Once the self-energy of Eq. (C13) is obtained, we have to calculate the interacting chemical potential μ to define the Green's function $G^{(2)}$ as

$$G^{(2)}(\mathbf{k},ik_n) = \frac{1}{ik_n - \epsilon_\mathbf{k} + \mu - \Sigma_\sigma^{(2)}(\mathbf{k},ik_n)}. \quad \text{(C17)}$$

For a given filling $\langle n \rangle$, μ is defined implicitly by the equation

$$\langle n \rangle = 2\frac{1}{N}\sum_\mathbf{k} G^{(2)}(\mathbf{k},\tau = 0^-)$$

$$= 2\frac{T}{N}\sum_{\mathbf{k},ik_n} e^{-ik_n 0^-} G^{(2)}(\mathbf{k},ik_n). \quad \text{(C18)}$$

However, this expression is not very practical numerically because of the convergence factor $e^{-ik_n 0^-}$ that is not well defined numerically. We use instead

$$2\frac{T}{N}\sum_{\mathbf{k},ik_n}[G^{(2)}(\mathbf{k},ik_n) - G^{(1)}(\mathbf{k},ik_n)] = 0, \quad \text{(C19)}$$

where it is assumed that $G^{(1)}$ contains the chemical potential μ_0 that gives the desired filling. No convergence factor is needed since the sum converges as the sum of $1/(k_n^2)$.

C. The current-current correlation function

Finally we come to the calculation of $\chi_{j_x j_x}$, Eq. (85). The first term, called the "bubble" contribution because

of its bubble shape in Fig. 1, can be written as

$$\chi_{j_x j_x}^b(iq_n)$$

$$= \frac{-2T}{N}\sum_\mathbf{k}\left(\frac{\partial \epsilon_\mathbf{k}}{\partial k_x}\right)^2 \sum_{ik_m} G^{(2)}(\mathbf{k},ik_m)G^{(2)}(\mathbf{k},ik_m + iq_n)$$

$$= \frac{-2}{N}\sum_\mathbf{k}\left(\frac{\partial \epsilon_\mathbf{k}}{\partial k_x}\right)^2 \int_0^\beta d\tau\, e^{iq_n\tau} G^{(2)}(\mathbf{k},\tau)G^{(2)}(\mathbf{k},-\tau). \quad \text{(C20)}$$

To use this formula we first have to compute $G^{(2)}(\mathbf{k},\tau)$ from $G^{(2)}(\mathbf{k},ik_n)$ defined in Eq. (C17). To do that we cannot simply perform a FT with respect to ik_n on $G^{(2)}(\mathbf{k},ik_n)$ including only a finite number of frequencies. This is because $G^{(2)}(\mathbf{k},\tau)$ has a discontinuity at $\tau = 0$ that will produce oscillations (the Gibbs phenomenon) close to $\tau = 0$ and $\tau = \beta$ [remember that $G(\mathbf{k},\beta - \tau) = -G(\mathbf{k},-\tau)$]. This problem can be solved by using the asymptotic form of $G^{(2)}(\mathbf{k},ik_n)$ to perform the transform on all frequencies. First, let us define $\bar{G}(\mathbf{k},\tau)$, the FT of some Green's function $G(\mathbf{k},ik_n)$, on a finite set of frequencies:

$$\bar{G}(\mathbf{k},\tau_j) = T\sum_{ik_n}' e^{-ik_n\tau_j} G(\mathbf{k},ik_n)$$

$$= e^{i\pi(N_\tau - 1)j/N_\tau} T\sum_{n=0}^{N_\tau - 1} e^{-i2\pi nj/N_\tau} G(\mathbf{k},ik_{n-\frac{N_\tau}{2}}). \quad \text{(C21)}$$

where $\sum'$ means that the sum is finite, N_τ is the number of values of τ, and we have used $k_n = (2n + 1)\pi T$ and $\tau_j = j/(N_\tau T)$. The sum in the second line has the form used in standard FFT routines. Now, to compute the self-energy, Eq. (C13), we have used FTs of cubic splines so that $\Sigma^{(2)}(\mathbf{k},ik_n)$ has the form of Eq. (E7). The asymptotic form of $G^{(2)}(\mathbf{k},ik_n)$ is therefore

$$G_{inf}^{(2)}(\mathbf{k},ik_n) = \frac{1}{ik_m - \tilde{\epsilon}_\mathbf{k} - \Sigma_{inf}(\mathbf{k},ik_n)}$$

$$= \frac{1}{ik_n - \tilde{\epsilon}_\mathbf{k} - \left(\frac{s_1}{ik_n} + \frac{s_2(\mathbf{k})}{(ik_n)^2} + \frac{s_3(\mathbf{k})}{(ik_n)^3}\right)}, \quad \text{(C22)}$$

where $\tilde{\epsilon}_\mathbf{k} = \epsilon_\mathbf{k} - \mu$. The FT over ik_n of this function can be done analytically using the residue theorem. For a function $g(z)$ having only simple poles, we have

$$T\sum_{ik_m} e^{-ik_m\tau} g(ik_m)$$

$$= \begin{cases} -\sum_j \underset{z=z_j}{Res}[g(z)]\, f(-z_j)e^{-z_j\tau}, & 0 < \tau < \beta \\ \sum_j \underset{z=z_j}{Res}[g(z)]\, f(z_j)e^{-z_j\tau}, & -\beta < \tau < 0, \end{cases} \quad \text{(C23)}$$

which, applied to Eq. (C22), gives

$$G_{inf}^{(2)}(\mathbf{k},\tau) = \mp\sum_{j=1}^4 e^{-z_j(\mathbf{k})\tau} f(\mp z_j(\mathbf{k}))\frac{[z_j(\mathbf{k})]^3}{[z_j(\mathbf{k}) - z_1(\mathbf{k})]\dots[z_j(\mathbf{k}) - z_{j-1}(\mathbf{k})][z_j(\mathbf{k}) - z_{j+1}(\mathbf{k})]\dots[z_j(\mathbf{k}) - z_4(\mathbf{k})]}, \quad \text{(C24)}$$

where the minus sign is for $0 < \tau < \beta$ and the plus sign for $-\beta < \tau < 0$. The $z_j(\mathbf{k})$ are the roots of the polynomial

$$z^4 - \tilde{\epsilon}_\mathbf{k} z^3 - s_1 z^2 - s_2(\mathbf{k}) z - s_3(\mathbf{k}) . \qquad (C25)$$

Those roots are given by quite imposing, but analytical, formulas. Finally, assuming that $\bar{G}^{(2)}_{inf}(\mathbf{k},\tau)$ is the finite FT of $G^{(2)}_{inf}(\mathbf{k},ik_n)$ as defined in Eq. (C21), we use

$$G^{(2)}(\mathbf{k},\tau) = \bar{G}^{(2)}(\mathbf{k},\tau) + \left[G^{(2)}_{inf}(\mathbf{k},\tau) - \bar{G}^{(2)}_{inf}(\mathbf{k},\tau) \right] \qquad (C26)$$

where the term between the brackets is the contribution from frequencies beyond the cutoff used in Eq. (C21). This expression will be very accurate if the asymptotic behavior is well obeyed beyond the cutoff. Using expression (C22) as the asymptotic form of $G^{(2)}(\mathbf{k},ik_n)$ may seem to complicate the calculations needlessly since the first term of the high-frequency expansion of $G^{(1)}(\mathbf{k},ik_n)$ is identical to that of $G^{(2)}(\mathbf{k},ik_n)$. However, to compute the cubic spline of the integrand in Eq. (C20), and then its FT, we need the derivatives of $G^{(2)}(\mathbf{k},\tau)$ at $\tau = 0$ and $\tau = \beta$ and, for that purpose, we have to use a more accurate asymptotic form. The reason will be explained shortly.

As we have just mentioned, we need to compute derivatives of Eq. (C26) with respect to τ at the boundaries. Let us first rewrite expression (C26) using Eq. (C21):

$$G^{(2)}(\mathbf{k},\tau) = T \sum_{ik_n}{}' e^{-ik_n\tau} \left[G^{(2)}(\mathbf{k},ik_n) - G^{(2)}_{inf}(\mathbf{k},ik_n) \right]$$
$$+ G^{(2)}_{inf}(\mathbf{k},\tau), \qquad (C27)$$

so that

$$\left.\frac{\partial G^{(2)}(\mathbf{k},\tau)}{\partial \tau}\right|_{\tau=0} = T \sum_{ik_n}{}' (-ik_n) \left[G^{(2)}(\mathbf{k},ik_n) - G^{(2)}_{inf}(\mathbf{k},ik_n) \right]$$
$$+ \left.\frac{\partial G^{(2)}_{inf}(\mathbf{k},\tau)}{\partial \tau}\right|_{\tau=0}, \qquad (C28)$$

where the last term is obtained from the derivative of Eq. (C24). If $G^{(2)}_{inf}$ was taken to be $G^{(1)}$, the sum in Eq. (C27) would converge like the sum of $1/(ik_n)^2$, but the sum in Eq. (C28) would not converge. Thus, $G^{(2)}_{inf}$ must have at least the same first two terms in its high-frequency expansion as $G^{(2)}$. If we use Eq. (C22), the first five terms in the expansion are equal; the sum in Eq. (C27) thus converges as the sum of $1/(ik_n)^6$, while the sum in Eq. (C28), converges as the sum of $1/(ik_n)^5$. This gives us a very precise evaluation of $G^{(2)}(\mathbf{k},\tau)$ and its derivatives. To obtain the derivatives at $\tau = \beta$ we use the relation

$$\left.\frac{\partial G(\mathbf{k},\tau)}{\partial \tau}\right|_{\tau=\beta} = \tilde{\epsilon}_\mathbf{k} + U n_{-\sigma} - \left.\frac{\partial G(\mathbf{k},\tau)}{\partial \tau}\right|_{\tau=0} \qquad (C29)$$

that is derived from the spectral representation of $G(\mathbf{k},\tau)$.

Once $G^{(2)}(\mathbf{k},\tau)$ and its derivatives are obtained, the integrals in expression (C20) are evaluated by computing the cubic splines for $G^{(2)}(\mathbf{k},\tau)G^{(2)}(\mathbf{k},-\tau)$ and using formula (E7) for the FT. The rest of the calculation is simply a sum over the Brillouin zone, where, of course, it is preferable to use the symmetries of the system to save computational resources.

The second term of Eq. (85) is

$$\chi^{v_1}_{j_x j_x}(iq_n) = -\frac{U}{4}\left(\frac{T}{N}\right)^2 \sum_{k_1 k_2} G^{(2)}(k_1) G^{(2)}(k_1 + iq_n)$$
$$\times G^{(1)}(k_2) G^{(1)}(k_2 + iq_n) \frac{\partial \epsilon_\mathbf{k}}{\partial k_x}(\mathbf{k}_1) \frac{\partial \epsilon_\mathbf{k}}{\partial k_x}(\mathbf{k}_2)$$
$$\times [3 U_{sp} \chi_{sp}(k_2 - k_1) + U_{ch} \chi_{ch}(k_2 - k_1)] \quad (C30)$$

where $k_1 + iq_n = (\mathbf{k}_1, ik_m + iq_n)$. If we define

$$f_n(k_2) = \frac{\partial \epsilon_\mathbf{k}}{\partial k_x}(\mathbf{k}_2) G^{(1)}(k_2) G^{(1)}(k_2 + iq_n),$$
$$\qquad\qquad (C31)$$
$$V(k_2 - k_1) = \frac{U}{8}[3 U_{sp} \chi_{sp}(k_2 - k_1) + U_{ch} \chi_{ch}(k_2 - k_1)],$$

then Eq. (C30) becomes

$$\chi^{v_1}_{j_x j_x}(iq_n) = -2\frac{T}{N} \sum_{k_1} \frac{\partial \epsilon_\mathbf{k}}{\partial k_x}(\mathbf{k}_1) G^{(2)}(k_1) G^{(2)}(k_1 + iq_n)$$
$$\times \frac{T}{N} \sum_{k_2} f_n(k_2) V(k_2 - k_1). \qquad (C32)$$

The sum over k_2 being a convolution, we have

$$\chi^{v_1}_{j_x j_x}(iq_n) = -\frac{T}{N} \sum_k \frac{\partial \epsilon_\mathbf{k}}{\partial k_x} G^{(2)}(k) G^{(2)}(k + iq_n)$$
$$\times \sum_{\bar{1}} e^{-ik\cdot\bar{1}} f_n(\bar{1}) V(\bar{1}). \qquad (C33)$$

Note that the sum over $\bar{1}$ written in explicit form is

$$\sum_j \int_0^\beta d\tau \, e^{-i\mathbf{k}\cdot\mathbf{r}_j} e^{ik_m\tau} f_n(\mathbf{r}_j,\tau) V(\mathbf{r}_j,\tau), \qquad (C34)$$

where the function $f_n(\mathbf{r},\tau)$ is given by

$$f_n(\mathbf{r},\tau) = \frac{1}{N} \sum_\mathbf{k} e^{i\mathbf{k}\cdot\mathbf{r}} \frac{\partial \epsilon_\mathbf{k}}{\partial k_x}$$
$$\times T \sum_{ik_m} e^{-ik_m\tau} G^{(1)}(\mathbf{k},ik_m) G^{(1)}(\mathbf{k},ik_m + iq_n).$$
$$\qquad\qquad (C35)$$

Since $G^{(1)}(\mathbf{k},ik_m)$ is the noninteracting Green's function, the Fourier transform over ik_m can be done analytically. Using Eq. (C23), we obtain, for $q_n \neq 0$,

$$T \sum_{ik_m} e^{-ik_m\tau} G^{(1)}(\mathbf{k},ik_m) G^{(1)}(\mathbf{k},ik_m + iq_n)$$
$$= \frac{e^{iq_n\tau} - 1}{iq_n} e^{-\tilde{\epsilon}_\mathbf{k}\tau} [\theta(\tau)(1 - f(\tilde{\epsilon}_\mathbf{k})) - \theta(-\tau) f(\tilde{\epsilon}_\mathbf{k})] . \quad (C36)$$

For $q_n = 0$, there is a double pole so that the calculation with the residue theorem is slightly different. However, we can use the following simple trick:

$$T \sum_{ik_m} e^{-ik_m\tau} G^{(1)}(\mathbf{k},ik_m)^2 = T \sum_{ik_m} e^{-ik_m\tau} \left(\frac{1}{ik_m - \tilde{\epsilon}_\mathbf{k}}\right)^2$$
$$= \frac{\partial}{\partial \tilde{\epsilon}_\mathbf{k}} T \sum_{ik_m} e^{-ik_m\tau} \left(\frac{1}{ik_m - \tilde{\epsilon}_\mathbf{k}}\right) \qquad (C37)$$

$$= \frac{\partial}{\partial \tilde{\epsilon}_k}(-e^{-\tilde{\epsilon}_k \tau}[(1 - f(\tilde{\epsilon}_k))\theta(\tau) - f(\tilde{\epsilon}_k)\theta(-\tau)])$$

$$= e^{-\tilde{\epsilon}_k \tau}\left(\tau[(1 - f(\tilde{\epsilon}_k))\theta(\tau) - f(\tilde{\epsilon}_k)\theta(-\tau)] + \frac{\partial f(\tilde{\epsilon}_k)}{\partial \tilde{\epsilon}_k}\right).$$

For $\tau > 0$ and $q_n \neq 0$, we have

$$f_n(\mathbf{r},\tau) = \frac{e^{iq_n \tau} - 1}{iq_n} \frac{1}{N} \sum_k e^{i\mathbf{k}\cdot\mathbf{r}} \frac{\partial \epsilon_k}{\partial k_x} f(-\tilde{\epsilon}_k)e^{-\tilde{\epsilon}_k \tau}$$

$$= \frac{e^{iq_n \tau} - 1}{iq_n} \frac{1}{N} \sum_k e^{i\mathbf{k}\cdot\mathbf{r}} \frac{\partial \epsilon_k}{\partial k_x} f(\tilde{\epsilon}_k)e^{(\beta-\tau)\tilde{\epsilon}_k}$$

$$= g_n(\tau)h(\mathbf{r},\tau). \qquad (C38)$$

The functions $f_n(\mathbf{r},\tau)$ for different values of n are thus obtained by multiplying the n independent function

$$h(\mathbf{r},\tau) = \frac{1}{N} \sum_k e^{i\mathbf{k}\cdot\mathbf{r}} \frac{\partial \epsilon_k}{\partial k_x} f(\tilde{\epsilon}_k)e^{(\beta-\tau)\tilde{\epsilon}_k} \qquad (C39)$$

by $g_n(\tau) = (e^{iq_n \tau} - 1)/(iq_n)$. Using this result, we find

$$\sum_{\bar{1}} e^{-i k_1 \cdot \bar{1}} f_n(\bar{1})V(\bar{1}) = \int d\tau \, e^{ik_m \tau} g_n(\tau)$$

$$\times \sum_j e^{-i\mathbf{k}_1 \cdot \mathbf{r}_j} h(\mathbf{r}_j,\tau)V(\mathbf{r}_j,\tau). \quad (C40)$$

Inserting this back into Eq. (C33), we obtain for the $q_n \neq 0$ terms,

$$\chi_{j_x j_x}^{v_1}(iq_n) = -2\frac{T}{N} \sum_k \sum_{ik_m} \frac{\partial \epsilon_k}{\partial k_x} G^{(2)}(\mathbf{k},ik_m)G^{(2)}(\mathbf{k},ik_m + iq_n)$$

$$\times \int d\tau \, e^{ik_m \tau} g_n(\tau) \sum_j e^{-i\mathbf{k}\cdot\mathbf{r}_j} h(\mathbf{r}_j,\tau)V(\mathbf{r}_j,\tau)$$

$$= -\frac{2}{iq_n} \frac{1}{N} \sum_k \frac{\partial \epsilon_k}{\partial k_x} T \sum_{ik_m} G^{(2)}(\mathbf{k},ik_m)G^{(2)}(\mathbf{k},ik_m + iq_n)$$

$$\times \left(\int d\tau \, e^{i(k_m + q_n)\tau} \sum_j e^{-i\mathbf{k}\cdot\mathbf{r}_j} h(\mathbf{r}_j,\tau)V(\mathbf{r}_j,\tau)\right.$$

$$\left. - \int d\tau \, e^{ik_m \tau} \sum_j e^{-i\mathbf{k}\cdot\mathbf{r}_j} h(\mathbf{r}_j,\tau)V(\mathbf{r}_j,\tau)\right). \quad (C41)$$

To make the convolutions more apparent, we define

$$J(\mathbf{k},ik_m) = G^{(2)}(\mathbf{k},ik_m) \int d\tau \, e^{ik_m \tau} \sum_j e^{-i\mathbf{k}\cdot\mathbf{r}_j} h(\mathbf{r}_j,\tau)V(\mathbf{r}_j,\tau) \qquad (C42)$$

so that

$$\chi_{j_x j_x}^{v_1}(iq_n) = -\frac{2}{iq_n} \frac{1}{N} \sum_k \frac{\partial \epsilon_k}{\partial k_x}\left(T\sum_{ik_m} G^{(2)}(\mathbf{k},ik_m)J(\mathbf{k},ik_m + iq_n)\right.$$

$$\left. - T\sum_{ik_m} G^{(2)}(\mathbf{k},ik_m + iq_n)J(\mathbf{k},ik_m)\right) \qquad (C43)$$

and we can use the convolution theorem to obtain

$$\chi_{j_x j_x}^{v_1}(iq_n) = -\frac{2}{iq_n} \frac{1}{N} \sum_k \frac{\partial \epsilon_k}{\partial k_x}\left(\int_0^\beta d\tau \, e^{-iq_n \tau} G^{(2)}(\mathbf{k},\tau)J(\mathbf{k}, -\tau)\right.$$

$$\left. - \int_0^\beta d\tau \, e^{iq_n \tau} G^{(2)}(\mathbf{k},\tau)J(\mathbf{k}, -\tau)\right). \qquad (C44)$$

Note that, since all the Matsubara sums have been transformed into FTs that can be done with FFTs and that an FFT gives all N values of an N point transform at the same time, we obtain the values of $\chi_{j_x j_x}^{v_1}(iq_n)$ for all iq_n except $iq_n = 0$ at the same time when the last FFT is done.

We still need to do the FT over τ in Eq. (C42) using cubic splines. For that we need the derivatives of $h(\mathbf{r}_j,\tau)V(\mathbf{r}_j,\tau)$ at $\tau = 0$ and $\tau = \beta$. The derivatives of $V(\mathbf{r}_j,\tau)$ have already been used to compute the self-energy and are obtained using Eq. (C16). For $h(\mathbf{r}_j,\tau)$, the derivative is obtained from definition (C39).

Next, we have to compute $J(\mathbf{k}, -\tau)$. First, we define the function

$$Q(\mathbf{k},ik_n) = \int d\tau \, e^{ik_n \tau} \sum_j e^{-i\mathbf{k}\cdot\mathbf{r}_j} h(\mathbf{r}_j,\tau)V(\mathbf{r}_j,\tau) \quad (C45)$$

so that definition (C42) reads as $J(\mathbf{k},ik_m) = G^{(2)}(\mathbf{k},ik_m)Q(\mathbf{k},ik_n)$. The FT over τ is done using the method described in Appendix E. The asymptotic form of $Q(\mathbf{k},ik_n)$ is

$$Q_{inf}(\mathbf{k},ik_n) = \frac{q_1(\mathbf{k})}{ik_n} + \frac{q_2(\mathbf{k})}{(ik_n)^2} + \frac{q_3(\mathbf{k})}{(ik_n)^3}, \qquad (C46)$$

so that, using Eq. (C22) for $G_{inf}^{(2)}(\mathbf{k},ik_m)$, the asymptotic form for $J(\mathbf{k},ik_m)$ is,

$$J_{inf}(\mathbf{k},ik_n) = \frac{1}{ik_n - \tilde{\epsilon}_k - \left(\frac{s_1}{ik_n} + \frac{s_2(\mathbf{k})}{(ik_n)^2} + \frac{s_3(\mathbf{k})}{(ik_n)^3}\right)}$$

$$\times \left(\frac{q_1(\mathbf{k})}{ik_n} + \frac{q_2(\mathbf{k})}{(ik_n)^2} + \frac{q_3(\mathbf{k})}{(ik_n)^3}\right) \qquad (C47)$$

and its FT is

$$J_{inf}(\mathbf{k}, -\tau) = \sum_{j=1}^4 e^{z_j(\mathbf{k})\tau} f(z_j(\mathbf{k}))$$

$$\times \frac{q_1(\mathbf{k})[z_j(\mathbf{k})]^2 + q_2(\mathbf{k})z_j(\mathbf{k}) + q_3(\mathbf{k})}{\prod_{i\neq j}[z_j(\mathbf{k}) - z_i(\mathbf{k})]}, \quad (C48)$$

where the $z_j(\mathbf{k})$ are the roots of polynomial (C25). By analogy with our previous calculations, the function $J(\mathbf{k}, -\tau)$ is then obtained from

$$J(\mathbf{k}, -\tau) = T\sum_{ik_n}^{\prime} e^{ik_n \tau}[J(\mathbf{k},ik_n) - J_{inf}(\mathbf{k},ik_n)] + J_{inf}(\mathbf{k}, -\tau) \qquad (C49)$$

where $\sum^{\prime}$ means that the sum is done up to a cutoff frequency.

Once these results are substituted into the expression for the MT term, Eq. (C44), we need the derivatives of $G^{(2)}(\mathbf{k},\tau)J(\mathbf{k}, -\tau)$ at $\tau = 0$ and $\tau = \beta$. For $G^{(2)}(\mathbf{k},\tau)$, they

are given by Eqs. (C28) and (C29). As for the derivatives of $J(\mathbf{k}, -\tau)$, they are obtained by differentiating Eq. (C49).

Finally, we need to evaluate separately the $q_n = 0$ term for $\tau > 0$. We have, from Eq. (C37),

$$f_0(\mathbf{r}, \tau) = \frac{1}{N} \sum_{\mathbf{k}} e^{i\mathbf{k}\cdot\mathbf{r}} \frac{\partial \epsilon_{\mathbf{k}}}{\partial k_x}(\mathbf{k}) \, T \sum_{ik_m} e^{-ik_m\tau} G^{(1)}(\mathbf{k}, ik_m)^2$$

$$= \frac{1}{N} \sum_{\mathbf{k}} e^{i\mathbf{k}\cdot\mathbf{r}} \frac{\partial \epsilon_{\mathbf{k}}}{\partial k_x}(\mathbf{k}) \, e^{-\tilde{\epsilon}_{\mathbf{k}}\tau} \left(\tau f(-\tilde{\epsilon}_{\mathbf{k}})) + \frac{\partial f(\tilde{\epsilon}_{\mathbf{k}})}{\partial \tilde{\epsilon}_{\mathbf{k}}} \right).$$

$$(C50)$$

so that

$$\chi_{j_x j_x}^{v_1}(0) = -2\frac{1}{N} \sum_{\mathbf{k}} \frac{\partial \epsilon_{\mathbf{k}}}{\partial k_x}(\mathbf{k}) \, T \sum_{ik_m} G^{(2)}(\mathbf{k}, ik_m) G^{(2)}(\mathbf{k}, ik_m)$$

$$\times \int_0^\beta d\tau \sum_j e^{-i\mathbf{k}_1\cdot\mathbf{r}_j} e^{ik_m\tau} f_0(\mathbf{r}_j, \tau) V(\mathbf{r}_j, \tau). \quad (C51)$$

Using our previous definition, Eq. (C31), for $f_n(k_2)$, the third term in Eq. (85) can be rewritten as

$$\chi_{j_x j_x}^{v_2}(iq_n) = \frac{U}{2} \left(\frac{T}{N}\right)^2 \sum_{k_1, q_1} \frac{\partial \epsilon_{\mathbf{k}}}{\partial k_x}(\mathbf{k}_1) G^{(2)}(k_1) G^{(2)}(k_1 + iq_n)$$

$$\times G^{(1)}(k_1 + q_1 + iq_n)$$

$$\times \left(3U_{sp} \frac{1}{1 - \frac{U_{sp}}{2}\chi_0(q_1)} \frac{1}{1 - \frac{U_{sp}}{2}\chi_0(q_1 + iq_n)} \right.$$

$$\left. + U_{ch} \frac{1}{1 + \frac{U_{ch}}{2}\chi_0(q_1)} \frac{1}{1 + \frac{U_{ch}}{2}\chi_0(q_1 + iq_n)} \right)$$

$$\times \frac{T}{N} \sum_{k_2} f_n(k_2)[G^{(1)}(k_2 + q_1 + iq_n) + G^{(1)}(k_2 - q_1)].$$

$$(C52)$$

The sum over k_2 is the sum of two convolutions and can be written as

$$\frac{T}{N} \sum_{k_2} f_n(k_2)[G^{(1)}(k_2 + q_1 + iq_n) + G^{(1)}(k_2 - q_1)] = \sum_{\bar{1}} (e^{i(q_1 + iq_n)\cdot\bar{1}} + e^{-iq_1\cdot\bar{1}}) f_n(\bar{1}) G^{(1)}(-\bar{1})$$

$$= \sum_j \int_0^\beta d\tau \, (e^{i\mathbf{q}_1\cdot\mathbf{r}_j} e^{-i(q_m + q_n)\tau} + e^{-i\mathbf{q}_1\cdot\mathbf{r}_j} e^{iq_m\tau}) f_n(\mathbf{r}_j, \tau) G^{(1)}(-\mathbf{r}_j, -\tau)$$

$$= \int_0^\beta d\tau \, (-e^{-i(q_m + q_n)\tau} + e^{iq_m\tau}) \sum_j e^{-i\mathbf{q}_1\cdot\mathbf{r}_j} f_n(\mathbf{r}_j, \tau) G^{(1)}(\mathbf{r}_j, -\tau), \quad (C53)$$

where we have used $f_n(-\mathbf{r}_j, \tau) = -f_n(\mathbf{r}_j, \tau)$ and $G^{(1)}(-\mathbf{r}_j, -\tau) = G^{(1)}(\mathbf{r}_j, -\tau)$. Using $f_n(\mathbf{r}, \tau) = g_n(\tau)h(\mathbf{r}, \tau)$, Eq. (C38), we have

$$\frac{T}{N} \sum_{k_2} f_n(k_2)[G^{(1)}(k_2 + q_1 + iq_n) + G^{(1)}(k_2 - q_1)] = \int d\tau \, (-e^{-i(q_m + q_n)\tau} + e^{iq_m\tau}) g_n(\tau) \sum_j e^{-i\mathbf{q}_1\cdot\mathbf{r}_j} h(\mathbf{r}_j, \tau) G^{(1)}(\mathbf{r}_j, -\tau)$$

$$= \frac{1}{iq_n} \int d\tau \, (-e^{-iq_m\tau} + e^{-i(q_m + q_n)\tau} + e^{i(q_m + q_n)\tau} - e^{iq_m\tau})$$

$$\times \sum_j e^{-i\mathbf{q}_1\cdot\mathbf{r}_j} h(\mathbf{r}_j, \tau) G^{(1)}(\mathbf{r}_j, -\tau), \quad (C54)$$

assuming $q_n \neq 0$. Inserting this expression into Eq. (C52), we get

$$\chi_{j_x j_x}^{v_2}(iq_n) = \frac{1}{iq_n} \frac{U}{2} \left(\frac{T}{N}\right)^2 \sum_{k_1, q_1} \frac{\partial \epsilon_{\mathbf{k}}}{\partial k_x}(\mathbf{k}_1) G^{(2)}(k_1) G^{(2)}(k_1 + iq_n) G^{(1)}(k_1 + q_1 + iq_n)$$

$$\times \left(3U_{sp} \frac{1}{1 - \frac{U_{sp}}{2}\chi_0(q_1)} \frac{1}{1 - \frac{U_{sp}}{2}\chi_0(q_1 + iq_n)} + U_{ch} \frac{1}{1 + \frac{U_{ch}}{2}\chi_0(q_1)} \frac{1}{1 + \frac{U_{ch}}{2}\chi_0(q_1 + iq_n)} \right)$$

$$\times \int d\tau \, (-e^{-iq_m\tau} + e^{-i(q_m + q_n)\tau} + e^{i(q_m + q_n)\tau} - e^{iq_m\tau}) \sum_j e^{-i\mathbf{q}_1\cdot\mathbf{r}_j} h(\mathbf{r}_j, \tau) G^{(1)}(\mathbf{r}_j, -\tau). \quad (C55)$$

Using the definitions

$$\bar{G}_n^{(1)}(k_1 + q_1) = G^{(1)}(k_1 + q_1 + iq_n) \quad (C56)$$

and

$$H_n(q_1) = \left(3U_{sp} \frac{1}{1 - \frac{U_{sp}}{2}\chi_0(q_1)} \frac{1}{1 - \frac{U_{sp}}{2}\chi_0(q_1 + iq_n)} + U_{ch} \frac{1}{1 + \frac{U_{ch}}{2}\chi_0(q_1)} \frac{1}{1 + \frac{U_{ch}}{2}\chi_0(q_1 + iq_n)} \right)$$
$$\times \int d\tau \, (e^{i(q_m+q_n)\tau} + e^{-i(q_m+q_n)\tau} - e^{iq_m\tau} - e^{-iq_m\tau}) \sum_j e^{-i\mathbf{q}_1\cdot\mathbf{r}_j} h(\mathbf{r}_j,\tau) G^{(1)}(\mathbf{r}_j, -\tau), \qquad \text{(C57)}$$

Eq. (C55) reads

$$\chi_{j_x j_x}^{v_2}(iq_n) = \frac{1}{iq_n} \frac{U}{2} \frac{T}{N} \sum_{k_1} \frac{\partial \epsilon_{\mathbf{k}}}{\partial k_x}(\mathbf{k}_1) G^{(2)}(k_1) G^{(2)}(k_1 + iq_n) \frac{T}{N} \sum_{q_1} \bar{G}_n^{(1)}(k_1 + q_1) H_n(q_1)$$
$$= \frac{1}{iq_n} \frac{U}{2} \frac{T}{N} \sum_{k_1} \frac{\partial \epsilon_{\mathbf{k}}}{\partial k_x}(\mathbf{k}_1) G^{(2)}(k_1) G^{(2)}(k_1 + iq_n) \sum_{\bar{1}} e^{ik_1\cdot\bar{1}} \bar{G}_n^{(1)}(-\bar{1}) H_n(\bar{1}), \qquad \text{(C58)}$$

where the sum over q_1 was written as a FT. Unfortunately, since this transform does not give a function of k_1 or $k_1 + iq_n$, or a sum of either, because the dependence on iq_n in $H_n(q_1)$ does not factor out as a sum of exponentials, the sum over k_1 does not have the form of a convolution or a sum of convolutions and has to be done in the form of Eq. (C58) for each different frequency iq_n.

Now, some work remains to be done before one can do the FT over $\bar{1}$ in Eq. (C58). First, $G_n^{(1)}(\mathbf{r},\tau)$ is explicitly given by

$$G_n^{(1)}(\mathbf{r},\tau) = \frac{1}{N} \sum_{\mathbf{k}} e^{i\mathbf{k}\cdot\mathbf{r}} T \sum_m e^{-ik_m\tau} \frac{1}{ik_m + iq_n - \tilde{\epsilon}_{\mathbf{k}}}, \quad \text{(C59)}$$

so that by changing the summation variable above or using Eq. (C23), we obtain

$$G_n^{(1)}(\mathbf{r},\tau) = e^{iq_n\tau} G^{(1)}(\mathbf{r},\tau). \qquad \text{(C60)}$$

Equation (C58) thus becomes

$$\chi_{j_x j_x}^{v_2}(iq_n) = \frac{1}{iq_n} \frac{U}{2} \frac{T}{N} \sum_{\mathbf{k},ik_m} \frac{\partial \epsilon_{\mathbf{k}}}{\partial k_x}(\mathbf{k}) G^{(2)}(\mathbf{k},ik_m) G^{(2)}(\mathbf{k},ik_m + iq_n)$$
$$\times \sum_{\mathbf{r}} \int d\tau \, e^{i\mathbf{k}\cdot\mathbf{r}} e^{-i(k_m+q_n)\tau} G^{(1)}(\mathbf{r},-\tau) H_n(\mathbf{r},\tau). \qquad \text{(C61)}$$

There is, however, a problem if we directly use $H_n(\mathbf{r},\tau)$ in Eq. (C61). From definition (C57), we notice that $H_n(\mathbf{q},iq_m)$ is peaked at the frequency $q_m = -q_n$ because of the factor

$$\frac{1}{1 - \frac{U_{sp}}{2}\chi_0(\mathbf{q},iq_m + iq_n)} \qquad \text{(C62)}$$

in the spin part. Therefore, $H_n(\mathbf{r},\tau)$ has oscillations in τ at the frequency q_n, and it is necessary to refine the grid in τ when q_n increases. $H_n(\mathbf{q},iq_m)$ is also peaked at $q_m = 0$ because of the factor

$$\frac{1}{1 - \frac{U_{sp}}{2}\chi_0(\mathbf{q},iq_m)}. \qquad \text{(C63)}$$

It is therefore not sufficient to express $H_n(\mathbf{r},\tau)$ using a function shifted in frequency multiplied by an oscillating function. By doing that we would reduce at most the oscillation frequency by half. Instead, we express $H_n(\mathbf{r},\tau)$ as a sum of two functions, one peaked at $q_m = 0$ and the other at $q_m = -q_n$. Then we

will be able to apply a translation in frequency to the latter and factor out the oscillating part. First, we write

$$\frac{1}{1 - \frac{U_{sp}}{2}\chi_0(\mathbf{q},iq_m + iq_n)} \frac{1}{1 - \frac{U_{sp}}{2}\chi_0(\mathbf{q},iq_m)}$$
$$= \frac{1}{\chi_0(\mathbf{q},iq_m) - \chi_0(\mathbf{q},iq_m + iq_n)} \frac{\chi_0(\mathbf{q},iq_m)}{1 - \frac{U_{sp}}{2}\chi_0(\mathbf{q},iq_m)}$$
$$+ \frac{1}{\chi_0(\mathbf{q},iq_m + iq_n) - \chi_0(\mathbf{q},iq_m)} \frac{\chi_0(\mathbf{q},iq_m + iq_n)}{1 - \frac{U_{sp}}{2}\chi_0(\mathbf{q},iq_m + iq_n)}. \qquad \text{(C64)}$$

If we define

$$D(\mathbf{q},iq_m) = \int d\tau \, (e^{iq_m\tau} + e^{-iq_m\tau})$$
$$\times \sum_j e^{-i\mathbf{q}\cdot\mathbf{r}_j} h(\mathbf{r}_j,\tau) G^{(1)}(\mathbf{r}_j, -\tau), \quad \text{(C65)}$$

the spin part of $H_n(\mathbf{q},iq_m)$ reads

$$-\frac{D(\mathbf{q},iq_m) - D(\mathbf{q},iq_m + iq_n)}{\chi_0(\mathbf{q},iq_m) - \chi_0(\mathbf{q},iq_m + iq_n)} \chi_{sp}(\mathbf{q},iq_m)$$
$$+ \frac{D(\mathbf{q},iq_m + iq_n) - D(\mathbf{q},iq_m)}{\chi_0(\mathbf{q},iq_m + iq_n) - \chi_0(\mathbf{q},iq_m)} \chi_{sp}(\mathbf{q},iq_m + iq_n). \qquad \text{(C66)}$$

Note that, since $D(\mathbf{q},iq_m)$ and $\chi_0(\mathbf{q},iq_m)$ are even functions, the function

$$\frac{D(\mathbf{q},iq_m) - D(\mathbf{q},iq_m + iq_n)}{\chi_0(\mathbf{q},iq_m) - \chi_0(\mathbf{q},iq_m + iq_n)} \qquad \text{(C67)}$$

is undetermined when $q_m = -q_n/2$, which happens when n is even. However, we know that $H_n(\mathbf{q}, -\frac{iq_n}{2})$ vanishes so that one can assume an arbitrary value for Eq. (C67) at that point. Numerically, it is better for that factor to be smooth. This is achieved by using a simple interpolation to fix that value.

Now, if we define the function

$$I_n(\mathbf{q},iq_m) \qquad \text{(C68)}$$
$$= 3U_{sp} \frac{D(\mathbf{q},iq_m) - D(\mathbf{q},iq_m + iq_n)}{\chi_0(\mathbf{q},iq_m) - \chi_0(\mathbf{q},iq_m + iq_n)} \frac{\chi_0(\mathbf{q},iq_m)}{1 - \frac{U_{sp}}{2}\chi_0(\mathbf{q},iq_m)}$$
$$+ U_{ch} \frac{D(\mathbf{q},iq_m) - D(\mathbf{q},iq_m + iq_n)}{\chi_0(\mathbf{q},iq_m) - \chi_0(\mathbf{q},iq_m + iq_n)} \frac{\chi_0(\mathbf{q},iq_m)}{1 + \frac{U_{ch}}{2}\chi_0(\mathbf{q},iq_m)},$$

which is peaked at $q_m = 0$, we make explicit that $H_n(\mathbf{q}, iq_m)$ is peaked at two values of frequency

$$H_n(\mathbf{q}, iq_m) = -I_n(\mathbf{q}, iq_m) + I_n(\mathbf{q}, -iq_m - iq_n). \quad \text{(C69)}$$

Using the bosonic Matsubara frequency representation for $I_n(\mathbf{q}, \tau)$ we obtain

$$H_n(\mathbf{q}, \tau) = T \sum_{iq_m} e^{-iq_m \tau} H_n(\mathbf{q}, iq_m)$$
$$= -I_n(\mathbf{q}, \tau) + e^{iq_n \tau} I_n(\mathbf{q}, -\tau). \quad \text{(C70)}$$

To compute $I_n(\mathbf{q}, \tau)$ from $I_n(\mathbf{q}, iq_m)$ we use the same procedure as for the previous FTs over Matsubara frequencies. Using

$$D_{inf}(\mathbf{q}, iq_m) = \frac{d(\mathbf{q})}{(iq_m)^2},$$
$$\chi_{0,inf}(\mathbf{q}, iq_m) = \frac{c(\mathbf{q})}{(iq_m)^2}, \quad \text{(C71)}$$

the asymptotic form for $I_n(\mathbf{q}, iq_m)$ is

$$I_n^{inf}(\mathbf{q}, iq_m) = 3U_{sp} \frac{d(\mathbf{q})}{(iq_m)^2 - \frac{U_{sp}}{2} c(\mathbf{q})}$$
$$+ U_{ch} \frac{d(\mathbf{q})}{(iq_m)^2 + \frac{U_{ch}}{2} c(\mathbf{q})}. \quad \text{(C72)}$$

Using a complex plane integration and the residue theorem, we get

$$I_n^{inf}(\mathbf{q}, \tau) = 3U_{sp} \frac{d(\mathbf{q})}{2z_{sp}(\mathbf{q})} \left(n_B(-z_{sp}(\mathbf{q})) e^{-z_{sp}(\mathbf{q})\tau} \right.$$
$$\left. - n_B(z_{sp}(\mathbf{q})) e^{z_{sp}(\mathbf{q})\tau} \right)$$
$$+ U_{ch} \frac{d(\mathbf{q})}{2iz_{ch}(\mathbf{q})} \left(n_B(-iz_{ch}(\mathbf{q})) e^{-iz_{ch}(\mathbf{q})\tau} \right.$$
$$\left. - n_B(iz_{ch}(\mathbf{q})) e^{iz_{ch}(\mathbf{q})\tau} \right), \quad \text{(C73)}$$

where $n_B(z)$ is the Bose–Einstein distribution and

$$z_{sp}(\mathbf{q}) = \sqrt{\frac{U_{sp}}{2} c(\mathbf{q})},$$
$$z_{ch}(\mathbf{q}) = \sqrt{\frac{U_{ch}}{2} c(\mathbf{q})}, \quad \text{(C74)}$$

or, using $n_B(-z) = -e^{\beta z} n_B(z)$,

$$I_n^{inf}(\mathbf{q}, \tau)$$
$$- 3U_{sp} \frac{d(\mathbf{q})}{z_{sp}(\mathbf{q})} n_B(z_{sp}(\mathbf{q})) e^{\frac{\beta}{2} z_{sp}(\mathbf{q})} \cosh\left[\left(\frac{\beta}{2} - \tau \right) z_{sp}(\mathbf{q}) \right]$$
$$- U_{ch} \frac{d(\mathbf{q})}{iz_{ch}(\mathbf{q})} n_B(iz_{ch}(\mathbf{q})) e^{i\frac{\beta}{2} z_{ch}(\mathbf{q})} \cos\left[\left(\frac{\beta}{2} - \tau \right) z_{ch}(\mathbf{q}) \right]. \quad \text{(C75)}$$

Using that result we write, as before, the transform in such a way that it converges quickly:

$$I_n(\mathbf{q}, \tau) = T \sum_{iq_m}' e^{-iq_m \tau} \left[I_n(\mathbf{q}, iq_m) - I_n^{inf}(\mathbf{q}, iq_m) \right]$$
$$+ I_n^{inf}(\mathbf{q}, \tau). \quad \text{(C76)}$$

There is, however, one last difficulty. The asymptotic form, Eq. (C72), approaches Eq. (C68) only when both q_m and $q_m + q_n$ are large with respect to the bandwidth. Thus, the frequency range of the finite sum in Eq. (C76) has to be chosen such that this condition is satisfied. If q_n is positive, the range of negative q_m must therefore be extended to make sure that, at the cutoff, $q_m + q_n$ is large.

Coming back to expression (C58), using results (C60) and (C70), the sum over $\bar{1}$ becomes

$$\sum_{\bar{1}} e^{ik_1 \cdot \bar{1}} G_n^{(1)}(-\bar{1}) H_n(\bar{1})$$
$$= \sum_{\mathbf{r}} \int d\tau\, e^{i\mathbf{k}\cdot\mathbf{r}} e^{-i(k_m + q_n)\tau} G^{(1)}(\mathbf{r}, -\tau)$$
$$\times [-I_n(\mathbf{r}, \tau) + e^{iq_n \tau} I_n(\mathbf{r}, -\tau)]$$
$$= \sum_{\mathbf{r}} \int d\tau\, e^{i\mathbf{k}\cdot\mathbf{r}} e^{-ik_m \tau} [-e^{-iq_n \tau} G^{(1)}(\mathbf{r}, -\tau) I_n(\mathbf{r}, \tau)$$
$$+ G^{(1)}(\mathbf{r}, -\tau) I_n(\mathbf{r}, -\tau)]. \quad \text{(C77)}$$

For $q_n = 0$, expression (C52) vanishes, as explained at the end of Appendix B.

To reach reasonably low temperatures without seeing any finite size effect, we use a system of 512×512 sites and 8192 frequencies. If we were using a brute force approach to compute Eq. (C52) we would have to sum $[(8192(512^2))^3 = 9.9 \times 10^{27}]$ terms. Assuming we could sum 10^9 terms per second, it would take about 300 billion years to calculate $\chi_{j_x j_x}^{v_2}(iq_n)$ for one value of q_n and thus about 30 000 billion years for a hundred values of q_n. Using the approach described above, this calculation is done in less than 2 days.

APPENDIX D: CHOICE OF MATSUBARA FREQUENCIES

While all external frequencies are obtained at the same time from the last FFT for the bubble and MT-like term in $\chi_{j_x j_x}(iq_n)$, this is not the case for the AL-like term, Eq. (C52), even in the form of Eq. (C58) that makes maximal use of FFTs. Hence, this term cannot be calculated for thousands of values of q_n or for the same number as that used in internal Matsubara frequency sums. Therefore we have to compute Eq. (C58) for a reasonable number of carefully chosen frequencies. Assuming that most of the information is in the low frequencies and that as their magnitude increases it becomes less important to include all the high frequencies, we use the following nonuniform Matsubara frequency index grid. That grid consists of subintervals within which the Matsubara frequencies are equally spaced, with larger space in between Matsubara frequencies at large frequency. The spacing between frequencies in different subintervals increases by powers of 2.

First we define

$N_0 = 2^r$: the last frequency index (cutoff), taken as a power of 2 (r integer);

m: integer that determines how dense the grid is. A large m gives a low density. $0 \leqslant m < r$;

$N_1 = \frac{N_0}{2^m}$: $N_1 + 1$ is the number of adjacent frequencies close to $n = 0$;

$N_2 = \frac{N_1}{2}$: number of frequencies in each subinterval with a fixed spacing between Matsubara frequencies;

$N = N_1 + m N_2 + 1$: total number of frequencies.

Then the indices of Matsubara frequencies on the grid are given by the following algorithm

$$
n(j) = \begin{cases} j, & j = 0, \ldots, N_1 - 1, \\ N_1 + 2^{l_j+1}\mathrm{mod}(j - N_1, N_2) + N_1(2^{l_j} - 1), \\ l_j = \mathrm{floor}\left(\frac{j - N_1}{N_2}\right), & j = N_1, \ldots, N - 1. \end{cases} \quad \text{(D1)}
$$

For example, taking $N_0 = 256$, $m = 5$, so that $N_1 = 8$, $N_2 = 4$ and a total number of frequencies $N = 29$, we obtain the following indices: $n = 0, 1, 2, 3, 4, 5, 6, 7, 8, 10, 12, 14,$ $16, 20, 24, 28, 32, 40, 48, 56, 64, 80, 96, 112, 128, 160, 192,$ $224, 256$.

With this kind of grid we greatly reduce the number of frequencies for which we have to calculate $\chi_{j_x j_x}^{v_2}$ with Eq. (C58) while retaining the essential information. Note that this also speeds up the analytical continuation with our maximum entropy method described in Appendix F.

APPENDIX E: FOURIER TRANSFORM OF A CUBIC SPLINE

Assume we have the following integral to do,

$$
f(k) = \int_{x_0}^{x_N} dx\, g(x)e^{-ikx}, \quad \text{(E1)}
$$

but that we know only $N + 1$ discrete values of $g(x_i)$. Let us approximate $g(x)$ in the interval using a cubic spline $S(x)$ defined as

$$
S(x) = \begin{cases} S_1(x) & x_0 < x < x_1 \\ S_2(x) & x_1 < x < x_2 \\ \quad \vdots \\ S_N(x) & x_{N-1} < x < x_N \end{cases}, \quad \text{(E2)}
$$

where the $S_n(x)$ are cubic polynomials, with the conditions

$$
\begin{aligned}
S_n(x_{n-1}) &= g(x_{n-1}), \quad S_n(x_n) = g(x_n), \\
S_n'(x_{n-1}) &= S_{n-1}'(x_{n-1}), \quad n > 1, \\
S_n''(x_{n-1}) &= S_{n-1}''(x_{n-1}), \quad n > 1, \quad \text{(E3)} \\
S_1'(x_0) &= g'(x_0), \quad S_N'(x_N) = g'(x_N),
\end{aligned}
$$

defining the $4N$ equations necessary to determine the $4N$ coefficients of the spline. The integral of Eq. (E1) becomes

$$
f(k) \approx \sum_{n=1}^{N} \int_{x_{n-1}}^{x_n} dx\, S_n(x)e^{-ikx}. \quad \text{(E4)}
$$

Integrating by parts we obtain

$$
\begin{aligned}
f(k) &= -\frac{1}{ik}\sum_{n=1}^{N}\left(e^{-ikx}S_n(x)\Big|_{x_{n-1}}^{x_n}\right) \\
&\quad + \frac{1}{ik}\sum_{n=1}^{N}\int_{x_{n-1}}^{x_n} dx\, S_n'(x)e^{-ikx} \\
&= \frac{e^{-ikx_0}S_1(x_0) - e^{-ikx_N}S_N(x_N)}{ik} \\
&\quad + \frac{1}{ik}\sum_{n=1}^{N}\int_{x_{n-1}}^{x_n} dx\, S_n'(x)e^{-ikx}, \quad \text{(E5)}
\end{aligned}
$$

where we have used the continuity of the spline at the points x_n to eliminate all the intermediate terms in the first sum. Now, if we integrate by parts in the second term and use the continuity of the derivatives $S_n'(x)$ at the points $x = x_n$, we obtain

$$
\begin{aligned}
f(k) &= \frac{e^{-ikx_0}S_1(x_0) - e^{-ikx_N}S_N(x_N)}{ik} \\
&\quad + \frac{e^{-ikx_0}S_1'(x_0) - e^{-ikx_N}S_N'(x_N)}{(ik)^2} \\
&\quad + \frac{1}{(ik)^2}\sum_{n=1}^{N}\int_{x_{n-1}}^{x_n} dx\, S_n''(x)e^{-ikx}. \quad \text{(E6)}
\end{aligned}
$$

Doing it one last time, using the fact that we also have the continuity of the second derivatives $S_n''(x)$ at x_n, we finally obtain

$$
\begin{aligned}
f(k) &= \frac{e^{-ikx_0}S_1(x_0) - e^{-ikx_N}S_N(x_N)}{ik} \\
&\quad + \frac{e^{-ikx_0}S_1'(x_0) - e^{-ikx_N}S_N'(x_N)}{(ik)^2} \\
&\quad + \frac{e^{-ikx_0}S_1''(x_0) - e^{-ikx_N}S_N''(x_N)}{(ik)^3} \\
&\quad + \frac{1 - e^{-ik\Delta x}}{(ik)^4}\sum_{n=0}^{N-1} S_{n+1}^{(3)}e^{-ikx_n}, \quad \text{(E7)}
\end{aligned}
$$

where $\Delta x = x_{n+1} - x_n$. The remaining discrete transform can be done using an FFT. The result of this transform will be periodic since it is discrete, but because of the factor $1/(ik)^4$ in front, it will have a relevant contribution only for small k. This periodicity in the sum therefore produces only a very small noise at high k, the remaining discretization noise, that decreases with increasing k. Note that expression (E7) is valid only for $k \neq 0$. For $k = 0$, the result is simply the sum, over all subintervals, of integrals of cubic polynomials with their respective coefficients.

Finally, note that we have chosen to fix the value of the derivatives at the boundaries to complete the system of equations (E3) defining the spline. But other interesting choices are also possible. For example, if we know the coefficients of the terms in $1/(k^2)$ and $1/(k^3)$, i.e., the numerator in the second and third terms of Eq. (E7), fixing those coefficients is a good alternative. In the case where k is a frequency, this choice is convenient because we often know the high-frequency expansion from sum rules.

APPENDIX F: ANALYTICAL CONTINUATION FOR THE CONDUCTIVITY

Let us start by rewriting the spectral representation for the Matsubara current-current correlation function $\chi_{j_x j_x}(iq_n)$,

$$
\begin{aligned}
\chi_{j_x j_x}(iq_n) &= \int \frac{d\omega}{\pi}\frac{\chi_{j_x j_x}''(\omega)}{\omega - iq_n} \\
&= iq_n\int\frac{d\omega}{\pi}\frac{\chi_{j_x j_x}''(\omega)}{\omega^2 + q_n^2} + \int\frac{d\omega}{\pi}\frac{\omega\,\chi_{j_x j_x}''(\omega)}{\omega^2 + q_n^2}. \quad \text{(F1)}
\end{aligned}
$$

Since $\chi''_{j_x j_x}(\omega)$ is odd,

$$\chi_{j_x j_x}(iq_n) = \int \frac{d\omega}{\pi} \frac{\omega \, \chi''_{j_x j_x}(\omega)}{\omega^2 + q_n^2}. \tag{F2}$$

The real part of the optical conductivity is

$$\sigma^r(\omega) = \frac{\chi''_{j_x j_x}(\omega)}{\omega}, \tag{F3}$$

so that we obtain

$$\chi_{j_x j_x}(iq_n) = 2 \int_0^\infty \frac{d\omega}{\pi} \frac{\omega^2}{\omega^2 + q_n^2} \sigma^r(\omega), \tag{F4}$$

using the fact that the integrand is even. This is our starting point. The objective is to obtain the real part of the conductivity, on the right-hand side, from the Matsubara expression for the susceptibility on the left-hand side. Most analytical continuation is done for imaginary-time data, but not in our case.[75]

Suppose we could be satisfied with $\sigma^r(\omega)$ on a discrete set of points ω_j. We can use a numerical integration method to approximate the integral of Eq. (F4), which would then have the form

$$\chi_{j_x j_x}(iq_n) \approx \sum_j K_{nj} \sigma_j^r, \tag{F5}$$

where $\sigma_j^r = \sigma^r(\omega_j)$ and K_{nj} is a $N_{q_n} \times N_\omega$ matrix, N_{q_n} being the size of the vector $\chi_{j_x j_x}(iq_n)$ and N_ω the size of the vector σ_j^r. Now, σ_j^r is the quantity we want to determine. If $N_{q_n} = N_\omega$ then σ_j^r is completely determined by the linear system (F5). However, the matrix K_{nj} is ill-conditioned so that a small noise in $\chi_{j_x j_x}(iq_n)$ would result in a very noisy solution σ_j^r. Also, N_{q_n} is generally smaller than N_ω, the number of real frequencies for which we want to determine $\sigma^r(\omega)$. We therefore need to include more information in the problem to find a unique σ_j^r. The way to do this is to use a maximum entropy approach. In this approach, we minimize the function

$$\chi^2 - \alpha S, \tag{F6}$$

where

$$\chi^2 = \sum_{\{iq_n\}} \left(\frac{\chi_{j_x j_x}(iq_n) - \sum_j K_{nj} \sigma_j^r}{\epsilon_n} \right)^2$$

$$= \sum_{\{iq_n\}} \left(\frac{\chi_{j_x j_x}(iq_n) - \bar{\chi}_{j_x j_x}(iq_n)}{\epsilon_n} \right)^2 \tag{F7}$$

measures the deviation of $\bar{\chi}_{j_x j_x}(iq_n) = \sum_j K_{nj} \sigma_j^r$ with respect to $\chi_{j_x j_x}(iq_n)$, ϵ_n being an estimate of the error of $\chi_{j_x j_x}(iq_n)$ with respect to the "exact" function. S is the differential entropy defined as

$$S = -\int_0^\infty d\omega \, \sigma^r(\omega) \ln \frac{\sigma^r(\omega)}{m(\omega)}, \tag{F8}$$

where $m(\omega)$ is called the default model. The value of α can be chosen according to different criteria. As is often done, we choose it such that $\chi^2 \approx N_{q_n}$, so that $|\chi_{j_x j_x}(iq_n) - \bar{\chi}_{j_x j_x}(iq_n)|$ is equal to ϵ_n on average.

Errors in the numerical evaluation of the integral of (F4), i.e., in the definition of K_{nj} in Eq. (F5), are equivalent to having larger errors in the data $\chi_{j_x j_x}(iq_n)$. Therefore, when

Eq. (F6) is minimized to find a solution σ_j^r, this could lead to large errors in σ_j^r with respect to the optimal solution because the inversion of expression (F4) is an ill-conditioned problem. It is thus clear that the error we make by replacing Eq. (F4) by Eq. (F5) must be smaller than the estimated error ϵ_n on the original data $\chi_{j_x j_x}(iq_n)$. That is why we need a very accurate numerical integration technique to define K_{nj}. Because we use the spectral representation in Matsubara frequencies, the weight function $\omega^2/(\omega^2 + q_n^2)$ in the integrand of Eq. (F4) is simple and can be integrated analytically. Hence, if we use, for example, a polynomial approximation for $\sigma^r(\omega)$ in a given interval $[\omega_{j-1}, \omega_j]$, the integral can also be done analytically in the interval. If we use a good piecewise polynomial approximation for $\sigma^r(\omega)$, then we can evaluate the integral of Eq. (F4) precisely.

Maybe the most efficient approach to integrate Eq. (F4) in one dimension is Gaussian quadratures. However, in the latter, both the weights and the grid points depend on the weight function, which in our case depends on q_n. We would therefore need a different grid in ω for each frequency iq_n. This is not possible because we can search for only a unique vector σ_j^r defined on a unique grid ω_j. Another very efficient way of doing the integrals of Eq. (F4) is to model $\sigma^r(\omega)$ using a cubic spline. This approach allows us to use a fixed grid and is very precise because cubic splines are very good to approximate smooth functions, which is the case of $\sigma^r(\omega)$. It seems therefore the best approach for our problem. However, to be able to perform the integral of Eq. (F4) over the whole frequency range $[0, \infty]$, and at the same time reduce the number of frequencies in the grid, which helps speed up the minimization of Eq. (F6), the spline we use is divided into two parts, a low-frequency part that is a cubic spline in ω and a high-frequency part cubic in $u = 1/\omega$. Then, to make the spline linear system well conditioned, we use a grid that is uniform in ω in the low-frequency part and uniform in u in the high-frequency part. Finally, integrating analytically in a piecewise manner, keeping the weight function $\omega^2/(\omega^2 + q_n^2)$ intact in the integrand is a great advantage as the temperature decreases since this function then becomes sharper and sharper and is thus increasingly difficult to integrate numerically. Of course the conductivity $\sigma^r(\omega)$ itself becomes also sharper as T decreases and we have to adjust the grid to resolve its structure. But the numerical integration is still much easier and precise with this approach. We describe below how the K_{nj} is defined and also our choice of grid in ω.

We start with the following representation for $\sigma^r(\omega)$,

$$\sigma^r(\omega) = \begin{cases} s_j(\omega), & \omega_{j-1} \leqslant \omega \leqslant \omega_j, & 1 \leqslant j \leqslant N \\ s_j(\frac{1}{\omega}), & \omega_{j-1} \leqslant \omega \leqslant \omega_j, & N < j \leqslant N+M \end{cases}, \tag{F9}$$

where $s_j(x) = a_j x^3 + b_j x^2 + c_j x + d_j$, with the conditions

$$\begin{aligned} s_j(\omega_{j-1}) &= \sigma_{j-1}^r, \\ s_j(\omega_j) &= \sigma_j^r, \\ s_j'(\omega_{j-1}) &= s_{j-1}'(\omega_{j-1}), \\ s_j''(\omega_{j-1}) &= s_{j-1}''(\omega_{j-1}), \\ s_1'(0) &= 0, \end{aligned} \tag{F10}$$

for $j \leqslant N$, while

$$s_{N+1}\left(\frac{1}{\omega_N}\right) = \sigma_N^r,$$

$$s_{N+1}\left(\frac{1}{\omega_{N+1}}\right) = \sigma_{N+1}^r,$$

$$s'_{N+1}\left(\frac{1}{\omega_N}\right) = s'_N(\omega_N), \qquad \text{(F11)}$$

$$s''_{N+1}\left(\frac{1}{\omega_N}\right) = s''_N(\omega_N),$$

and

$$s_j\left(\frac{1}{\omega_{j-1}}\right) = \sigma_{j-1}^r,$$

$$s_j\left(\frac{1}{\omega_j}\right) = \sigma_j^r,$$

$$s'_j\left(\frac{1}{\omega_{j-1}}\right) = s'_{j-1}\left(\frac{1}{\omega_{j-1}}\right), \qquad \text{(F12)}$$

$$s''_j\left(\frac{1}{\omega_{j-1}}\right) = s''_{j-1}\left(\frac{1}{\omega_{j-1}}\right),$$

$$\left.\frac{\partial s_{N+M}\left(\frac{1}{\omega}\right)}{\partial \frac{1}{\omega}}\right|_{\omega=\infty} = 0,$$

for $N + 1 < j \leqslant N + M$. All the derivatives noted with $'$ and $''$ are taken with respect to ω. The second condition for $j = N + M$ and the last condition in Eq. (F12) make sure that there is no constant and no $1/\omega$ terms in $s_{N+M}(1/\omega)$ so that the integral of the spline converges. Note that this spline is not physically correct for $\omega \to \infty$ since the moments of $\sigma^r(\omega)$ are not defined. But this does not have any significant importance in the numerical solution if ω_{N+M-1} is chosen large enough. The advantage of this spline is that it is very easy to implement.

Let us now define the kernel K_{nj} in Eq. (F5). For the low-frequency part of Eq. (F4) we have

$$\chi_{j_x j_x}^{lf}(iq_n) = 2\int_0^{\omega_N} \frac{d\omega}{\pi} \frac{\omega^2}{\omega^2 + q_n^2}\sigma^r(\omega)$$

$$= \frac{2}{\pi}\sum_{j=1}^N \int_{\omega_{j-1}}^{\omega_j} d\omega \frac{\omega^2}{\omega^2 + q_n^2}s_j(\omega)$$

$$= \frac{2}{\pi}\sum_{j=1}^N \int_{\omega_{j-1}}^{\omega_j} d\omega \frac{a_j\omega^5 + b_j\omega^4 + c_j\omega^3 + d_j\omega^2}{\omega^2 + q_n^2}, \qquad \text{(F13)}$$

where $\omega_0 = 0$. For $q_n \neq 0$, we obtain

$$\chi_{j_x j_x}^{lf}(iq_n) = \frac{2}{\pi}\sum_{j=1}^N \left(\left[\frac{q_n^4}{2}\ln\left(q_n^2 + \omega^2\right) - \frac{q_n^2}{2}\omega^2 + \frac{\omega^4}{4}\right]_{\omega_{j-1}}^{\omega_j} a_j\right.$$

$$+ \left[q_n^3 \arctan\left(\frac{\omega}{q_n}\right) - q_n^2\omega + \frac{\omega^3}{3}\right]_{\omega_{j-1}}^{\omega_j} b_j$$

$$+ \left[\frac{\omega^2}{2} - \frac{q_n^2}{2}\ln\left(q_n^2 + \omega^2\right)\right]_{\omega_{j-1}}^{\omega_j} c_j$$

$$+ \left[\omega - q_n \arctan\left(\frac{\omega}{q_n}\right)\right]_{\omega_{j-1}}^{\omega_j} d_j\right), \qquad \text{(F14)}$$

and, for $q_n = 0$,

$$\chi_{j_x j_x}^{lf}(0) = \frac{2}{\pi}\sum_{j=1}^N \int_{\omega_{j-1}}^{\omega_j} d\omega\,(a_j\omega^3 + b_j\omega^2 + c_j\omega + d_j)$$

$$= \frac{2}{\pi}\sum_{j=1}^N \left(\frac{\omega_j^4 - \omega_{j-1}^4}{4}a_j + \frac{\omega_j^3 - \omega_{j-1}^3}{3}b_j\right.$$

$$\left. + \frac{\omega_j^2 - \omega_{j-1}^2}{2}c_j + (\omega_j - \omega_{j-1})d_j\right) \qquad \text{(F15)}$$

The high-frequency part of Eq. (F4) is

$$\chi_{j_x j_x}^{hf}(iq_n) = 2\int_{\omega_N}^{\infty} \frac{d\omega}{\pi} \frac{\omega^2}{\omega^2 + q_n^2}\sigma^r(\omega). \qquad \text{(F16)}$$

Using

$$\omega = \frac{1}{u}, \quad \Rightarrow \quad d\omega = -\frac{1}{u^2}du, \qquad \text{(F17)}$$

it becomes

$$\chi_{j_x j_x}^{hf}(iq_n) = \frac{2}{\pi}\int_0^{u_M} du \frac{1}{u^2 + u^4 q_n^2}\sigma^r\left(\frac{1}{u}\right), \qquad \text{(F18)}$$

where $u_M = 1/\omega_N$. Now, with Eq. (F9), we have

$$\chi_{j_x j_x}^{hf}(iq_n) = \frac{2}{\pi}\sum_{j=1}^M \int_{u_{j-1}}^{u_j} du \frac{1}{u^2 + u^4 q_n^2}s_j(u)$$

$$= \frac{2}{\pi}\sum_{j=1}^M \int_{u_{j-1}}^{u_j} du \frac{\alpha_j u^3 + \beta_j u^2 + \gamma_j u + \delta_j}{u^2 + u^4 q_n^2}, \qquad \text{(F19)}$$

where $1 \leqslant j \leqslant M$, $u_0 = 0$, and we have used a different notation for the coefficients to match their indices with those of grid points in u, which are indexed in order of decreasing ω. For $q_n \neq 0$, we obtain

$$\chi_{j_x j_x}^{hf}(iq_n) = \frac{2}{\pi}\sum_{j=1}^M \left(\left[\frac{1}{2q_n^2}\ln\left(1 + q_n^2 u^2\right)\right]_{u_{j-1}}^{u_j}\alpha_j\right.$$

$$+ \left[\frac{1}{q_n}\arctan(q_n u)\right]_{u_{j-1}}^{u_j}\beta_j$$

$$+ \left[\ln(u) - \frac{1}{2}\ln\left(1 + q_n^2 u^2\right)\right]_{u_{j-1}}^{u_j}\gamma_j$$

$$+ \left[-\frac{1}{u} - q_n \arctan(q_n u)\right]_{u_{j-1}}^{u_j}\delta_j\right), \qquad \text{(F20)}$$

and, for $q_n = 0$,

$$\chi_{j_x j_x}^{hf}(0) = \frac{2}{\pi}\sum_{j=1}^M \int_{u_{j-1}}^{u_j} du \left(\alpha_j u + \beta_j + \frac{\gamma_j}{u} + \frac{\delta_j}{u^2}\right)$$

$$= \frac{2}{\pi}\sum_{j=1}^M \left[\frac{u_j^2 - u_{j-1}^2}{2}\alpha_j + (u_j - u_{j-1})\beta_j\right.$$

$$\left. + \left(\ln\frac{u_j}{u_{j-1}}\right)\gamma_j + \left(\frac{1}{u_{j-1}} - \frac{1}{u_j}\right)\delta_j\right]. \qquad \text{(F21)}$$

Note that $\gamma_1 = 0$ and $\delta_1 = 0$, so that this expression has no problem with $u = 0$.

The spline coefficients for the complete spline are obtained at the same time for both the low-frequency and high-frequency parts using conditions (F10), (F11), and (F12). Because the spline has two parts made of polynomials in ω and $u = 1/\omega$, one must define the spline linear system for that particular case, but this is a rather straightforward task. Note that, for the high-frequency part, the condition of continuity of the first derivatives with respect to u or ω are the same, but that is not true for the continuity of the second derivatives. However, we do not observe any loss of accuracy if the continuity of the second derivatives with respect to u instead of ω is used.

Conditions (F10), (F11), and (F12), put in matrix form, are written as $Av = \bar{\sigma}$, where v is a vector containing the spline coefficients and $\bar{\sigma}$ is a vector containing the values σ_j^r (that are repeated) and zeros otherwise. We want to obtain the coefficients as linear forms of the vector σ^r. For that we have to invert the matrix A and first obtain a linear form for v. The first two lines of condition (F10) tell us that $\bar{\sigma}$ contains the elements σ_j^r repeated twice each, except for σ_0^r, and the other elements of $\bar{\sigma}$ are zeros. So if we define the matrix $P_{A\sigma}$ that sums up the pairs of columns in A^{-1} corresponding to the same σ_j^r and remove all columns that correspond to zeros in $\bar{\sigma}$ we get

$$v = A^{-1} P_{A\sigma} \sigma^r$$
$$= T_{v\sigma} \sigma^r. \tag{F22}$$

Then the vectors formed with the coefficients are given by expressions like

$$a = P_a v, \quad b = P_b v, \ldots, \tag{F23}$$

where P_a extracts a column formed of all the coefficients of the cubic terms, P_b are the coefficients of the quadratic terms, etc. Now, expressions (F14) and (F15) have the matrix form

$$\chi_{j_x j_x}^{lf}(iq_n) = \frac{2}{\pi}\left(\bar{K}_n^a a + \bar{K}_n^b b + \bar{K}_n^c c + \bar{K}_n^d d\right), \tag{F24}$$

which becomes, using Eqs. (F23) and (F22),

$$\chi_{j_x j_x}^{lf}(iq_n) = \frac{2}{\pi}\left(\bar{K}_n^a P_a + \bar{K}_n^b P_b + \bar{K}_n^c P_c + \bar{K}_n^d P_d\right)T_{v\sigma}\sigma^r. \tag{F25}$$

Similarly, if we define the projectors for the vectors α, β, γ, and δ, then Eqs. (F20) and (F21) take the form

$$\chi_{j_x j_x}^{hf}(iq_n) = \frac{2}{\pi}\left(\bar{K}_n^\alpha P_\alpha + \bar{K}_n^\beta P_\beta + \bar{K}_n^\gamma P_\gamma + \bar{K}_n^\delta P_\delta\right)T_{v\sigma}\sigma^r. \tag{F26}$$

Summing Eqs. (F25) and (F26) we obtain

$$\chi_{j_x j_x}(iq_n) = K_n \sigma^r, \tag{F27}$$

with

$$K_n = \frac{2}{\pi}\left(\bar{K}_n^a P_a + \bar{K}_n^b P_b + \bar{K}_n^c P_c + \bar{K}_n^d P_d\right.$$
$$\left. + \bar{K}_n^\alpha P_\alpha + \bar{K}_n^\beta P_\beta + \bar{K}_n^\gamma P_\gamma + \bar{K}_n^\delta P_\delta\right)T_{v\sigma}. \tag{F28}$$

To conclude this section, a few other points must be addressed. First, the form of expression (F14) becomes numerically unstable when q_n/ω are large. For example, the first two terms in the high q_n/ω expansion of $\frac{q_n^4}{2}\ln(q_n^2 + \omega^2)$ in $\bar{K}_n^a$ cancel out the terms $-\frac{q_n^2}{2}\omega^2$ and $\frac{\omega^4}{4}$. When q_n/ω increases, the magnitude of those terms becomes much larger than $\bar{K}_n^a$ itself so that if one computes numerically the three terms of $\bar{K}_n^a$ separately and then adds them, the finite precision error becomes larger than the true result. To overcome this problem one simply has to use the large q_n/ω expansion of $\bar{K}_n^a$ starting at a certain cutoff, instead of directly the form appearing in Eq. (F14). The same kind of cancellation appears in the other terms of Eq. (F14) so that the large q_n/ω expansions must be used for those terms as well. In the case of Eq. (F20) it is when $q_n u$ is small that some simplifications occur when replacing the expressions by their expansions, which will also improve the accuracy of the numerical result.

Second, since we invert the spline matrix A to define $T_{v\sigma}$ in Eq. (F22), it is preferable that this matrix be well conditioned. For that purpose we define our grid to be uniform in ω for the low-frequency part of the spline and uniform in u for the high-frequency part. The grid in u is

$$u = 0, \frac{1}{\omega_{N+M-1}}, \quad \frac{1}{\omega_{N+M-2}}, \ldots, \frac{1}{\omega_N}. \tag{F29}$$

If $u_j - u_{j-1}$ is constant we have

$$\omega_{N+M-2} = \frac{\omega_{N+M-1}}{2},$$
$$\omega_{N+M-3} = \frac{\omega_{N+M-1}}{3}, \ldots, \quad \omega_N = \frac{\omega_{N+M-1}}{M} \tag{F30}$$

or

$$\omega_{N+1} = \frac{M\omega_N}{M-1},$$
$$\omega_{N+2} = \frac{M\omega_N}{M-2}, \ldots, \quad \omega_{N+M-1} = M\omega_N. \tag{F31}$$

Also, to have a density of points ω_j that varies continuously when we change from high to low frequency, we assume that $\omega_{N+1} - \omega_N = \omega_N - \omega_{N-1}$. Defining $\Delta\omega_{lf} = \omega_N - \omega_{N-1}$, we have

$$\frac{M\omega_N}{M-1} - \omega_N = \Delta\omega_{lf}, \tag{F32}$$

so that

$$M = \frac{\omega_N}{\Delta\omega_{lf}} + 1, \tag{F33}$$

and, if $\omega_j - \omega_{j-1}$ is constant for $j \leqslant N$,

$$\Delta\omega_{lf} = \frac{\omega_N}{N}, \tag{F34}$$

so that $M = N + 1$. Note that when choosing ω_N and N, we have to check that the last frequency $\omega_{N+M-1} = (N+1)\omega_N$ is large enough while not so large that it would uselessly make the calculation heavy. To further improve the conditioning of the matrix A, we use normalized frequencies $\omega_j' = \omega_j/\omega_N$ so

that $\omega'_N = 1$ and $u'_M = 1$. In the jth interval, if a'_j, b'_j, c'_j, and d'_j are the coefficients in the normalized grid, we have

$$\sigma^r(\omega_j) = a_j\omega_j^3 + b_j\omega_j^2 + c_j\omega_j + d_j,$$

$$= a'_j\frac{\omega_j^3}{\omega_N^3} + b'_j\frac{\omega_j^2}{\omega_N^2} + c'_j\frac{\omega_j}{\omega_N} + d'_j, \quad \text{(F35)}$$

and therefore,

$$a_j = \frac{a'_j}{\omega_N^3}, \quad b_j = \frac{b'_j}{\omega_N^2}, \quad c_j = \frac{c'_j}{\omega_N}, \quad d_j = d'_j. \quad \text{(F36)}$$

Finally, for the high-frequency part of the spline, we have

$$\alpha_j = \omega_N^3\alpha'_j, \quad \beta_j = \omega_N^2\beta'_j, \quad \gamma_j = \omega_N\gamma'_j, \quad \delta_j = \delta'_j. \quad \text{(F37)}$$

To end this section, we comment on the differential entropy and the minimization procedure. For the differential entropy of Eq. (F8), we use a default model that is almost flat in the region where $\sigma^r(\omega)$ is expected to have its main structure, and that decreases gradually to very small values for frequencies much larger than the bandwidth. This ensures that the solution that we find is as unbiased as possible. The minimization of Eq. (F6) is performed using a Matlab routine called *fmincon*, which uses a trust-region-reflective algorithm that has been proven quite efficient with not as much tendency to get trapped into local minima as other optimization routines. Our procedure is to start with a very large value of α such that the minimization process gives a solution very close to the default model $m(\omega)$ [the minimization of Eq. (F8) alone has in fact a solution proportional to $m(\omega)$]. Then, α is decreased and a new optimal solution is found, using the previous solution as a starting point in the optimization routine. This step is then repeated until $\chi^2 \approx N_{q_n}$ or χ^2 does not decrease anymore when α is reduced. Using an augmented lagrangian method, we also include inequality constraints to restrict the roughness of the solution $\sigma^r(\omega_j)$. This roughness appears at some point in the procedure when we try to make $K_n\sigma^r$ closer to $\chi_{j_x j_x}(iq_n)$. It is related to oscillations present in K_{nj} as a function of the frequency index j for a given n. Those oscillations are in fact the price to pay to work with an accurate numerical integration method since they are present in all approximations more sophisticated than a piecewise linear function for $\sigma^r(\omega)$ in the numerical integration (think about the unequal weights in a Simpson 1/3 or in Gaussian quadratures). In fact, the oscillations in our K_{nj} have an extremely small relative amplitude, but they appear greatly amplified in the solution $\sigma^r(\omega_j)$ when the relative distance $|\chi_{j_x j_x}(iq_n) - K_n\sigma^r|$ becomes very small. The link between oscillations in $\sigma^r(\omega_j)$ and oscillations in K_{nj} for n fixed is clear because they are correlated in the two functions. So they are not related to noise in the data $\chi_{j_x j_x}(iq_n)$. However, those inequality constraints are not absolutely necessary to obtain good, quantitative results with our approach. They just ensure that $\sigma^r(\omega_j)$ is a smooth function.

---

*dominic.bergeron@usherbrooke.ca

†tremblay@physique.usherbrooke.ca

[1] P. Anderson, Science **235**, 1196 (1987).

[2] B. J. Powell and R. H. McKenzie, J. Phys. Condens. Matter **18**, R827 (2006).

[3] H. Nakano and M. Imada, J. Phys. Soc. Jpn. **68**, 1458 (1999).

[4] T. Tohyama, Y. Inoue, K. Tsutsui, and S. Maekawa, Phys. Rev. B **72**, 45113 (2005).

[5] E. Dagotto, A. Moreo, F. Ortolani, J. Riera, and D. Scalapino, Phys. Rev. B **45**, 10107 (1992).

[6] J. Riera and E. Dagotto, Phys. Rev. B **50**, 452 (1994).

[7] W.-Z. Li, F. Chen, T.-F. Xu, and H.-P. Ying, Commun. Theor. Phys. **22**, 273 (1994).

[8] D. J. Scalapino, S. R. White, and S. C. Zhang, Phys. Rev. Lett. **68**, 2830 (1992).

[9] A. Comanac, L. De' Medici, M. Capone, and A. J. Millis, Nat. Phys. **4**, 287 (2008).

[10] S. Chakraborty, D. Galanakis, and P. Phillips, Phys. Rev. B **78**, 212504 (2008).

[11] F. Mancini and A. Avella, Adv. Phys. **53**, 537 (2004).

[12] T. A. Maier, Condens. Matter (2003); e-print arXiv:cond-mat/0312447.

[13] M. H. Hettler, M. Mukherjee, M. Jarrell, and H. R. Krishnamurthy, Phys. Rev. B **61**, 12739 (2000).

[14] K. Haule and G. Kotliar, Phys. Rev. B **76**, 104509 (2007).

[15] K. Haule and G. Kotliar, Europhys. Lett. **77**, 6 (2007).

[16] N. Lin, E. Gull, and A. J. Millis, Phys. Rev. B **80**, 161105 (2009).

[17] S. Okamoto, D. Sénéchal, M. Civelli, and A.-M. S. Tremblay, Phys. Rev. B **82**, 180511 (2010).

[18] G. Kotliar, S. Y. Savrasov, G. Pálsson, and G. Biroli, Phys. Rev. Lett. **87**, 186401 (2001).

[19] T. Maier, M. Jarrell, T. Pruschke, and M. H. Hettler, Rev. Mod. Phys. **77**, 1027 (2005).

[20] G. Kotliar, S. Y. Savrasov, K. Haule, V. S. Oudovenko, O. Parcollet, and C. A. Marianetti, Rev. Mod. Phys. **78**, 865 (2006).

[21] T. Moriya, Y. Takahashi, and K. Ueda, J. Phys. Soc. Jpn. **59**, 2905 (1990).

[22] R. Hlubina and T. Rice, Phys. Rev. B **51**, 9253 (1995).

[23] A. Rosch, Phys. Rev. Lett. **82**, 4280 (1999).

[24] H. v. Löhneysen, A. Rosch, M. Vojta, and P. Wölfle, Rev. Mod. Phys. **79**, 1015 (2007).

[25] S. Wermbter and L. Tewordt, Phys. Rev. B **48**, 10514 (1993).

[26] T. Dahm, L. Tewordt, and S. Wermbter, Phys. Rev. B **49**, 748 (1994).

[27] H. Kontani, J. Phys. Soc. Jpn. **76**, 074707 (2007).

[28] H. Kontani, K. Kanki, and K. Ueda, Phys. Rev. B **59**, 14723 (1999).

[29] H. Kontani, Rep. Prog. Phys. **71**, 026501 (2008).

[30] Y. Yanase, J. Phys. Soc. Jpn. **71**, 278 (2002).

[31] S. A. Hartnoll, D. M. Hofman, M. A. Metlitski, and S. Sachdev (private communication).

[32] M. V. Sadovskii and N. A. Strigina, J. Exp. Theor. Phys. Lett. **95**, 526 (2002).

[33] J. Lin and A. J. Millis, Phys. Rev. B **83**, 125108 (2011).

[34] H. Maebashi and H. Fukuyama, J. Phys. Soc. Jpn. **66**, 3577 (1997).

[35] H. Maebashi and H. Fukuyama, J. Phys. Soc. Jpn. **67**, 242 (1998).

[36] Y. M. Vilk, L. Chen, and A.-M. S. Tremblay, Phys. Rev. B **49**, 13267 (1994).

[37] Y. Vilk and A.-M. Tremblay, J. Phys. I (France) **7**, 1309 (1997).

[38] S. Allen, A.-M. Tremblay, and Y. M. Vilk, in *Theoretical Methods for Strongly Correlated Electrons*, edited by D. Sénéchal, C. Bourbonnais, and A.-M. Tremblay (Springer, New York, 2003); e-print arXiv:cond-mat/0110130.

[39] A.-M. S. Tremblay, *Theoretical Methods for Strongly Correlated Systems*, edited by A. Avella and F. Mancini (Springer, New York, 2011), Chap. 13, p. 409; e-print arXiv:1107.1534 [cond-mat].

[40] N. D. Mermin and H. Wagner, Phys. Rev. Lett. **17**, 1133 (1966).

[41] P. C. Hohenberg, Phys. Rev. **158**, 383 (1967).

[42] Y. Vilk and A.-M. Tremblay, J. Phys. Chem. Solids **56**, 1769 (1995).

[43] S. Moukouri, S. Allen, F. Lemay, B. Kyung, D. Poulin, Y. M. Vilk, and A.-M. S. Tremblay, Phys. Rev. B **61**, 7887 (2000).

[44] B. Kyung, V. Hankevych, A.-M. Daré, and A.-M. S. Tremblay, Phys. Rev. Lett. **93**, 147004 (2004).

[45] N. Bickers and D. Scalapino, Ann. Phys. USA **193**, 206 (1989).

[46] N. E. Bickers, D. J. Scalapino, and S. R. White, Phys. Rev. Lett. **62**, 961 (1989).

[47] T. Moriya and K. Ueda, Rep. Prog. Phys. **66**, 1299 (2003).

[48] G. G. Lonzarich and L. Taillefer, J. Phys. C **18**, 4339 (1985).

[49] T. Moriya, *Spin Fluctuations in Itinerant Electron Magnetism* (Springer-Verlag, Berlin, 1985).

[50] I. Dzyaloshinskii, Sov. Phys. JETP **66**, 848 (1987).

[51] H. J. Schulz, Europhys. Lett. **4**, 609 (1987).

[52] P. Lederer, G. Montambaux, and D. Poilblanc, J. Phys. **48**, 1613 (1987).

[53] C. Honerkamp and M. Salmhofer, Phys. Rev. Lett. **87**, 187004 (2001).

[54] M. A. Tusch, Y. H. Szczech, and D. E. Logan, Phys. Rev. B **53**, 5505 (1996).

[55] E. Motoyama, G. Yu, I. Vishik, O. Vajk, P. Mang, and M. Greven, Nature (London) **445**, 186 (2007).

[56] A. F. Veilleux, A.-M. Daré, L. Chen, Y. M. Vilk, and A.-M. S. Tremblay, Phys. Rev. B **52**, 16255 (1995).

[57] B. Kyung, J. S. Landry, D. Poulin, and A.-M. S. Tremblay, Phys. Rev. Lett. **90**, 099702 (2003).

[58] A. M. S. Tremblay, B. Kyung, and D. Senechal, Low Temp. Phys. **32**, 424 (2006).

[59] G. Baym, Phys. rev. **127**, 1391 (1962).

[60] L. Kadanoff and G. Baym, *Quantum Statistical Mechanics* (Benjamin, New York, 1962).

[61] I. Paul and G. Kotliar, Phys. Rev. B **67**, 115131 (2003); e-print arXiv:cond-mat/0211538.

[62] Y. Vilk and A.-M. Tremblay, Europhys. Lett. **33**, 159 (1996).

[63] P. C. Martin and J. Schwinger, Phys. Rev. **115**, 1342 (1959).

[64] J. M. Luttinger and J. C. Ward, Phys. Rev. **118**, 1417 (1960).

[65] M. R. Hedayati and G. Vignale, Phys. Rev. B **40**, 9044 (1989).

[66] G. Mahan, *Many-Particle Physics*, 3rd ed. (Kluwer/Plenum, New York, 2000), Sec.6.4.4 .

[67] N. F. Berk and J. R. Schrieffer, Phys. Rev. Lett. **17**, 433 (1966).

[68] A. Larkin and A. Varlamov, Condens. Matter (2001); e-print arXiv:cond-mat/0109177.

[69] K. Maki, Prog. Theor. Phys. **39**, 897 (1968).

[70] K. Maki, Prog. Theor. Phys. **40**, 193 (1968).

[71] K. Maki, J. Low Temp. Phys. **1**, 513 (1969).

[72] R. S. Thompson, Phys. Rev. B **1**, 327 (1970).

[73] L. Aslamasov and A. Larkin, Phys. Lett. A **26**, 238 (1968).

[74] V. S. Oudovenko and G. Kotliar, Phys. Rev. B **65**, 075102 (2002).

[75] M. Jarrell and J. E. Gubernatis, Phys. Rep. **269**, 133 (1996).

[76] K. S. D. Beach, R. J. Gooding, and F. Marsiglio, Phys. Rev. B **61**, 5147 (2000).

[77] S. Roy and A.-M. S. Tremblay, Europhys. Lett. **84**, 37013 (2008).

[78] A.-M. Daré, Y. M. Vilk, and A.-M. S. Tremblay, Phys. Rev. B **53**, 14236 (1996).

[79] Y. Onose, Y. Taguchi, K. Ishizaka, and Y. Tokura, Phys. Rev. B **69**, 24504 (2004).

[80] A. Zimmers, J. Tomczak, R. Lobo, N. Bontemps, C. Hill, M. Barr, Y. Dagan, R. Greene, A. Millis, and C. Homes, Europhys. Lett. **70**, 225 (2005).

[81] T. Moriya and K. Ueda, Adv. Phys. **49**, 555 (2000).

[82] B. Kyung, J.-S. Landry, and A. M. S. Tremblay, Phys. Rev. B **68**, 174502 (2003).

[83] V. Hankevych, B. Kyung, A.-M. Daré, D. Sénéchal, and A.-M. Tremblay, in *Proceedings of SNS2004* (2005); e-print arXiv:cond-mat/0407085.

[84] D. Bergeron, *Conductivité dans le modèle de Hubbard bidimensionnel a faible couplage*, Ph.D. thesis, Université de Sherbrooke, 2011.

[85] A. Kaminski, S. Rosenkranz, H. M. Fretwell, Z. Z. Li, H. Raffy, M. Randeria, M. R. Norman, and J. C. Campuzano, Phys. Rev. Lett. **90**, 207003 (2003).

[86] N. E. Hussey, J. Phys. Condens. Matter **20**, 123201 (2008).

[87] R. A. Cooper, Y. Wang, B. Vignolle, O. J. Lipscombe, S. M. Hayden, Y. Tanabe, T. Adachi, Y. Koike, M. Nohara, H. Takagi, C. Proust, and N. E. Hussey, Science **323**, 603 (2009); [http://www.sciencemag.org/content/323/5914/603.full.pdf].

[88] N. Doiron-Leyraud, P. Auban-Senzier, S. R. de Cotret, A. Sedeki, C. Bourbonnais, D. Jerome, K. Bechgaard, and L. Taillefer, (2009); e-print arXiv:0905.0964 [cond-mat.supr-con].

[89] N. Doiron-Leyraud, P. Auban-Senzier, S. René de Cotret, C. Bourbonnais, D. Jérome, K. Bechgaard, and L. Taillefer, Phys. Rev. B **80**, 214531 (2009).

[90] M. Abdel-Jawad, J. G. Analytis, L. Balicas, A. Carrington, J. P. H. Charmant, M. M. J. French, and N. E. Hussey, Phys. Rev. Lett. **99**, 107002 (2007).

[91] Y. Ando, S. Komiya, K. Segawa, S. Ono, and Y. Kurita, Phys. Rev. Lett. **93**, 267001 (2004).

[92] G. Pálsson, *Computational Studies of Thermoelectricity in Strongly Correlated Electron Systems*, Ph.D. dissentaion, Rutgers University, 2001.

[93] H. Terletska, J. Vucicević, D. Tanasković, and V. Dobrosavljević, e-print arXiv:1012.5833 [cond-mat.str-el].

[94] A.-M. Daré, L. Chen, and A.-M. S. Tremblay, Phys. Rev. B **49**, 4106 (1994).

[95] G. Mahan, *Many-Particle Physics* (Kluwer Academic, Dordrecht, The Netherlands, 2000).